AD-683304

ULTRASONIC COUPLING LOSSES

By W. L. Ghering

Technical Memorandum
File No. TM 603.2811-09
November 1, 1967
Contract NOw 65-0123-d
Copy No. 18

THIS DOCUMENT HAS BEEN APPROVED
FOR PUBLIC RELEASE AND SALE;
ITS DISTRIBUTION IS UNLIMITED

The Pennsylvania State University
Institute for Science and Engineering
ORDNANCE RESEARCH LABORATORY
University Park, Pennsylvania

DDC
RECEIVED
MAR 1 8 1969

NAVY DEPARTMENT · NAVAL ORDNANCE SYSTEMS COMMAND

Reproduced by the
CLEARINGHOUSE
for Federal Scientific & Technical
Information Springfield Va. 22151

UNCLASSIFIED

File No. 603.2811
November 1, 1967
FWB:dlt

ABSTRACT

Coupling losses must be considered in ultrasonic measurements of small specimens of high Q materials. In these measurements, the energy loss in the bonding material is often of the same magnitude or larger than the loss in the specimen. This study is an investigation of the characteristics of coupling losses.

The energy losses due to a coupling film or coupling by placing surfaces in optical contact were measured as a function of such varied parameters as frequency, bond thickness, bond composition, mechanical loading, surface conditions, relative alignment of transducer and specimen, and temperature. The equipment used in the measurements was designed so that the energy dissipation due to the mounting of the quartz crystal in order to measure its damping was negligible.

The experimental data obtained for small volumes of liquids, free films, and for loaded films were initially puzzling: the magnitude of the losses was much larger than would be expected on the basis of the theory of longitudinal vibrations. An investigation of the vibrational modes for a disc according to the Aggarwal solution indicated that the resonant modes near the fundamental thickness resonance exhibited shear displacements at the surface of the disc which were comparable to the longitudinal displacement. Such radial or shear motion of the disc-shaped vibrator leads to considerable losses when a liquid coupling film is used. A liquid does not support a shear wave and the transverse component of the vibration in the film is rapidly damped out.

The energy losses for a free film on the surface of a vibrator agree with the theory of shear losses. Still higher accuracy could be obtained if a shear transducer were used with a suitable support arrangement. The viscosity of films could then be determined accurately as a function of frequency.

When the film was loaded, the energy dissipation increased much more than would be expected even when shear is taken into account. The vibrational modes of the system in a loaded condition are unknown, but even larger shear motions would not account for the magnitude of the energy losses.

In order to account for the energy losses, it must be assumed that a component of the losses is due to surface imperfections such as microscopic surface cracks and surface dislocations, and that loading the crystal increases these losses. The addition of a $\lambda/2$

UNCLASSIFIED

increased the losses for a glycerin film by approximately a factor of 10, while a $\lambda/4$ load increased the losses about a factor of 40 relative to that of a free glycerin film. Surface cracks and dislocations generate acoustic near fields and near field coupling may account for another part of the loss. Whereas for most of the investigated liquids, the loaded film measurements indicated that the energy losses were not directly proportional to the film thickness, some liquids like glycerin have a high bulk viscosity and the losses are then found to increase with the film thickness.

Further indication of surface effects were noted when the losses due to a coupling film on a commercially obtained "ground finish" transducer increased as a function of an increase in the surface tension of the liquid. In contrast to this, the damping of an optically polished crystal was not affected by the variation of the surface tension of the film.

A study of the energy dissipation due to surfaces in optical contact was made. Through variation of temperature and other relevant parameters, a temperature activated hysteresis was observed for many of the measurements. According to the theory of temperature activated hysteresis, the loss is proportional to the number of dislocations; the surfaces in optical contact seemed to act like a plane of dislocations. Energy losses due to optical contact also show dependency on the mode of vibration.

With the knowledge derived, it ought now to be possible to proceed in a systematic manner and obtain detailed results. It was only through these studies, however, that the significant properties involved in the acoustical behavior of thin films, bonded surfaces, and surfaces in optical contact could be made apparent. Apart from deriving a method to measure viscosity in a wide frequency range, the study showed that acoustic measurements can give a considerable amount of information about the mechanical behavior of surfaces of solids which cannot be obtained by other methods.

TABLE OF CONTENTS

LIST OF FIGURES

LIST OF FIGURES (cont.)

LIST OF FIGURES (cont.)

LIST OF FIGURES (cont.)

I. INTRODUCTION

Statement of the Problem

The original task of the study described here was the measurement of the acoustic properties of small specimens, such as liquid volumes of drop size, single crystals, thin films, and small samples of random configuration. There is a need for such measurements. For example, medical analysis of small volumes of body fluids such as the fluid in the ventricles of the human brain would be useful. Surface relaxation effects of liquids[1] could be studied by investigating the damping of drops of liquids. Many materials are available in single crystal forms only in small quantities.

Ultrasonic measurements are usually taken by employing a separate transducer with a coupling medium between the transducer and the material under investigation. The coupled system of transducer-bond-sample is excited to forced vibrations and the decay of the vibration is observed as a function of time. The measurement gives the energy dissipation of the total system, consisting of the quartz crystal, the bonding, and the test piece. In testing small samples, or materials with low loss factors, the bonding losses cannot be neglected. Because the characteristics of the bonding losses are not well known, most experimenters try to reduce them to an acceptable level and then neglect them. At a recent lecture W. P. Mason[2] referred to bonding techniques as still one of the "black arts" with various experimenters devising their own technique or ritual.

In previous studies, as well as in the present measurements, bonding and surface losses were found to be predominant in many small specimen measurements. In fact, these losses turned out to be so great that accurate measurements of small specimens possessing low loss factors could not be made; thus, there exists a need for a better understanding of the characteristics of a bond. The main emphasis of this study, therefore, was placed on the determination of the characteristics of ultrasonic coupling losses. Particular attention was paid to developing experimental techniques and to interpreting the experimental results.

Experimental Methods and Equipment

The measurements were performed by loading a vibrator with the samples to be tested and studying their effect on the decay of the resonant vibration after the power source had been disconnected. The amplitude of the vibrations were relatively small and witnin the range of Hooke's law. Non-linear effects have been excluded.

In general, the change of the loss factor (see next section) of the composite resonant system of transducer-bond-sample was determined as a function of the various parameters such as: frequency, bond thickness, bond composition, mechanical loading of the bond, surface conditions, relative alignment, and temperature. To obtain accurate results, the vibrator had to have a small energy dissipation so that the energy dissipation of the sample had a measurable effect on the decay time of the vibrator-sample system.

Quartz transducers were chosen because of their small internal energy dissipation. The crystals were manufactured by the Valpey Corporation by the following process:[3] The raw material was cut with No. 100 abrasive. The first 0.038 cm stock was removed with 30 micron grit; the next 0.010 cm by 9 micron grit; another 0.010 cm was removed by 2 micron grit and the final polish was done with 1 micron grit, removing about 0.0010 cm of the material. The grinding and polishing grit was single crystal AlO_2 (99% pure) of Moh hardness 9, and specific gravity 3.85.

Studies of films of various bonding agents or special test solutions were performed at frequencies from 400 KHz to 5 MHz and from 30 MHz to 210 MHz. The crystal transducers were excited in their fundamental thickness resonance for frequencies up to 5 MHz. Their thickness is given by

$$d\ (\text{cm}) = 2.85 \times 10^5 / f_o\ , \qquad 1.1$$

where f_o is the frequency of the fundamental thickness resonance. Crystal diameter was 2.936 cm for the lower frequency film measurements. The crystals used for studying the effect of optical contact and the higher frequency film measurements were optically polished 0.952 cm diameter crystals and were driven in overtones (3^{rd} to 21^{st} harmonic).

The quartz vibrator had to be supported in some way so that the measurements could be performed. It was necessary to support it in such a manner that the supports had as little effect on the measurement of the losses as possible. To determine the effect of the supports, the internal dissipation of the crystal for thickness vibration had to be

measured. Many papers have been published on the damping of shear modes of quartz, but very little is known about that for thickness vibrations.

To measure the damping of a free quartz crystal, a free fall device was constructed. Figure 1 shows the top portion of the apparatus. The crystal is excited to a resonant mode of vibration and then dropped between the electrodes that are approximately 110 cm long. These electrodes sense the electric field due to the direct piezoelectric effect generated by the decaying vibration of the freely falling quartz crystal. The time of fall is about 0.5 second which would correspond to the time for the amplitude of the vibrations of a crystal with a Q of 800,000 to decay to 1/e.

Plating a crystal substantially increases the damping; therefore, most of the measurements in this study were made with unplated crystals. Unplated crystals also provided unobstructed surfaces on which to work and dispensed with the troublesome electrical connections. The electrodes were stiff plates that were approached to a distance of about 0.015 cm to the surface of the crystal transducers. The small air gaps between the vibrating surfaces of the crystal and the non-vibrating, relatively stiff electrodes acted like low loss compliances. Most of the radiation damping that would have occurred with plated crystals not placed in proximity of plane electrodes could thus be eliminated and measurements could be performed in air. However, the entire apparatus fitted into a desiccator vessel and the space around the crystal could be evacuated in order to eliminate losses due to

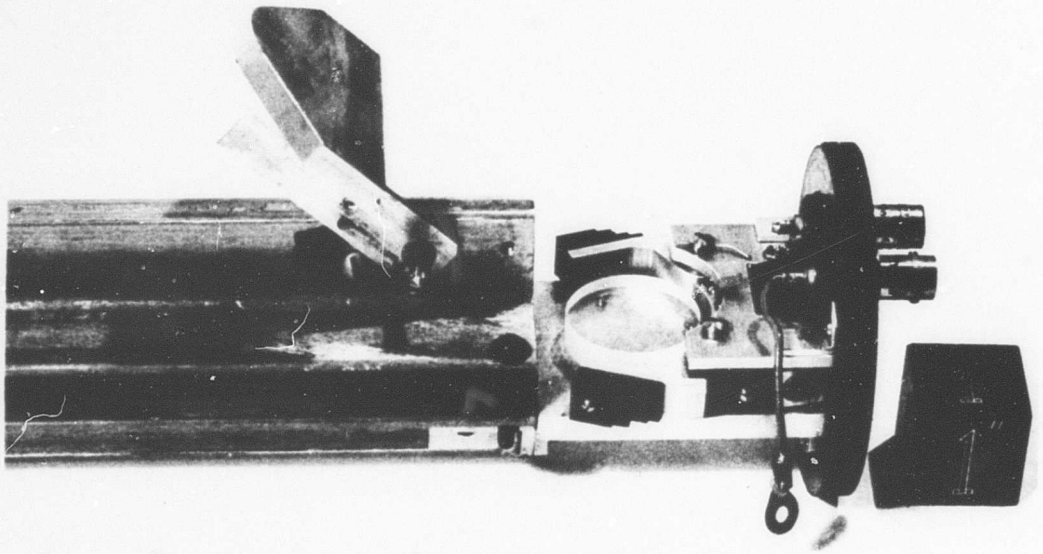

Figure 1. Apparatus to Measure the Quality Factor of a Crystal in Free Fall

radiation and the air film between crystal and electrode. This was done whenever the energy losses of the composite system were small.

The measurement of the vibration amplitude usually absorbs a certain power which must be furnished by the vibrating system. This extraction of power has the same effect as an additional damping applied to the system and the decay time is shortened because of the measurement. To reduce this damping, which is coupled into the mechanical system, the coupling capacitors to the electrodes of the quartz vibrators were made as small as possible, and the output coupled to a cathode follower of high impedance. Figure 2 shows the electronic arrangement.

Considerable effort was spent on developing a holder that would not increase the damping of the crystal. The initial holders employed radial steel points such as phonograph needles to hold the crystal. These holders were not satisfactory because of crystal-support interaction and crystal fracture at the point of contact. Initially it was assumed that the central plane of the disc shaped crystal was a nodal plane for thickness vibrations. However, vibration studies showed that for a quartz crystal vibrating in a thickness mode there is a considerable radial component of motion at its central plane (Figure 24). It was necessary, therefore, to employ supports that were compliant enough to allow for this radial component of the vibration.

Figure 3 shows the crystal support arrangement. In Figure 3a the crystal is held by circumferential spring steel points, in Figure 3b by thin spring steel supports fitted with sapphire phonograph needles

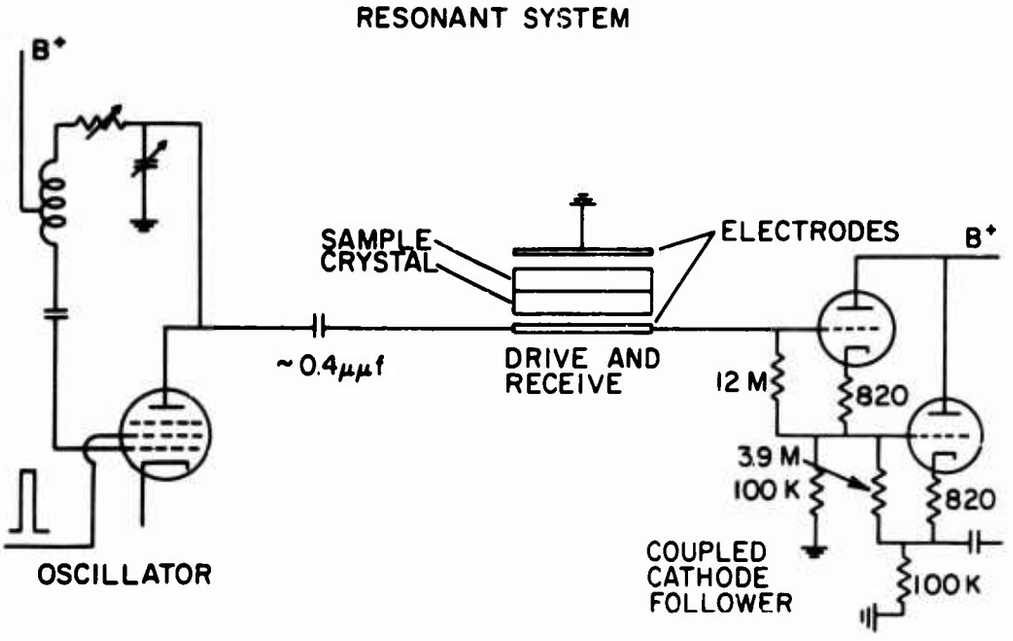

Figure 2. Diagram of the Electromechanical Resonant System

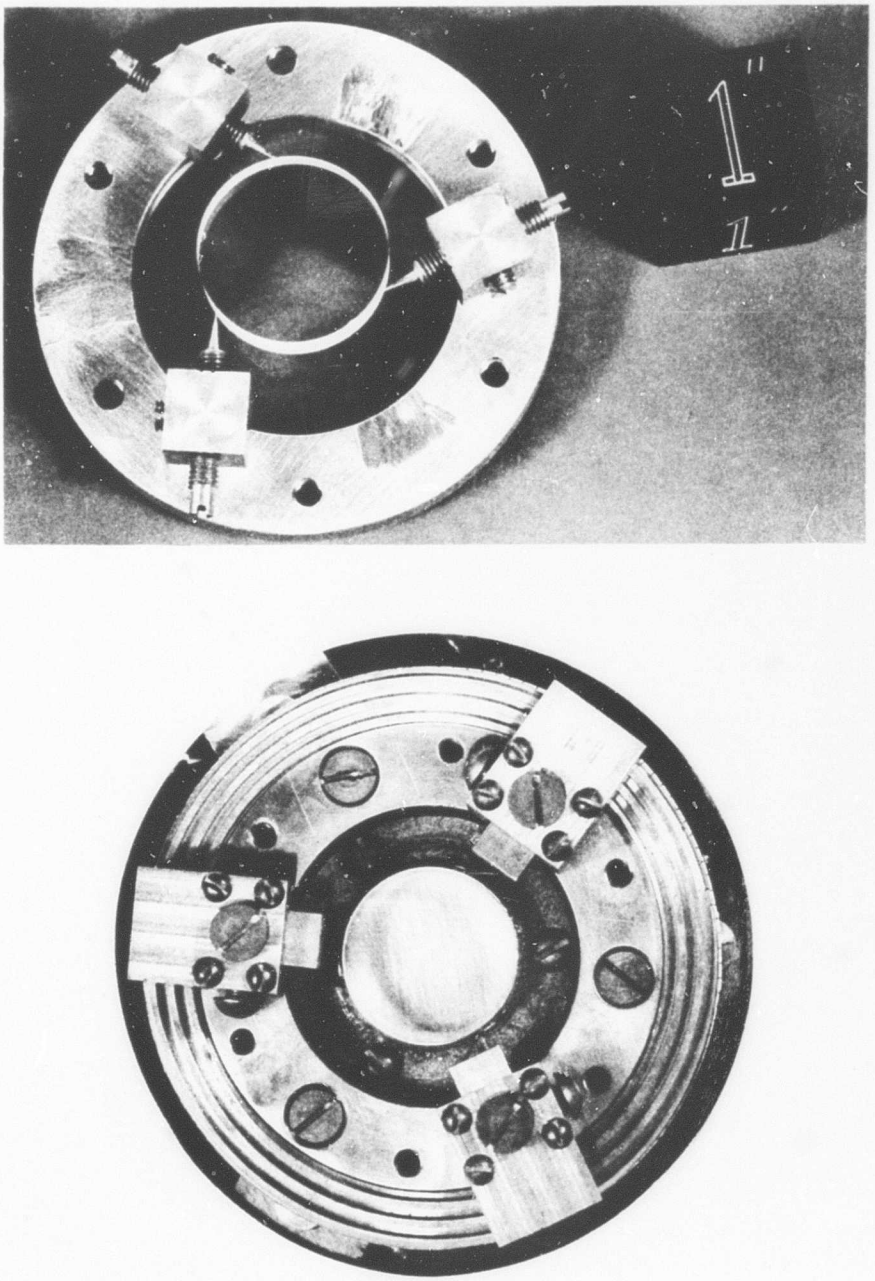

Figure 3. Crystal Support Arrangement (a) Crystal Held by Circumferential Spring Steel Supports (b) Crystal Held by Spring Steel Supports Fitted with Sapphire Phonograph Needles

that fit into slits lapped along the circumference of the crystal in its central plane. Both types of support were sufficiently compliant so that they exerted little radial force on the crystal; thus, the crystal was essentially suspended freely in space. A rack-differential screw arrangement allowed easy and accurate repeated insertion of the crystal into the holder. The crystal holders fit into an adjustable stand, as shown in Figure 4. Two electrodes at a small distance from the crystal serve to drive it through the external electric field created by application of a suitable drive voltage.

For a given energy of the vibration, the vibration amplitudes decrease inversely proportional to the square of the frequency. The vibration amplitudes are, therefore, very small at high frequencies; dust particles and surface roughnesses, as they occur on non-optically flat surfaces, usually lead to complete isolation between two surfaces.

It was found that at frequencies greater than about 10 MHz the coupling between the crystal and the electrode was small and that the microscopic air film because of room dust and surface roughnesses was sufficient to decouple the crystal and electrodes. The simple holder shown in Figure 5 thus proved practical; the holder was small enough to be immersed in a dewar, so that measurements could be made at low temperatures. The electronic setup for a frequency range 30 to 210 MHz is shown in Figure 6a. For 10 MHz measurements arrangement shown in Figure 6b was used.

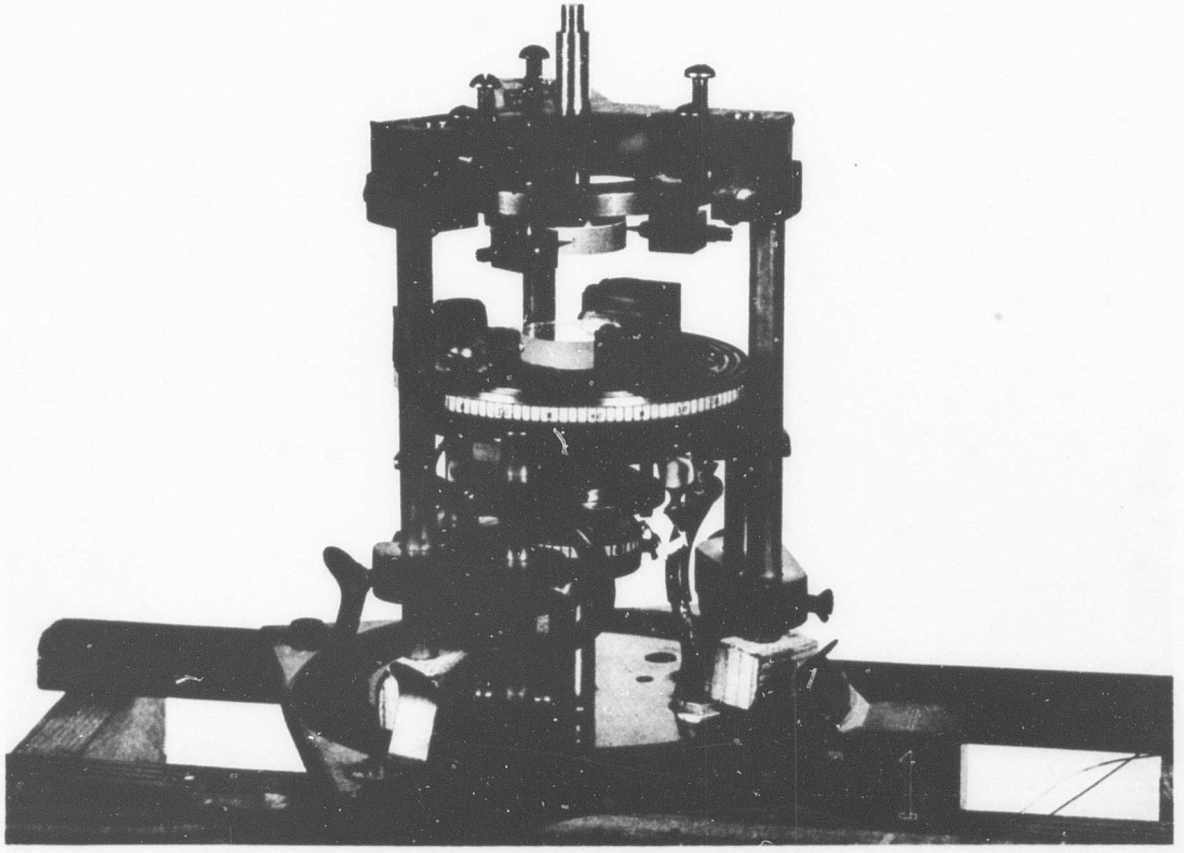

Figure 4. Adjustable Stand to Support Crystal Holders

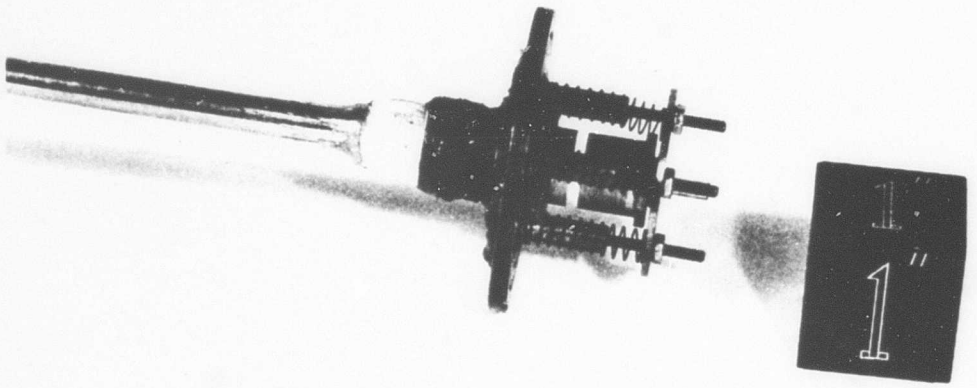

Figure 5. High Frequency Crystal Holder

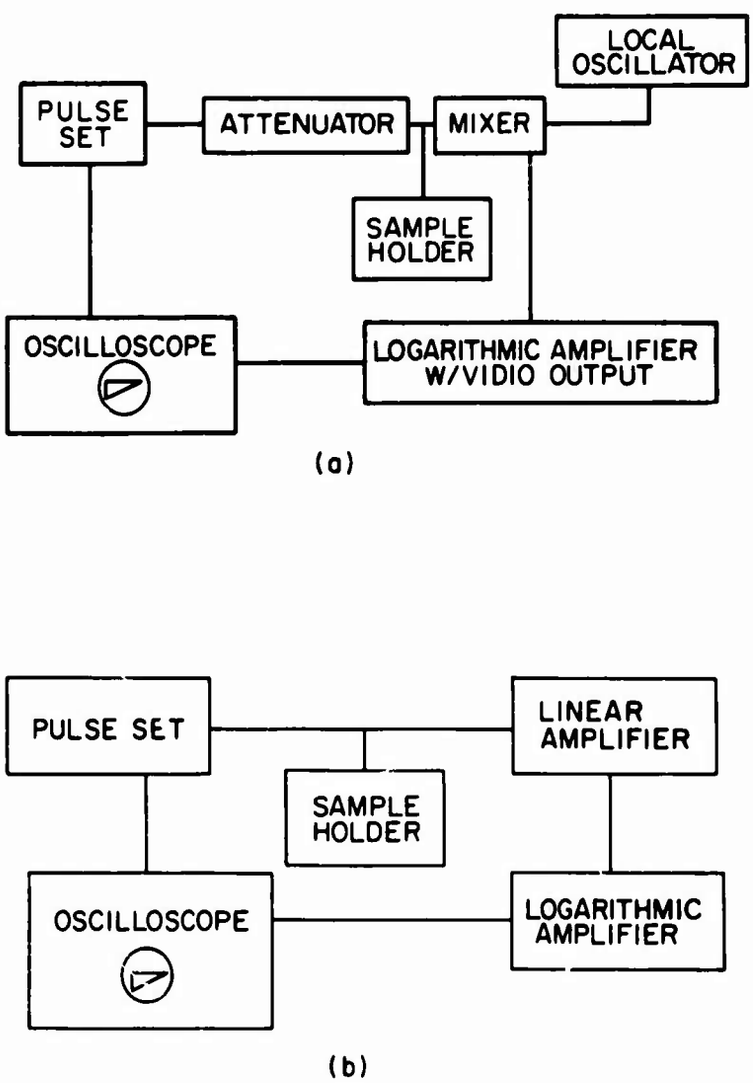

Figure 6. Block Diagram of Electronic Arrangement (a) Setup for 30 to 210 MHz (b) Setup for 10 MHz

The first series of investigations was devoted to a study of drops and small volumes of liquids placed on the surface of a resonating quartz crystal. Later in the program, test pieces such as discs of various metals or quartz were placed on the quartz vibrator to measure their acoustic properties. Because of the great effect of the contact between vibrator and test pieces on the experimental results, a thorough study of the acoustical behavior of films and of surfaces in optical contact was initiated.

Films were formed on the surface of a single quartz crystal by evaporation from a solution of the film material and a solvent. Glycerin and petroleum jelly formed a stable film for a wide range of thicknesses when the quartz surface had a ground finish (i.e., not polished). It was also of interest to measure the effect of loaded films; i.e., of films sandwiched between two vibrating surfaces, so that both film surfaces are under mechanical stress (see Theory section). The films were of standard bonding materials such as glycerin, vaseline, vacuum grease, different silicone oils, Eastman 910 cement, or of solutions of sugar in water. To load a free film, a mechanism was devised that dropped a metal disc or a second quartz crystal from a small distance above the film onto it. The disc supports could be drawn back rapidly by solenoids. This arrangement is shown in Figure 7. A quartz crystal or a disc of thickness $\lambda/2$ (half a wavelength) represented a small loading as far as longitudinal stresses are concerned; one of a thickness of $\lambda/4$, because it vibrates in anti-resonance, a very large loading (see Theory section).

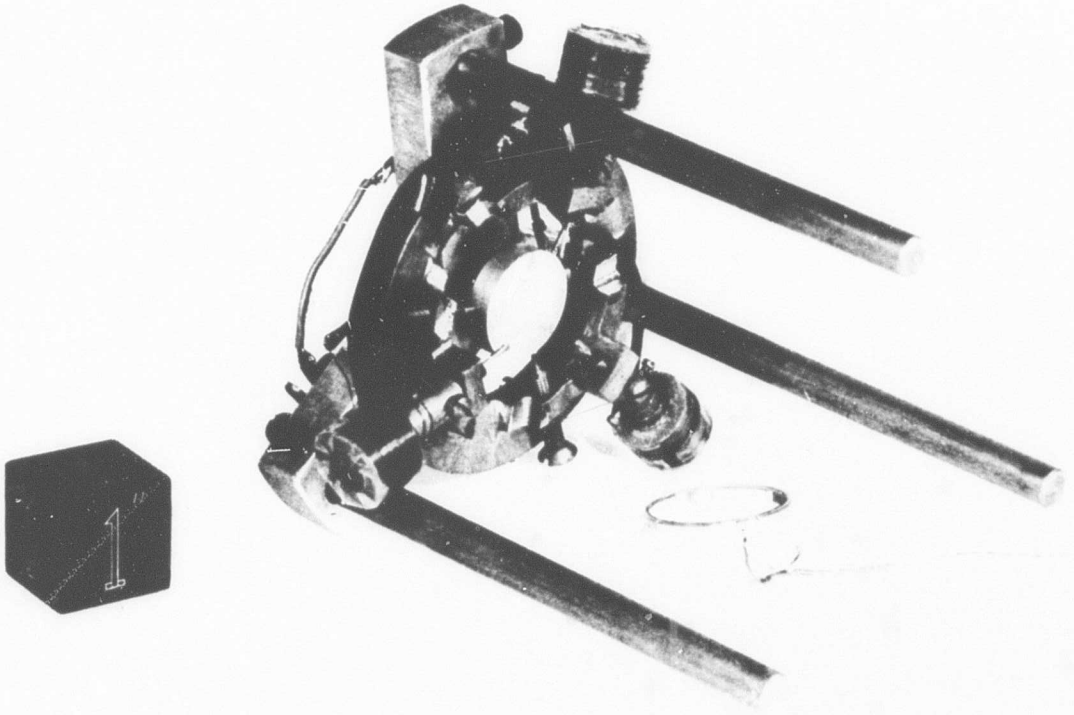

Figure 7. Apparatus to Place a Metal Disc Load on a Free Film

As the thickness of a film was reduced, its energy dissipation approached that for optical contact. To obtain optical contact, the surfaces had to be optically polished. Particular care had to be taken to eliminate room dust and other particles. Room dust in normal laboratory air is usually sufficient to spoil the optical contact between two optically flat surfaces. Several industrial models of air cleaners are available, but at rather high cost, so the laboratory model shown in Figure 8 was designed and constructed using American Air Filter components. The final filter was an 'Astrocel' which had a guaranteed efficiency of 99.9% on 0.3 micron particles. With the addition of an air flow stabilizing grid following the 'Astrocel', the air flow was uniform in the work area. This design was satisfactory for excluding atmospheric contamination of the contact surfaces.

The properties of optical contact were investigated in the frequency range from 30 MHz to 210 MHz and for temperatures between 90°K and 370°K.

The results obtained for the energy damping of films and contact surfaces could not be easily interpreted. The mechanism of thermal damping, for instance, leads to loss factors that were 10 times smaller than those actually measured. More information was needed about the vibration pattern and in particular, about the transverse motion of a vibrating quartz crystal. Theoretical studies on the basis of a simplified theory were supplemented by measurements. To obtain information about the surface motion of a crystal vibrating at 400 KHz, a

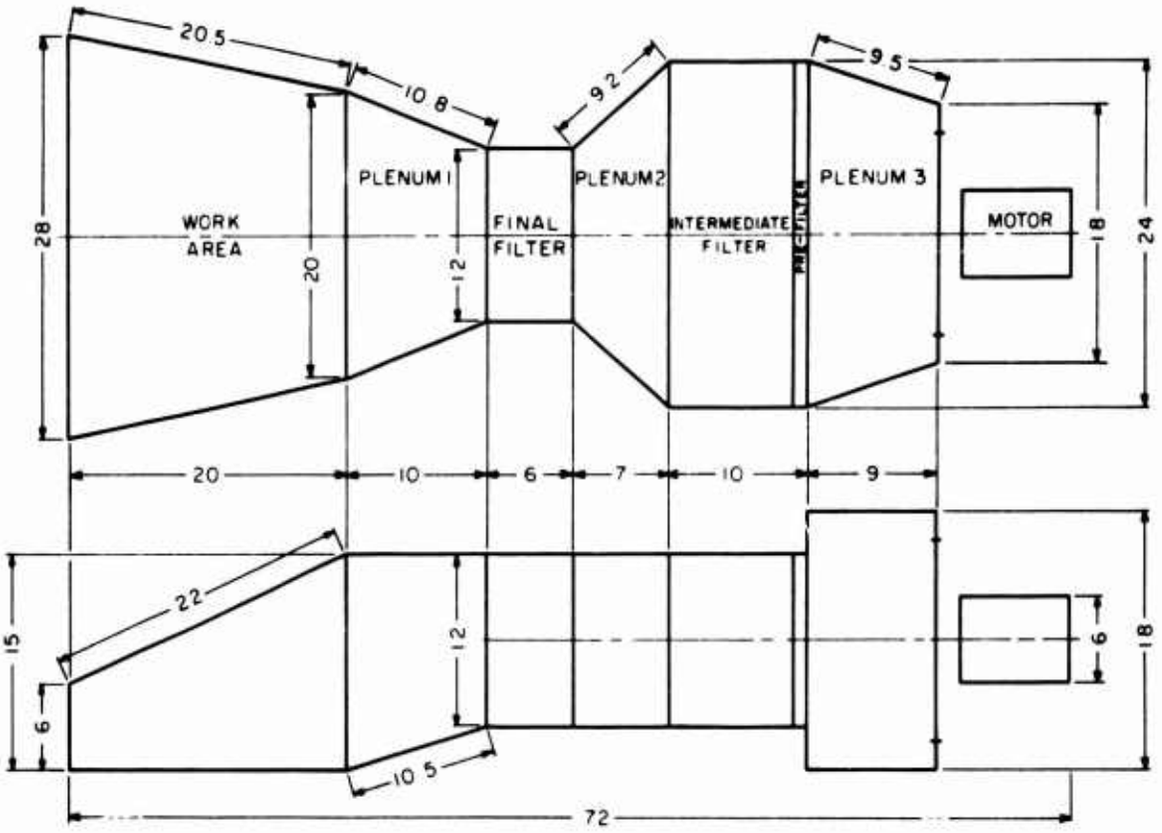

Figure 8. Top and Side View of Laboratory Model of Clean Air Station

probe pickup was constructed. Figure 9 illustrates the pickup and the method used to measure the transverse component of the vibration of a crystal as a function of the polar angle. A multiple half-wavelength probe attached to a piezoelectric crystal sensed the radial component of the vibration at the cylindrical surface of the crystal as it was driven in a thickness mode.

To determine the effect of the orientation of the crystallographic axes on the contact loss between two crystals, the axes were determined as shown in Figure 10. The crystal was rotated about its X-axis until the rays of light formed the circular (bullseye) pattern characteristic of the Z (optic) axis. This arrangement was sufficient to locate the Z or optical axis and to determine the left- or right-handedness of a quartz crystal whose fundamental thickness resonance was not greater than 10 MHz. Higher frequency crystals were too thin to be investigated by this method.

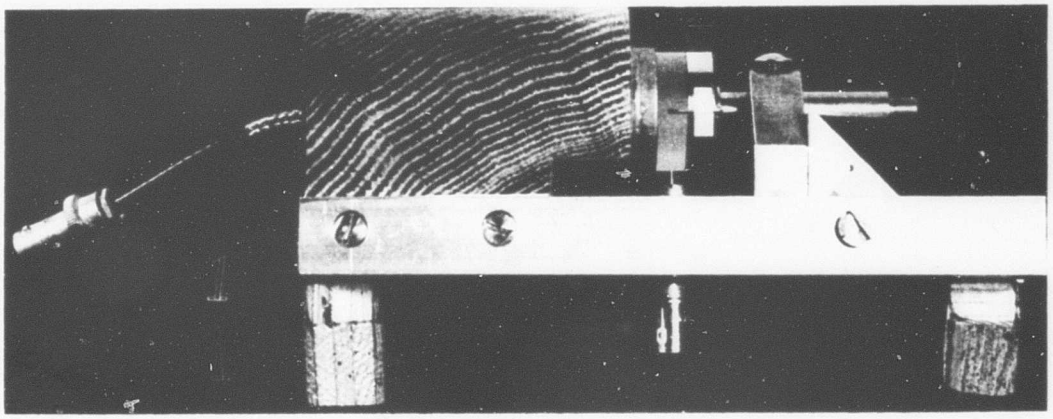

Figure 9. Probe Pickup to Measure the Transverse Component of Crystal Vibration

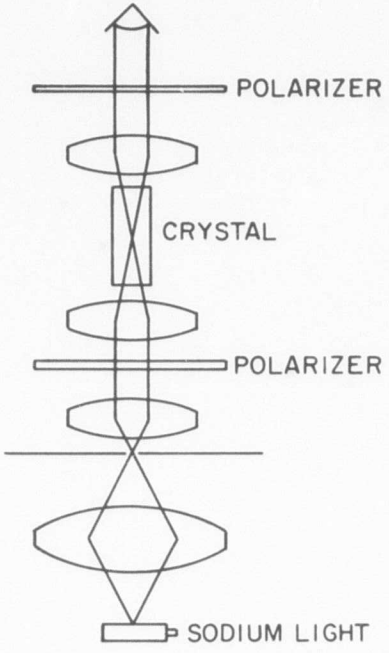

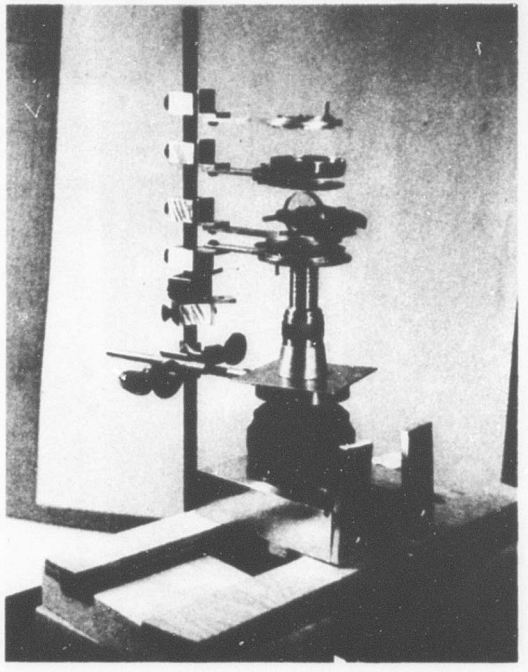

Figure 10. Optical Arrangement to Locate Crystallographic Axes of Quartz Crystals

II. THEORY

Loss Factor and Energy Dissipation

In acoustics it is standard practice to describe the internal dissipation of a material or system by a dimensionless constant such as the loss factor:

$$\eta \equiv \frac{\text{energy dissipated per period}}{2\pi \times \text{energy of the system}} = \frac{\partial E}{\partial t} \Big/ \omega E \ , \qquad 2.1$$

where $\frac{\partial E}{\partial t}$ is the energy dissipation per unit time, E is the total energy of the system and ω the angular frequency. The loss factor thus defined is closely related to quantities that can be measured directly. For instance, the loss factor is equal to the relative bandwidth of a resonance curve

$$\eta = \omega_\beta / \omega_o \qquad 2.2$$

where ω_β is the bandwidth at the half energy points, and ω_o is the resonant frequency. The loss factor can also be deduced from the time t_e for the amplitude of the vibration to decay to 1/e of its initial value:

$$\eta = \frac{2}{\omega t_e} \ . \qquad 2.3$$

If the system consists of several separate parts, such as a quartz vibrator carrying a film and a disc that loads the film, the resultant loss factor, denoted as the system loss factor η_s, is given by

$$\eta_s = \frac{\sum_\nu \frac{\partial E_\nu}{\partial t}}{\omega \sum_\nu E_\nu} = \frac{\sum_\nu \left(\frac{1}{\omega E_\nu} \frac{\partial E_\nu}{\partial t} \right) E_\nu}{\sum_\nu E_\nu} = \sum_\nu \frac{\eta_\nu E_\nu}{E_t} \qquad 2.4$$

where

$$E_t = \Sigma E_\nu$$

is the total vibrational energy of the system and E_ν the vibrational energy of its νth part. If the quartz vibrator of mass M_1 is coupled to a similar vibrator or to a disc of mass M_2 that vibrates in a $\lambda/2$ or a $\lambda/4$ thickness mode, the space distribution of the vibration amplitude is sinusoidal, and the effective masses are half of the masses of the vibrator and the loading disc. The mass of the film is negligible. The above expression then becomes

$$\eta = \eta_1 \frac{M_1}{M_1+M_2} + \eta_2 \frac{M_2}{M_1+M_2} + \frac{2}{\omega V^2} \frac{\partial E_f}{\partial t} \frac{1}{M_1+M_2} \qquad 2.5$$

where V is the maximum of the velocity amplitude and $\frac{dE_f}{dt}$ the energy dissipation of the film per unit time. The film has been assumed to vibrate with the velocity V and all its energy to be kinetic.

Frequently, it is convenient to define a loss factor for the film alone and to refer this loss factor to the velocity amplitude of the film surface that is generated by the thickness vibration of the quartz crystal.

$$\eta_f = \frac{1}{\omega} \frac{\partial E_f}{\partial t} \cdot \frac{1}{\frac{1}{2} M_f V_o^2} \qquad 2.6$$

as if V_o were the velocity that determined the energy losses of the film. The film loss factor is that which the film would have to have

to account for the change in the system loss factor when all the additional losses are ascribed to the film. Actually, the energy losses turn out to be predominantly due to the shear motion of the quartz surface; and the loss factor as defined above will not only depend on the film, but also on the amplitude pattern of the quartz vibrator. However, the above definition is useful as this loss factor describes the effect of the film on the particular vibrator which was used in the experiment. The above equations show that the energy dissipation of the film increases the loss factor of the system by

$$\Delta\eta_s = \frac{2}{\omega_o V_o^2} \frac{\partial E_f}{\partial t} \frac{1}{M_1+M_2} = \frac{2}{\omega_o V_o^2} \frac{\partial E_f}{\partial t} \frac{1}{M} = \eta_f \frac{M_f}{M} \qquad 2.7$$

where $\Delta\eta_s$ is the change in the system loss factor because of the film. For two crystals in contact, the mass $M = M_1+M_2$ is proportional to the thickness of the system. The thickness d of a quartz crystal is inversely proportional to the resonant frequency (see Eqn 1.1), the mass is also inversely proportional to the resonant frequency; $\omega_o = \pi c/d$, where c is the sound velocity in quartz. Then $M = \sigma\rho d = \sigma\rho c\pi/\omega_o = \text{const.}/\omega_o = a/\omega_o$ where σ is the cross section area and a is a constant as defined above. We then have

$$\Delta\eta_s = \frac{1}{\omega_o V_o^2} \frac{\partial E_f}{\partial t} \frac{\omega_o}{a} = \frac{1}{V_o^2} \frac{R V_o^2}{a} = \frac{R}{a} \qquad 2.8$$

where R is the equivalent dissipation resistance of the film per unit area and is defined by

$$\frac{\partial E_f}{\partial t} = R V_o^2 \ . \qquad 2.9$$

The increase in loss factor of the system thus is proportional to the effective dissipation resistance per unit area of the film referred to the surface velocity of the quartz vibration.

Properties of Liquid Surfaces

The molecular force field in a liquid is greatly disturbed near and at its surface. Klemm[1] has stated that surface relaxation is to be expected and that the surface layer can have a very high viscosity. He estimates that for water, the surface viscosity would be about 10,000 times greater than the viscosity measured within a liquid volume. Thus, there is reason to expect that the properties of a film differ from those of the same liquid in bulk. Also it is questionable if properties such as viscosity are unchanged in the region of interaction of the liquid and the solid material. No experimental results that verify or contradict Klemm's theory have yet been published.

Energy Dissipation of Films Because of Heat Conduction

The effect of heat conduction in the air gap of a condenser microphone on its damping has been studied by Pfriem.[4] Similar computations were performed for liquid films. The computations are relatively lengthy with the result that heat effects are about 10 times too small to account for the energy dissipation of thin films sandwiched between two heat conducting surfaces. The energy dissipation is considerably smaller if one or more of the surfaces in question are of poor heat conductors such as quartz.

Thin Films and Optical Contact

When two crystals with optically flat surfaces are brought together, Van der Waals or London dispersion forces are generated. The forces between surfaces for distances greater than 1000 Å have been found to be proportional to $1/d^4$.[5] Optical contact is said to occur when the surfaces seize one another; the distance of separation is about 200 Å. The molecular forces that act between the two surfaces then attain a strength of the order of 14 kg/cm^2 whether the contact was made in air or in vacuum.[6] The true mechanism of optical contact bonding is not well understood. The bonding has been shown not to depend on the surface tension of a thin film of water on the surface of the crystal.[6] For thin films the interaction of the surfaces must be considered. As the thickness of the film goes to zero, the coupling must change to that of optical contact.

Energy Dissipation in Films Because of Shear Waves in Liquids

When this study was started, the transverse motion of the vibrating quartz was neglected and the loss due to a liquid film was computed as if it transmitted a simple standing wave pattern from which the energy densities and hence the loss factor could be determined. However, this theory could not explain the experimentally observed losses. The more exact theory shows that a disc vibrator generates a considerable shear motion even when vibrating in a thickness mode.

When shear is taken into account, an additional component of loss is generated due to the attenuation of the shear component in the

bonding film. The longitudinal component of the motion is transmitted as is assumed in the elementary theory, however the transverse component is largely lost due to the inability of a fluid to support a shear wave. The shear attenuation leads to a loss factor much larger than that of the plane wave theory.

Lord Rayleigh[7] investigated the motion generated in a viscous medium by a plane moving parallel to itself with a velocity V_o. The displacement of the fluid is parallel to the plate and varies with the distance x from it. The equation of motion is

$$\rho \frac{dv}{dt} = \mu \frac{\partial^2 v}{\partial x^2} \qquad 2.10$$

where ρ is the density and μ the viscosity of the fluid. For harmonic motion, the solution is

$$v = A\,(e^{-jkx} + Re^{jkx})\, e^{j\omega t} \qquad 2.11$$

where A and R are constants,

$$k = \pm\,(1-j)\sqrt{\frac{\omega\rho}{2\mu}} = \pm\,\frac{2\pi}{\lambda_s}\,(1-j) = \pm\,(1-j)\,k_o, \text{ and}$$

$$k_o = \sqrt{\frac{\omega\rho}{2\mu}}\,.$$

The solution represents two waves, one propagating in the positive X direction, the other in the negative X direction. The wave number is complex and its real part is equal to the imaginary part, like that for heat waves. The shear motion propagates in the viscous liquid in the form of heavily damped waves; their amplitude decreases by a

factor $e^{-2\pi} \approx 1/520$ per wavelength. The wavelength is given by

$$\lambda_s = \frac{2\pi}{k_o} = \sqrt{\frac{8\pi^2(\mu/\rho)}{\omega}} \ .$$

The preceding formula shows that the shear wave wavelength λ_s in a viscous liquid is extremely short. For example, for water at 500 KHz $\lambda_s \approx 5\ 10^{-4}$ cm.

In studying the propagation of shear waves in a viscous liquid, R in Eq. 2.11 is the amplitude reflection coefficient. Reflection at the opposite face can thus be neglected and R = 0 if the thickness of the film is greater than about 1/3 the shear wavelength λ_s. The solution then simplified to

$$v = V_o e^{-k_o x} \cos(\omega t - k_o x) \ . \qquad 2.12$$

The viscous force acting on the plate is given by

$$(f)_{x=0} = -\mu \left(\frac{\partial v}{\partial x}\right)_{x=0} = \mu\, k_o V_o(\cos \omega t - \sin \omega t) = \mu\, k_o V_o \sqrt{2} \cos\left(\omega t + \frac{\pi}{4}\right) \ . \qquad 2.13$$

The energy dissipation dE/dt (i.e., the work performed by the plate on the viscous film) is

$$N_o \equiv \left.\frac{dE}{dt}\right|_{x=0} = \lim_{T\to\infty} \frac{1}{T} \int_0^T f \cdot v \, dt = \mu\, k_o \sqrt{2}\, V_o^2\, \frac{1}{T} \int_0^T \cos \omega t \cos(\omega t + \pi/4)\, dt =$$

$$\mu \frac{k_o V_o^2}{2} \qquad 2.14$$

and the change of the observed system loss factor because of the presence of a viscous film becomes

$$\frac{dE}{dt}\Big/\omega E \equiv \Delta\eta_s = \frac{\frac{1}{2}\mu k_o V_o^2}{\frac{1}{2}\left(\frac{M_{total}}{2} \times V_{total}^2\right)\omega} = \frac{2\mu k_o}{\omega M_{total}(1+R^2)}$$

$$= \frac{2\mu\sqrt{\frac{\omega\rho}{2\mu}}}{\omega M_{total}(1+R^2)} = \frac{2\sqrt{\frac{\mu\rho}{2\omega}}}{M_{total}(1+R^2)}$$

where $V_{total}^2 = V_o^2 + V_{long}^2$, $R^2 = \frac{V_{long}^2}{V_o^2}$ 2.15

and M_t is the total mass of the system. It has been assumed that the amplitude distribution over the thickness of the vibrator is sinusoidal so that the mode mass is half the total mass.

If the film is sandwiched between two vibrating discs of similar dimensions, the longitudinal component of the vibration will be the same below and above the film. The transverse velocities of the two surfaces will have the same magnitude but their phase will be opposite. If the thickness of the film is greater than about half a shear wave wavelength, the two shear components will not interact and the losses will be twice as great as that given by the above formula.

For films that are sandwiched between two surfaces and are not thicker than half a shear wave wavelength, a more exact computation is needed. If one of the two surfaces is at $x = d$ moving with the velocity V_o in its plane and the other is at $x = 0$ completely at rest, the boundary conditions are

$$V = 0 \quad \text{at } x = 0$$

$$V = V_o \quad \text{at } x = d \; . \tag{2.16}$$

The first condition yields

$$0 = 1 + R \; .$$

Consequently

$$v = -2Aj \sin kx$$

and

$$V_o = -2Aj \sin kd \; . \tag{2.17}$$

Substituting A from the last equation into the preceding equation, we get

$$v = \frac{V_o \sin kx}{\sin kd} \; . \tag{2.18}$$

The force on the surface at x = d is given by

$$f = -\mu \left(\frac{\partial v}{\partial x} \right)_{x=d} = \frac{-V_o k \cos kd}{\sin kd}$$

$$= - V_o k \cot kd \; . \tag{2.19}$$

The component of the force in phase with V_o is given by the real part

$$\mathrm{Re}(f) = \mathrm{Re} \{\mu V_o k_o (1-j) \cot [k_o d (1-j)]\}$$

$$= \mu V_o k_o \, \mathrm{Re} \{\cot (\alpha - j\alpha) - j \cot (\alpha - j\alpha)\}$$

$$= \frac{1}{2} \frac{\sin 2\alpha + \sinh 2\alpha}{\cosh^2 \alpha - \cos^2 \alpha} \cdot \mu V_o k_o \tag{2.20}$$

where $\alpha = k_o d$.

The power dissipated per unit area of the film thus is given by

$$N_o = \frac{\mu V_o^2 k_o}{4} \frac{\sin 2a + \sinh 2a}{\cosh^2 a - \cos^2 a} \quad . \qquad 2.21$$

Figure 11 shows the theoretical curve.

When the film is thick, Eq. 2.21 reduces to Eq. 2.14, and the preceding result is obtained. But when the film is very thin the equation predicts that the absorption becomes infinite. However, the transmitted shear force then would be very large and the second surface would not be at rest but would move transversely. The relative velocity and consequently also the loss would then be much smaller. The large values of l s factor thus cannot be realized in practice.

We thus arrive at the conclusion that if the thickness of the film is reasonably great the viscosity dependent losses of the film correspond to those of an infinitely thick film. The losses may increase considerably when the film becomes thin and the test piece is forced to vibrate.

Some of the measurements were performed with free films placed on the surface of a vibrating quartz crystal. The boundary conditions then are

$$v = V_o \qquad \text{at } x = 0$$

$$\frac{\partial v}{\partial x} = 0 \qquad \text{at } x = d \; . \qquad 2.22$$

We then have

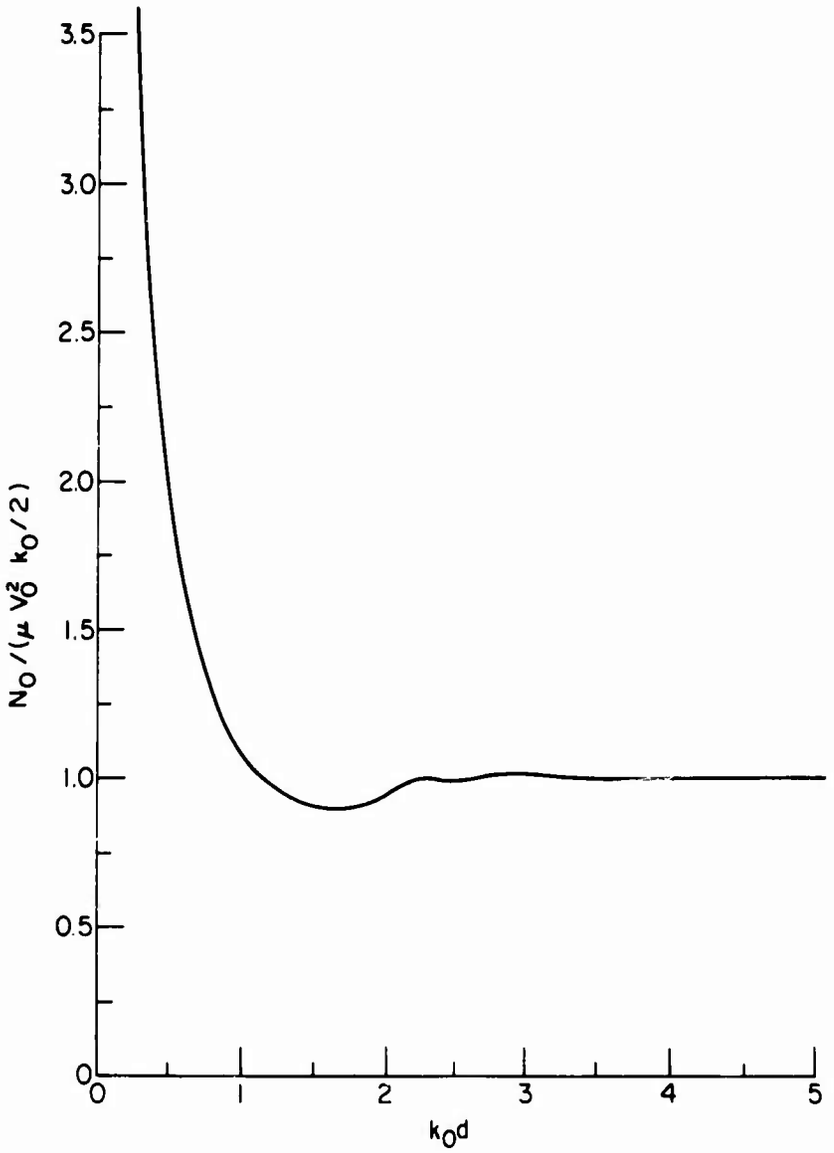

Figure 11. Theoretical Loss Curve for Sandwiched Film

$$v = A(e^{-jkx} + R\, e^{jkx}) \ ,$$

$$(v)_{x=0} = V_o = A\,(1 + R) \ , \text{ and}$$

$$\left(\frac{\partial v}{\partial x}\right)_{x=d} = 0 = jkA\,(-e^{-jkd} + Re^{jkd}) \ . \qquad 2.23$$

Hence $$1 + R = \frac{V_o}{A} \ ,$$

$$R = e^{-2jkd} \ , \text{ and}$$

$$A = \frac{1}{1 + e^{-2jkd}}\, V_o \ ; \qquad 2.24$$

the solution then reduces to

$$v = \frac{V_o}{1 + e^{-2jkd}}\, [e^{-jkx} + e^{-2jkd}.e^{jkx}] \ . \qquad 2.25$$

The force that acts on the surface x = 0 of the film is given by

$$f = -\mu \left(\frac{\partial v}{\partial x}\right)_{x=0} = \frac{\mu\, V_o jk}{1 + e^{-2jkd}}\, [1 - e^{-2jkd}]$$

$$= -\mu\, V_o k\, [\tan kd]$$

$$= -\mu\, V_o k_o\, [(1-j)\, \tan\, (\alpha - j\alpha)] \ , \qquad 2.26$$

where $\alpha = k_o d$. The power dissipated is determined by the component of the force in phase with the velocity, that is

$$\mathrm{Re}(f) = -\mu_o V_o k_o\, \mathrm{Re}\, [\tan\, (\alpha - j\alpha) - j\, \tan\, (\alpha - j\alpha)] \ . \qquad 2.27$$

But $$\tan\, (\alpha - \alpha j) = \frac{1}{2}\, \frac{[\sin 2\alpha - j\, \sinh 2\alpha]}{\cosh^2 \alpha - \sin^2 \alpha} \ . \qquad 2.28$$

Hence

$$\text{Re}\{f\} = \frac{1}{2} \frac{-\mu_o V_o k_o [\sin 2\alpha - \sinh 2\alpha]}{\cosh^2\alpha - \sin^2\alpha} \qquad 2.29$$

and the power dissipated per unit surface area is

$$N_o = \frac{1}{2} V_o \, \text{Re}(f) = \frac{\mu_o V_o^2 k_o (\sinh 2\alpha - \sin 2\alpha)}{4 (\cosh^2\alpha - \sin^2\alpha)}. \qquad 2.30$$

If $\alpha \to \infty$, $\cosh\alpha = \sinh \alpha = e^{\alpha}/2$ and

$$N_o = \frac{\mu_o V_o^2 k_o}{2} . \qquad 2.31$$

The maximum is obtained for $\alpha \sim \pi/2 = k_o d$ and its value is nearly equal to

$$1.1 \times \frac{\mu V_o^2 k_o}{2} . \qquad 2.32$$

Figure 12 shows the theoretical curve.

Elementary Theory of the Thickness Vibration of a Quartz Crystal

Most books on acoustics derive the properties of quartz vibrators on the basis of some elementary theory. The transducer is approximated by a short rod free at both ends which is excited by a spatially constant force distribution, the vibration is assumed to be one dimensional and displacements transverse to the axis of the quartz are neglected.

The natural mode solution of a rod free at both ends is

$$\xi_\nu = A_\nu \cos k_\nu x . \qquad 2.33$$

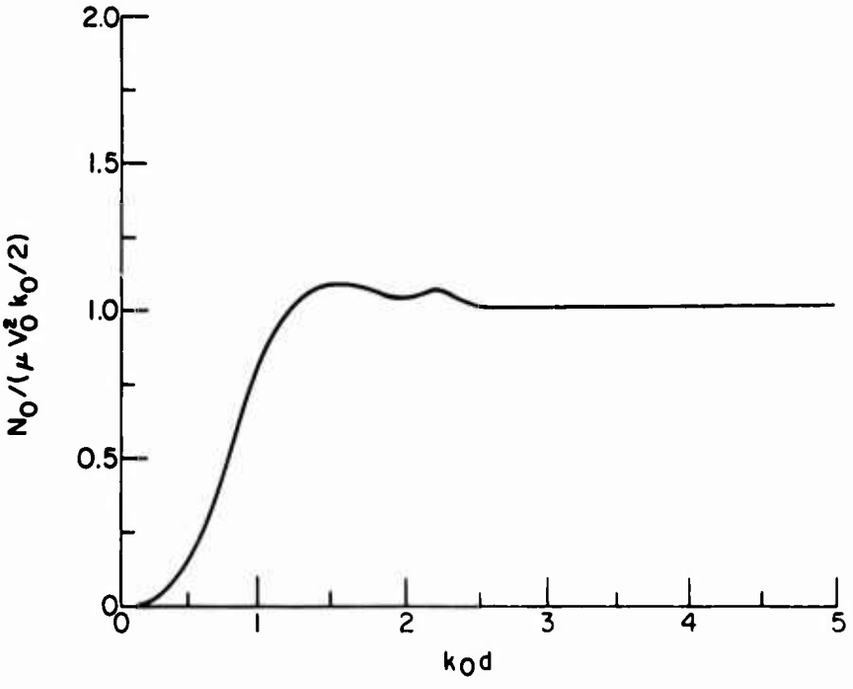

Figure 12. Theoretical Loss Curve for Free Film

The equation of motion is $\frac{\partial^2 \xi}{\partial x^2} = \frac{1}{c^2} \frac{\partial^2 \xi}{\partial t^2}$. For the rod free at both ends with a spatially constant driving force and the observation point at a free end we get the following solution

$$\xi = \sum_{\nu} \xi_{\nu} = \sum_{\nu} [\kappa_{\nu} f_o / M_{\nu} (\omega_{\nu} - \omega^2)]$$

where $$\kappa_{\nu} = \frac{1}{f_o} \int f(x) \, \xi_{\nu}(x) \, dx$$

and $$f_o = \int f(x) \, dx ,$$

$$M_{\nu} = M/2 , \qquad 2.34$$

f(x) is the force distribution function which in this case is a constant. The excitation constant κ_{ν} is

$$\kappa_{\nu} = \frac{2}{f_o} \int_0^{\ell/2} \frac{f_o \, dx}{\ell} \left|\cos (\nu\pi x/\ell)\right| = \frac{2}{\ell} \frac{\sin (\nu\pi x/\ell)}{\nu\pi/\ell} \Bigg|_0^{\ell/2}$$

$$= \frac{2}{\nu\pi} \sin (\nu\pi/2) = \begin{cases} 0 & \nu = 0,2,4,6, \ \ldots \\ \frac{2}{\nu\pi} & \nu = 1,3,5,7, \ \ldots \ . \end{cases} \qquad 2.35$$

The solution for the displacement at the free end thus becomes

$$\xi = \sum_{\nu,\text{odd}} \xi_{\nu} = \sum_{\nu,\text{odd}} \frac{2}{\nu\pi} \frac{f_o}{(M/2)(\omega_{\nu}^2 - \omega^2)}$$

$$= \sum_{\nu,\text{odd}} \frac{4}{\nu\pi M} \frac{f_o}{(\omega_{\nu}^2 - \omega^2)} \ . \qquad 2.36$$

This is the solution of displacement for the free-free rod with no loss and shows that only the odd multiples of the fundamental frequency are excited and the excitation is inversely proportional to the order ν of

the mode. Losses are taken into account by making ω_ν complex $\bar{\omega}_\nu^2 = \omega_\nu^2 (1 + j\eta)$, then we have

$$\xi(A) = \sum_{\nu,\text{odd}} \frac{4}{\pi M} \frac{F_o}{(\bar{\omega}_\nu^2 - \omega^2)} \quad . \tag{2.37}$$

Advanced Theory of the Thickness Vibration of a Quartz Crystal

If we are interested in a more detailed description of the thickness vibration of a disc the elementary theory is inadequate. In fact, the thickness vibration of a quartz crystal or a disc is of a complex nature as shown by observers such as Osterberg,[8] and Dye,[9] and more recently by Shaw,[10] Arnold and Martner,[11] Midlin,[12] and Gazis.[13] Instead of identifying the transducer with a short rod we may identify it with a small plate. Classical plate theory is applied primarily to plates of infinite or semi-infinite extension. Because the transducer is finite, edge effects must be expected. A pure extensional wave in a plate does not satisfy the boundary conditions at the edges; Midlin et al[12] have shown that the edge effects are important for finite plates.

One possibility to deal with the quartz vibrator is to assume it to be equivalent to a cylinder of short length. Pochhammer-Chree[14] derived mode solutions that satisfy the boundary conditions at the free cylindrical surface, but do not contain enough free constants to satisfy end conditions. Therefore, these solutions apply only to the infinite cylinder. McNiven[15] showed that even at low frequencies a

longitudinally propagating wave generates a distortion wave as it is reflected from a traction free end surface of a cylinder. The general solution for a finite cylinder is obtained by adding a finite number of Pochhammer-Chree mode function with real, complex, and imaginary propagation constants.

An approximate solution for the vibration of a finite disc has been published by Aggarwal,[16] and this solution is confirmed by the mode studies of Shaw,[10] and Arnold and Martner.[11] Aggarwal's solution applies to homogeneous, isotropic discs, and represents the dual to the Pochhammer-Chree solution of the cylinder. In the Aggarwal solution the boundary conditions are satisfied on the flat surfaces of the disc but only for a small number of positions on its curved surfaces. By adding a number of modes a reasonably good approximation to the conditions at a cylindrical surface is obtained. As this solution is important in transducer considerations its derivation will be outlined here.

The equation of motion of an isotropic solid is expressed by the vector equation

$$(\lambda + \mu)\ \text{grad div}\ \vec{s} + \mu\ \nabla^2\ \vec{s} = \rho\ \frac{\partial^2 \vec{s}}{\partial t^2}\ .^{17}$$

In cylindrical coordinates the radial and axial components are

$$(\lambda + 2\mu)\left[\frac{\partial^2 U}{\partial r^2} + \frac{1}{r}\frac{\partial U}{\partial r} - \frac{U}{r^2}\right] + \mu\frac{\partial^2 U}{\partial z^2} + (\lambda+2\mu)\frac{\partial^2 W}{\partial r \partial z} = \rho\frac{\partial^2 U}{\partial t^2}$$

$$\mu\left[\frac{\partial^2 W}{\partial r^2} + \frac{1}{r}\frac{\partial W}{\partial r}\right] + (\lambda+2\mu)\frac{\partial^2 W}{\partial z^2} + (\lambda+\mu)\frac{\partial}{\partial z}\left(\frac{\partial U}{\partial r} + \frac{U}{r}\right) = \rho\frac{\partial^2 W}{\partial t^2} \qquad 2.38$$

where λ and μ are Lamé constants, ρ is the density, the radial displacement: $U = u \exp(ipt)$, and the axial displacement: $W = w \exp(ipt)$. The Z axis is chosen to coincide with the disc axis and the origin to lie in the medial plane. It is then shown that the displacement functions U and W may be expressed in terms of potential functions ψ and φ, where

$$U = \left(\frac{\partial \psi}{r \partial z} + \frac{\partial \varphi}{\partial r} \right) \exp(ipt)$$

and

$$W = \left(- \frac{\partial \psi}{r \partial r} + \frac{\partial \varphi}{\partial z} \right) \exp(ipt) \ .$$

Introducing the potential functions ψ and φ , the differential equations become

$$\frac{\partial^2 \psi}{\partial r^2} - \frac{1}{r} \frac{\partial \psi}{\partial r} + \frac{\partial^2 \psi}{\partial z^2} + k^2 \psi = 0$$

and

$$\frac{\partial^2 \varphi}{\partial r^2} + \frac{1}{r} \frac{\partial \varphi}{\partial r} + \frac{\partial^2 \varphi}{\partial z^2} + h^2 \varphi = 0 \qquad 2.39$$

using

$$k^2 = p^2 \rho / \mu \quad \text{and} \quad h^2 = p^2 \rho / (\lambda + 2\mu) \ . \qquad 2.40$$

The stress equations for the normal and tangential components are

$$\sigma_{rr} = \mu \left[(2h^2 - k^2) \varphi + 2 \frac{\partial^2 \varphi}{\partial r^2} + 2 \frac{\partial}{\partial r} \left(\frac{1}{r} \frac{\partial \psi}{\partial z} \right) \right]$$

$$\sigma_{zz} = \mu \left[(2h^2 - k^2) \varphi^2 + 2 \frac{\partial^2 \varphi}{\partial z^2} - 2 \frac{\partial}{\partial z} \left(\frac{1}{r} \frac{\partial \psi}{\partial r} \right) \right]$$

$$\sigma_{rz} = \mu \left[2 \frac{\partial^2 \varphi}{\partial r \partial z} + \frac{2}{r} \frac{\partial^2 \psi}{\partial z^2} + \frac{k^2}{r} \psi \right] . \qquad 2.41$$

The wave solution is obtained by separating the variables, assuming that

$$\psi = r\, f(r)\, F(z) \qquad \text{and} \qquad \varphi = r\, g(r)\, G(z)\ . \tag{2.42}$$

Ruling out singularities at the origin and keeping only the functions that correspond to symmetric vibrations it is shown that the functions ψ and φ can be written

$$\begin{aligned} \psi &= A r\, J_1(\alpha r)\, \sin\left[(k^2 - \alpha^2)^{\frac{1}{2}} z\right] \\ \varphi &= D\ J_0(\beta r)\, \cos\left[(h^2 - \beta^2)^{\frac{1}{2}} z\right] \end{aligned} \tag{2.43}$$

where α and β are arbitrary constants to be determined. Up to this point, the solution follows closely the classical approach. It is in the matching of the boundary conditions that the difference arises. The boundary conditions are:

$$\left.\begin{aligned} \sigma_{zz} &= 0 \\ \sigma_{zr} &= 0 \end{aligned}\right\} \text{at } z = \pm c \text{ and } \left.\begin{aligned} \sigma_{rr} &= 0 \\ \sigma_{rz} &= 0 \end{aligned}\right\} \text{at } r = a \tag{2.44}$$

for a disc of thickness 2c and diameter 2a.

As it is impossible to satisfy all these conditions with a finite number of terms, we look for solutions that satisfy them approximately. Aggarwal choses to satisfy the boundary conditions on the flat surfaces exactly, but only approximately on the cylindrical surface. The conditions that are satisfied rigorously yield

$\sigma_{rz} = 0$ at $z = \pm c$,

$$2Da\,(h^2 - a^2)^{\frac{1}{2}} \sin\,[(h^2 - a^2)^{\frac{1}{2}}\, c] + A\,(2a^2 - k^2) \sin\,[(k^2 - a^2)^{\frac{1}{2}}\, c] = 0$$

and from $\sigma_{zz} = 0$ at $z = \pm c$ we get

$$D(2a^2 - k^2) \cos\,[h^2 - a^2)^{\frac{1}{2}}\, c] - 2\,Aa\,(k^2 - a^2)^{\frac{1}{2}} \cos\,[(k^2 - a^2)^{\frac{1}{2}}\, c] = 0\ .$$

2.45

The last two equations lead to the frequency equation

$$-\frac{\tan\,[(k^2 - a^2)^{\frac{1}{2}}\, c]}{\tan\,[[h^2 - a^2)^{\frac{1}{2}}\, c]} = \frac{4\,a^2\,(h^2 - a^2)^{\frac{1}{2}}\,(k^2 - a^2)^{\frac{1}{2}}}{(k^2 - 2a^2)^2}\ . \qquad 2.46$$

Figure 13 shows a graphical solution of this equation. For a value of $kc < 2.765$ there is only one real value of ac. Aggarwal chose to determine a by using $\sigma_{rr} = 0$ at $Z = \pm c$, $r = a$ leading to the solutions $aa = 2.05$, 5,39, 8.57, ... If several values of a satisfy the above equation (for a given frequency) all these individual solutions are superimposed. In the frequency vicinity of the first fundamental thickness controlled mode, three values are obtained for a so that the complete solution can be built up by adding up three different functions ψ and φ with different multipliers. In a rigorous computation, also the complex roots would have to be taken into account. However, the justification being the agreement with experiment, the three terms that correspond to real or imaginary values of a lead to a fairly good solution.

Furthermore, the Aggarwal theory leads to three modes of different resonant frequencies near the frequency that corresponds to the

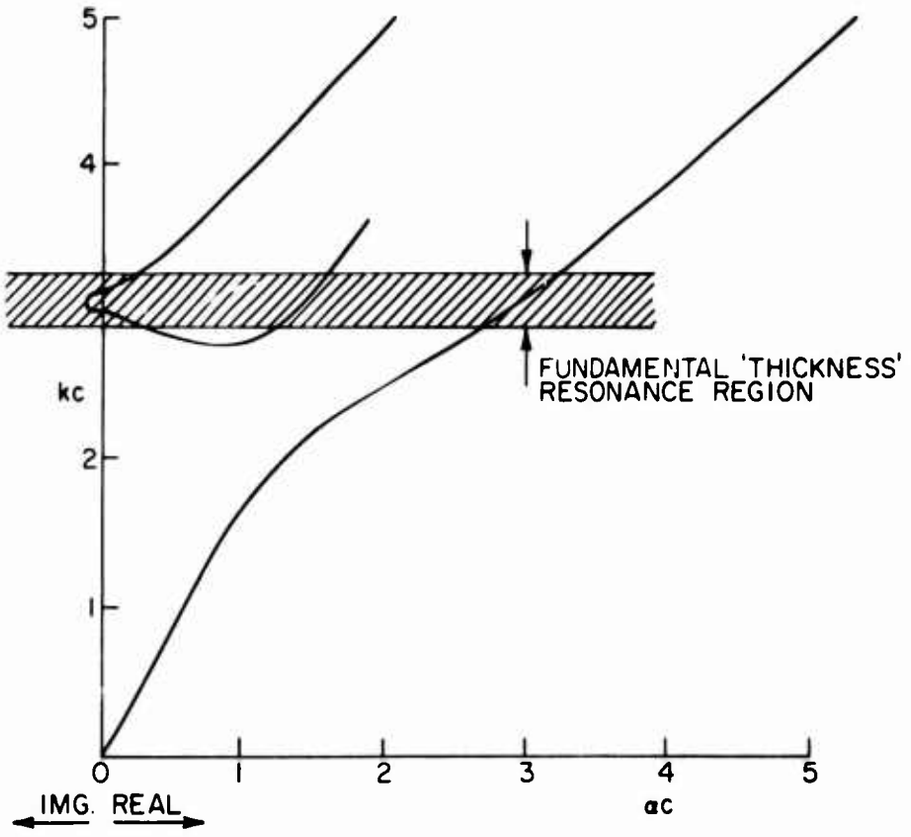

Figure 13. Graphical Solution of Dispersion Relation, Eq. 2.46, for a Disc of Diameter to Thickness Ratio 3.86

fundamental thickness resonance of the elementary theory, and thus explains the multiplicity of resonance peaks that will be discussed in connection with Figure 25.

In the study reported here we were interested in the complex motion of the transducer, i.e., both the axial and radial components, and thus it was necessary to derive also the solutions of the radial displacements. The first six modes have been studied; the three low frequency 'radial' modes and the three modes in the 'thickness' resonance region. The computations for the first three modes are straightforward. With the first three values of α, u and v are given by

$$u = A\, k\, J_1 (\alpha\, a\, \frac{r}{a})\, \frac{(1-y)^{\frac{1}{2}}}{1-2y}\, \cos [(1-y)^{\frac{1}{2}}\, kc]$$

$$w = -A\, k\, J_0 (\alpha\, a\, \frac{r}{a})\, \frac{1}{2y^{\frac{1}{2}}}\, \sin [(1-y)^{\frac{1}{2}}\, kc]$$

where $y = \frac{\alpha^2}{k^2}$. 2.47

For the thickness modes, the three independent boundary conditions were chosen to be

$$\sigma_{rr} = 0 \text{ at } r = a,\ z = \pm c\ ;$$

$$\sigma_{rr} = 0 \text{ at } r = a,\ z = 0\ ;$$

and $$\sigma_{rz} = 0 \text{ at } r = a,\ z = \pm c\ .$$ 2.48

For a given frequency the allowed values of α represent the solutions of the equations:

$$- \mu \left[D_1\sigma_1 + D_2\sigma_2 + D_3\sigma_3\right] = 0 \quad \text{at} \quad r = a,\ z = \pm c$$

$$- \mu \left[D_1\sigma_4 + D_2\sigma_5 + D_3\sigma_6\right] = 0 \quad \text{at} \quad r = a,\ z = 0$$

$$- \mu \left[D_1\sigma_7 + D_2\sigma_8 + D_3\sigma_9\right] = 0 \quad \text{at} \quad r = a,\ z = \pm \frac{c}{2} . \qquad 2.49$$

The resonant frequency may be identified with the frequency for which the determinant of the above equations vanishes. The expressions for the stresses are of the form, e.g.,

$$\sigma_{rr} = \mu \frac{2A}{c^2} \left[\left[(1-y)^{\frac{1}{2}} kc\right] ac \left\{ \frac{\left[\cos (1-y)^{\frac{1}{2}} kc\right]}{\left[\cos (\varepsilon-y)^{\frac{1}{2}} kc\right]} \left[\frac{(2\varepsilon-1)}{(2y-1)} J_0 (ar) \right.\right.\right.$$

$$\left.\left.\left. - \frac{2y}{2y-1} \left(J_0(ar) - \frac{J_1(ar)}{ar} \right) \right] + J_0(ar) - \frac{J_1(ar)}{ar} \right\} \right] . \qquad 2.50$$

With the solution of the resonant frequency, the values of kc and ac were found and substituted into the above simultaneous equations; the ratio of the constants D_1, D_2, D_3 were then computed. The displacement functions $u = u_1 + u_2 + u_3$ and $w = w_1 + w_2 + w_3$ are given by:

$$u_1 = K_{11}\ D_1\ J_1(a_1 r) , \quad w_1 = K_{10}\ D_1\ J_0(a_1 r)$$

$$u_2 = K_{21}\ D_2\ J_1(a_2 r) , \quad w_2 = K_{20}\ D_2\ J_0(a_2 r)$$

$$u_3 = K_{31}\ D_3\ J_1(a_3 r) , \quad w_3 = K_{30}\ D_3\ J_0(a_3 r)$$

and

$$u = D_1\ K_{11} \left\{ J_1(a_1 r) + \frac{D_2}{D_1} \frac{K_{21}}{K_{11}} J_1(a_2 r) + \frac{D_3}{D_1} \frac{K_{31}}{K_{11}} J_1(a_3 r) \right\}$$

$$w = D_1\ K_{10} \left\{ J_0(a_1 r) + \frac{D_2}{D_1} \frac{K_{20}}{K_{10}} J_0(a_2 r) + \frac{D_3}{D_1} \frac{K_{30}}{K_{10}} J_0(a_3 r) \right\} . \qquad 2.51$$

The above equations were evaluated and plotted, using the Penn State University IBM 7074 Computer. The first six mode solutions, normalized to maximum component of displacement ~1, are:

kc	Mode functions
0.897	$w = 0.558\ A\ J_0(2.05\ r/a)$
	$u = -2.04\ A\ J_1(2.05\ r/a)$
2.050	$w = 0.75\ A\ J_0(5.37\ r/a)$
	$u = -0.2355\ A\ J_1(5.39\ r/a)$
2.628	$w = 0.563\ A\ J_0(8.57\ r/a)$
	$u = 0.2515\ A\ J_1(8.57\ r/a)$
2.897	$w = 0.4661\ A\ [J_0(10.42\ r/a) - 0.7818\ J_0(1.10\ r/a) - 0.8500\ J_0(4.86\ r/a)]$
	$u = -0.2447\ A\ [J_1(10.42\ r/a) - 1.122\ J_1(1.10\ r/a) - 3.490\ J_1(4.86\ r/a)]$
3.061	$w = 0.3887\ A\ [J_0(11.36\ r/a) + 0.4038\ J_0(5.61\ r/a) - 0.0996\ I_0(0.46\ r/a)]$
	$u = -0.2161\ A\ [J_1(11.36\ r/a) + 2.296\ J_1(5.61\ r/a) - 0.1744\ I_1\ (0.46\ r/a]$
3.231	$w = 0.2776\ A\ [J_0(12.27\ r/a) - 0.1004\ J_0(6.19\ r/a) + 0.2068\ J_0\ (0.82\ r/a)]$
	$u = -0.1601\ A\ [J_1(12.27\ r/a) - 0.8433\ J_1(6.19\ r/a) - 0.5758\ J_1(0.82\ r/a)]$.

2.52

The basic correctness of these solutions has been confirmed by the experimental data of Shaw[10] and that of Arnold and Martner.[11] The solutions are represented in Figures 14 through 19. The curves show that the axial displacement is not constant but varies greatly over the cross section and that the radial component of motion is significant.

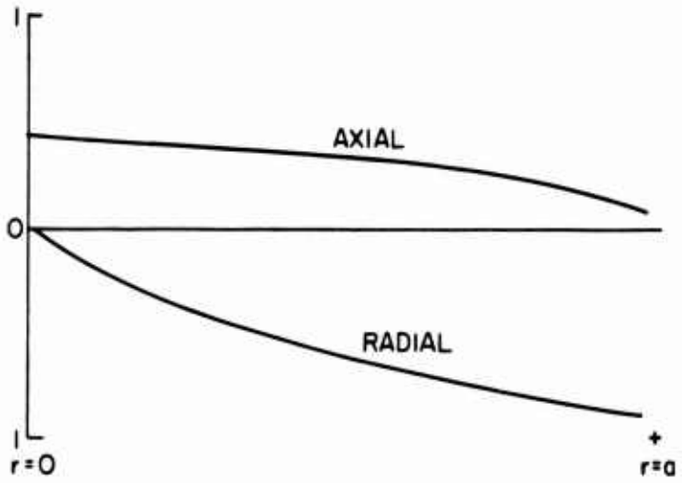

Figure 14. Displacement Amplitudes for Axial and Radial Component of Vibration for kc = 0.897

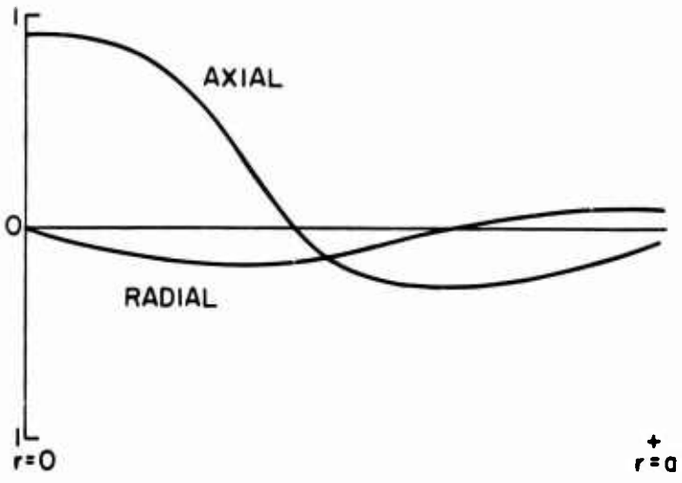

Figure 15. Displacement Amplitudes for Axial and Radial Component of Vibration for kc = 2.050

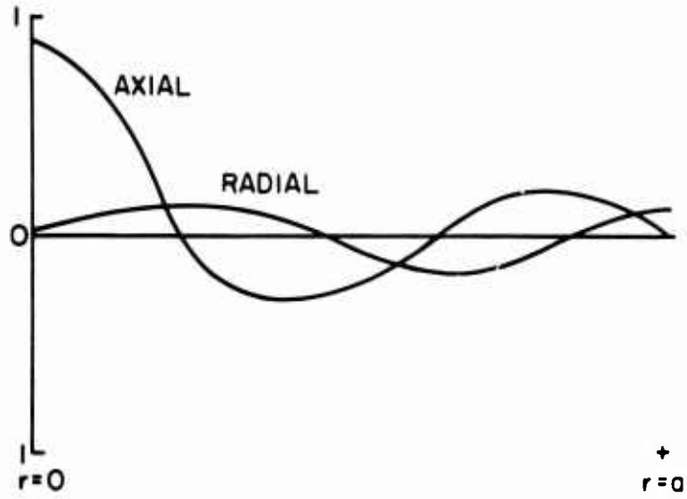

Figure 16. Displacement Amplitudes for Axial and Radial Component of Vibration for kc = 2.628

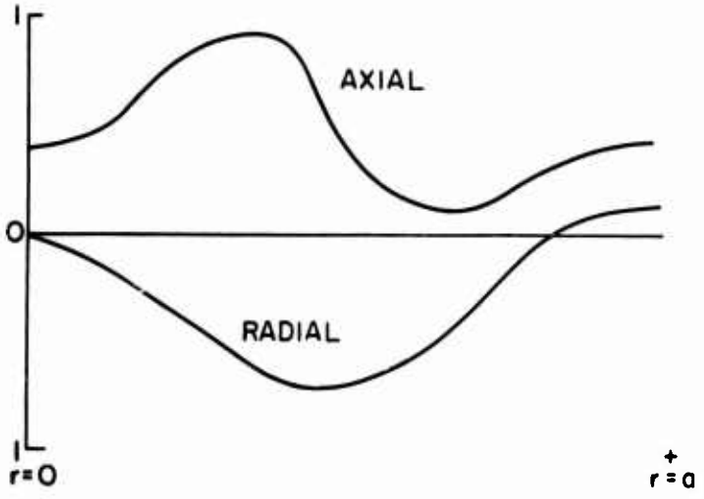

Figure 17. Displacement Amplitudes for Axial and Radial Component of Vibration for kc = 2.897

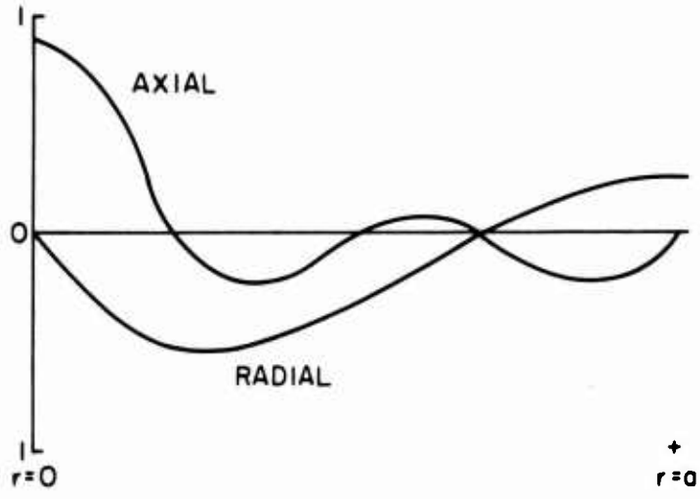

Figure 18. Displacement Amplitudes for Axial and Radial Component of Vibration for kc = 3.061

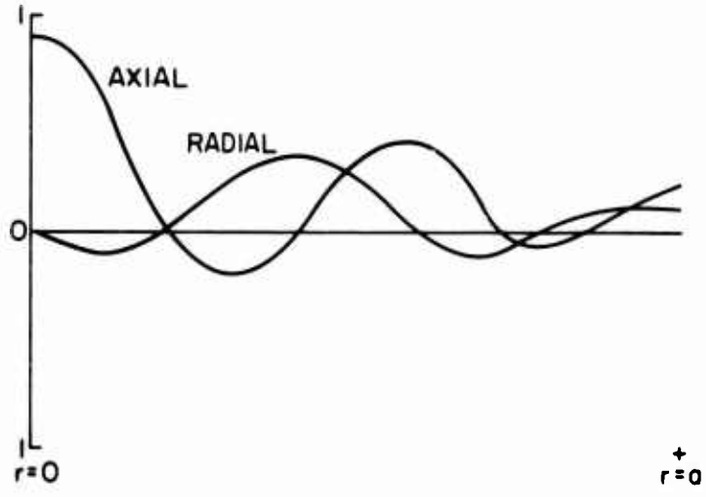

Figure 19. Displacement Amplitudes for Axial and Radial Component of Vibration for kc = 3.231

It is important to note the great change in amplitude distributions and relative amplitude distributions of axial and radial displacement from one mode to the next.

Half Wavelength Load

If a load has a thickness of half a wavelength, or of an integer number of half wavelengths, it vibrates in resonance and represents a purely resistive load. If the load is a $\lambda/2$ quartz crystal, its resonant impedance per unit area is

$$R = \eta_{\omega M} \approx \eta \frac{2\pi c \rho d}{2d} \quad , \tag{2.53}$$

where d is the thickness and c the propagation velocity for longitudinal waves in the material. If the surfaces in contact would introduce no energy loss, $\eta \simeq 10^{-6}$ and

$$R = 10^{-6}\ \rho c \pi = 10^{-6}\ \frac{\rho c \pi}{\rho_o c_o}\ \rho_o c_o = 10^{-6} \left(\frac{1.45 \times 10^{-6}}{42} \right) \pi\ \rho_o c_o \sim \frac{1}{8}\ \rho_o c_o$$

where $\rho c = 1.45 \times 10^6$ g/sec cm^2 for quartz, $\rho_o c_o = 42$ g/sec cm^2 for air . (2.54)

Thus loading a half wavelength quartz crystal by a second similar crystal represents a load that is small. It can be assumed that such a load does not increase significantly the normal stress at the surface of the crystal. However such a load introduces another surface that moves in its plane and generates a shear force that acts on the film and increases the energy losses. These losses decrease the Q of the resultant system by about a factor 1000, and the resultant Q is only

about 1000. The normal loading effect of the $\lambda/2$ quartz then is equivalent to a resistive load of about 1/300 of the ρc of quartz or to about 100 times that of the radiation damping in air. This load resistance is not negligible, but it is still relatively small. Thus, a $\lambda/2$ disc represents essentially a shear load.

Quarter Wavelength Load

If a vibrator is exactly one quarter wavelength thick, it represents an infinite impedance and would act like a rigid clamping for the surface of the film with which it is in contact. But because of the clamping, the crystal would have a different resonant frequency. The fundamental resonant frequency should be smaller by 1/3, the second harmonic by 1/3 higher than the fundamental of the half wave single crystal.

However, because of the compressibility of the film and its relatively high energy dissipation, coupling is far from perfect and the resulting system represents two coupled circuits as shown in Figure 20. The $\lambda/4$-crystal that vibrates below its resonance then represents only a finite impedance that is in parallel with the impedance of the film.

For instance, if a $\lambda/2$ quartz resonating at 500 KHz is coupled by a film of thickness of $1.5\ 10^{-3}$ cm to a $\lambda/4$ crystal, the fundamental resonance of the system should be 333 KHz if the coupling were infinitely strong. The measured value is 410 KHz. However, coupling

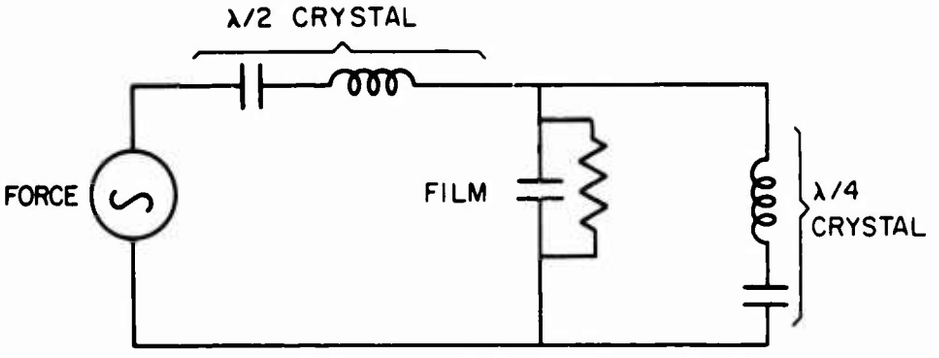

Figure 20. Coupled Circuit for λ/4 Load

is strong enough to ensure that the coupled systems vibrate with the amplitude it would exhibit if coupling were perfect.

Because of the energy dissipation in the film and in the load, a ~ $\lambda/4$ crystal does not represent an infinite but only a finite load of magnitude $\omega M\eta$; an estimate based on the experimental results shows that its loading impedance is much greater than the ρc of the quartz. A $\lambda/4$ disc represents a normal load and a shear load, both of considerable magnitude.

Temperature Activated Hysteresis.

A temperature activated hysteresis was reported by Cook and Breckenridge[18] and further documented and explained by Mason.[19] Some general comments on hysteresis are given by Mason:[20] The losses in solids and even in liquids for very high frequencies appear to be of the hysteresis type; the stress strain curve is not a straight line, but a hysteresis loop in which the strain is a double valued function of the stress. This type of hysteresis can be represented by giving the elastic constants an imaginary component whose magnitude represents the ratio of the breadth of the hysteresis loop to its length. Since the width will be proportional to the length, the total area is proportional to the square of the maximum strain and hence the loss factor generated by it is independent of the amplitude.

The loss factor of a hysteresis type loss is also independent of the frequency in contrast to that resulting from relaxation losses. Relaxation mechanisms introduce loss factors that are proportional

to the frequency below the resonant frequency and inversely proportional to the frequency above the resonant frequency. The high temperature loss in quartz is attributed to the breakaway of dislocations from their impurity pinning points and the increase in the loss factor follows the equation $\delta Q^{-1} = 7\ 10^{-4}\ e^{-5000/kT}$.[19]

The theory of this type of loss has been derived by Mason.[21] The pinning points can be momentarily torn loose from the dislocation and energy can thus be transmitted from one loop to another. All the loops undergo thermal vibration with a velocity that is determined by the equation $1/2(\dot{x}_t)^2 m = kT$ where $m = \pi\rho b^2 \ell$ is the mass of the loop, ρ is the density of the medium, $\dot{x}_t$ the thermal velocity as the loop crosses the equilibrium position, ℓ the length, and b the magnitude of Burgers vector. The particle motion u can add to or conteract the thermal motion if it is in or out of phase; the thermal velocities are as likely to be opposite to the particle velocity as to be in the same direction. An energy $\dot{u}^2 m$ is abstracted from the crystal vibration on the average for each unpinned impurity atom. As long as the loop is pinned on the ends the vibrations are coherent; the excess energy of the loop is returned to the crystal vibration and no loss is experienced. If a pinning point is momentarily lost, energy can feed from one loop to another and the vibrations are no longer coherent. In this case the average amount of energy that is returned to the crystal vibrations is zero and energy of the amount $\dot{u}^2 m$ is consumed by each unpinned impurity atom for each vibration.

The equations of motion of a dislocation in its potential well is

$$\pi b^2 \rho \ell \frac{d^2 d}{dt^2} + 2\pi T_{13} \ell d = 0 \qquad 2.55$$

where $F = 2\pi T_{13} \ell d$ is the restoring force and m is the mass if the dislocation as given above.[22] For simple harmonic motion the frequency is $\nu = \frac{1}{2\pi b}\left(\frac{2T_{13}}{\rho}\right)^{\frac{1}{2}}$ and to this order of accuracy the frequency is independent of the loop length. To calculate the acoustic loss because of this source let us consider the distribution of shear strain shown in Figure 21.

The particle displacement is zero at x = 0 and u at $x = \ell_t$ for t = 0. After an interval of time dt the same shape will be present at a distance V_s dt where V_s is the shear velocity. The velocity $\dot{u}$ that a given particle will have is considered constant over the time of the wave (small loss theory assumption). The loss from one unpinned vibration per interval of time dt is the loss per dislocation vibration multiplied by the number of vibrations or frequency times the time,

$$\dot{u}^2 m\nu \, dt = \dot{u}^2 \, (\pi \rho b^2 \ell) \frac{1}{2\pi b}\left(\frac{2T_{13}}{\rho}\right)^{\frac{1}{2}} dt =$$

$$\dot{u}^2 \, b \ell \left(\frac{T_{13} \rho}{2}\right)^{\frac{1}{2}} dt \, . \qquad 2.56$$

From Boltzmann's principle the number of unpinned atoms per cm^3 will be $N_o \, e^{-U/kT}$. The volume of the disturbance is V_s dt per unit cross section. Hence the total loss per interval of time dt is

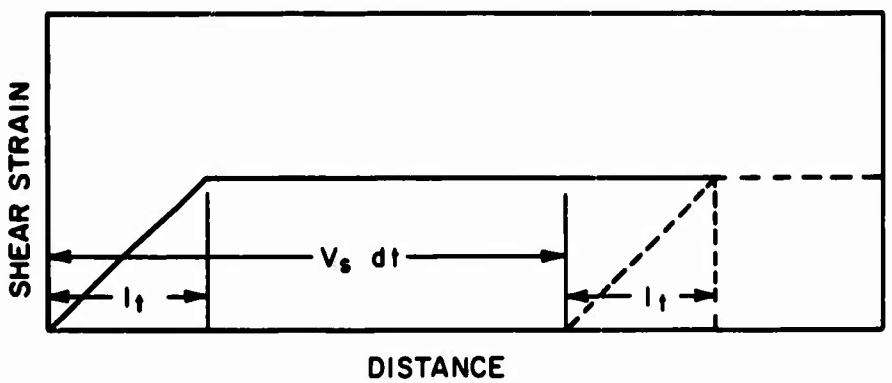

Figure 21. Model of Shear Waved used in Dislocation Energy Loss Theory

$$\left[\dot{u}^2 \, b \, (\mu\rho)^{\frac{1}{2}} \left(\frac{T_{13}}{2\mu} \right)^{\frac{1}{2}} V_s \, N_o \ell \, e^{-U/kT} \right] (dt)^2 \, . \qquad 2.57$$

Total input energy for the wave in the interval of time dt is

$$W_o = \dot{u}^2 \, \rho c \, dt = \dot{u}^2 (\mu\rho)^{\frac{1}{2}} \, dt \text{ (this equation defines } \mu). \qquad 2.58$$

The energy transmission for the first time interval dt takes the form

$$W = W_o \, \{1 - [2 \, T_{13}/\mu) \, b \, V_s \, N_o \ell \, e^{-U/kT}]/2\} \, dt \, . \qquad 2.59$$

This is the first term of the expansion of the equation

$$W = W_o \exp \left\{ \frac{\left(\frac{2 \, T_{13}}{\mu} \right)^{\frac{1}{2}} b \, V_s \, N_o \ell \, e^{-U/kT}}{2} \, t \right\}$$

$$= W_o \exp (-\delta t) \text{ where } \delta \text{ is the decrement} \, . \qquad 2.60$$

The decrement $\delta = \pi \, \eta$, thus we have finally

$$\eta = \frac{1}{Q} = \left[\left(T_{13}/\mu \right)^{\frac{1}{2}} b \, V_s \, (N_o \ell) \, e^{-U/kT} \right] / \sqrt{2} \, \pi \, . \qquad 2.61$$

Mason[19] gives the following data for quartz:

$$(T_{13}/\mu) = 8.8 \, 10^{-8}, \; b = 4.5 \, 10^{-8}, \; N_o \ell \sim 600 \, . \qquad 2.62$$

Impurity binding energy is 2 to 5 kilocalories per mole. Thus

$$\eta \sim \frac{3 \, 10^{-4} \; 4.5 \, 10^{-8} \; 3.4 \, 10^{5} \; 600}{1.4 \; 3.14} \, e^{-U/kT}$$

$$\eta \sim 6.3 \, 10^{-4} \, e^{-U/kT} \text{ for bulk quartz.} \qquad 2.63$$

III. EXPERIMENTAL RESULTS

Free Fall Measurements of a Quartz Crystal in Vacuum

To determine the Q of the quartz crystals used in the experiments and to evaluate the effect of the supports on the Q of a quartz crystal, a quartz crystal was dropped in vacuum between two electrodes. A time exposure photograph of the decay of the vibration of a free falling quartz crystal vibrating at 400 KHz is shown in Figure 22. Evaluation of this curve leads to a loss factor of 3.0×10^{-6}. The quartz crystals that were available at the time of the measurement had defects and small parts chipped off. This measurement would have to be repeated with undamaged polished crystals if a more accurate determination of intrinsic quartz loss in a dilatational mode were desired. The method, however, is one of the most accurate measuring techniques possible to obtain the damping of a quartz crystal. Comparison of the free fall results with those obtained for the crystal in its mounts showed that the support loss was at most of the same order of magnitude as that of the quartz transducer in vacuum.

Velocity Distribution and Mode Pattern of a Quartz Crystal Vibrating in a Thickness Mode

For an understanding of the energy dissipation of bonded surfaces and surfaces in optical contact it is necessary to obtain a knowledge of the longitudinal and transverse velocity distribution of a quartz crystal in a thickness mode. It has already been shown in the theory

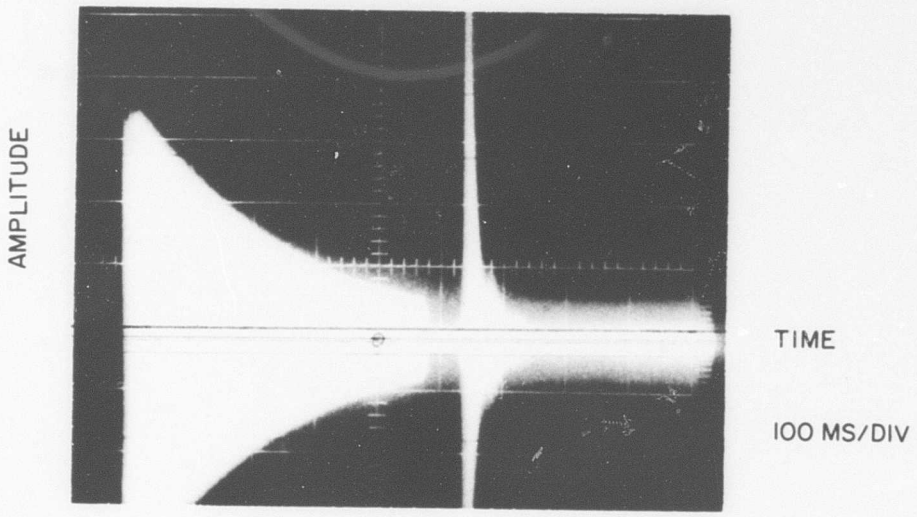

Figure 22. Time Exposure Photograph of the Decay of the Vibration of a 400 KHz Quartz Crystal in Free Fall

section that the motion of a quartz crystal that vibrates in a thickness mode is very complex. The quality factor Q of quartz is a complex function of the frequency and the temperature. Figure 23 shows the Q of various crystals as a function of frequency at room temperature. The situation can be expected to be considerably more complex when the temperature is also varied, and when the system is made up of two quartz crystals in optical contact with each other.

When the crystals were excited in overtones most of the measurements could be made in air. The limit of their Q (without taking into account the improvement because of the shielding effect of the rigid electrode) because of air damping then would be 28×10^3 n, where n is the number of the harmonic that has been excited. The Q values actually measured were much lower and most of the measurements shown in Figure 23 could be made in air. The curves show that in general the Q increases with the thickness of the crystal. The 400 KHz crystal, for instance, when excited at a frequency of 70 MHz has a Q that is about 30 times as great as that of a 10 MHz crystal excited in its seventh overtone. This shows, as is already known, that most of the energy losses in a quartz crystal are generated at or near its surface. This is the reason that surface treatment, etching, and grinding are important if high Q, high frequency vibrators are desired. Similar results had already been obtained by B. Droney,[23] who found that for aluminum and other substances (if the effect of scattering is eliminated) at frequencies about 20 MHz most of the energy losses occur at or near the surface of the test piece.

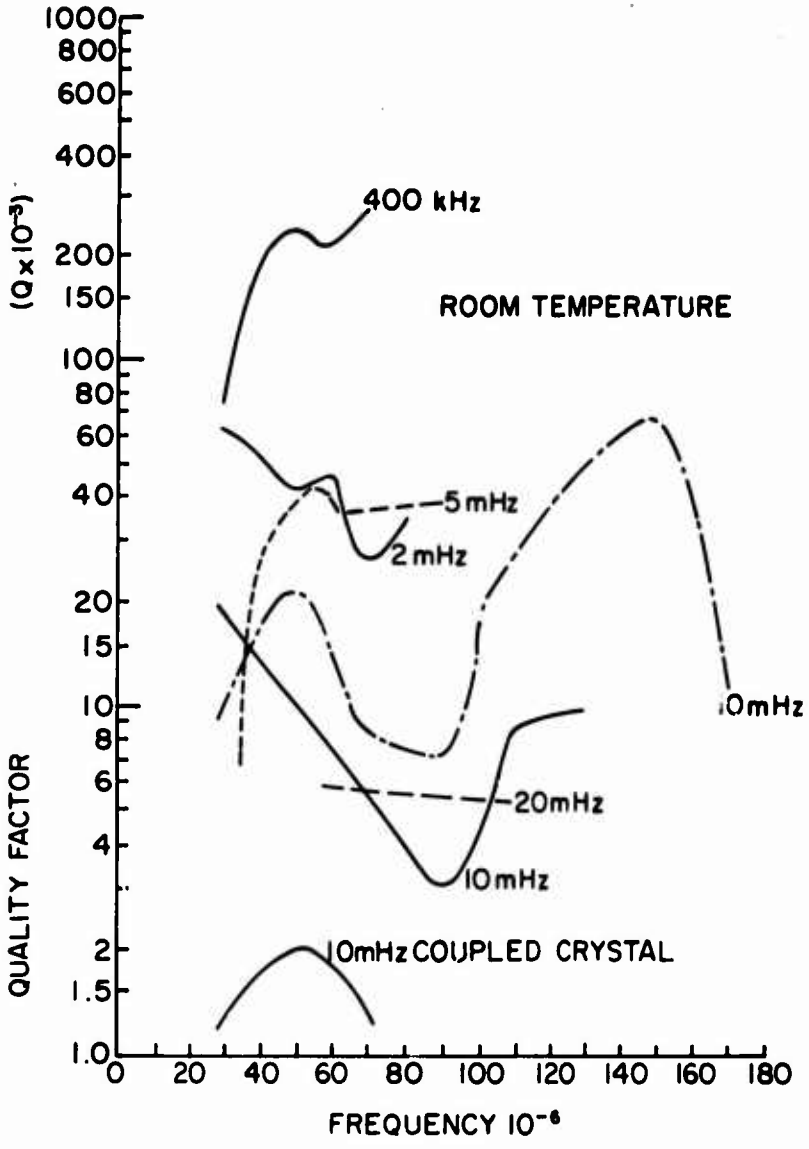

Figure 23. The Quality Factor of Various Quartz Crystals Plotted as a Function of Frequency

To see the effect of the anisotropy of quartz on the vibration pattern, the transverse amplitude at the edge of a longitudinally vibrating free crystal was recorded with a small vibration pickup. Figure 24 shows some measurements of the edge vibration of a free crystal in a thickness mode as measured with a small crystal probe. The angles are measured from an arbitrary point and are not referred to the axes of the crystal. The curve shows a strong sensitivity of the edge vibration on the orientation; this fact indicates that the anisotropy of quartz has an important effect on the vibration, and that more exact theories would have to take account of it.

To gain insight into the mode structure of quartz the electric field along the Y direction can be monitored as the crystal is driven by an electric field in the direction of the X axis. For quartz, an electric field in the X direction excites the stresses X_x, Y_y, and Y_z as shown in Appendix A. The Y axis electric field is generated by the stresses Z_x and Y_y. This field does not measure the Y axis mechanical response of the crystal, but measures the magnitude of the above shear deformation that accompany the complex vibration of the crystal; there is no direct coupling between these two sets of stresses. To find the Y axis, the electrodes (Figure 7 inset) were rotated until the voltage was a maximum; for the Z axis this voltage was a minimum. Figure 25 shows the frequency response of the X and Y electric field when the crystal is excited at and near its fundamental thickness frequency. Instead of exhibiting a single thickness resonance as the elementary theory predicts, the crystal vibrator exhibits a whole series

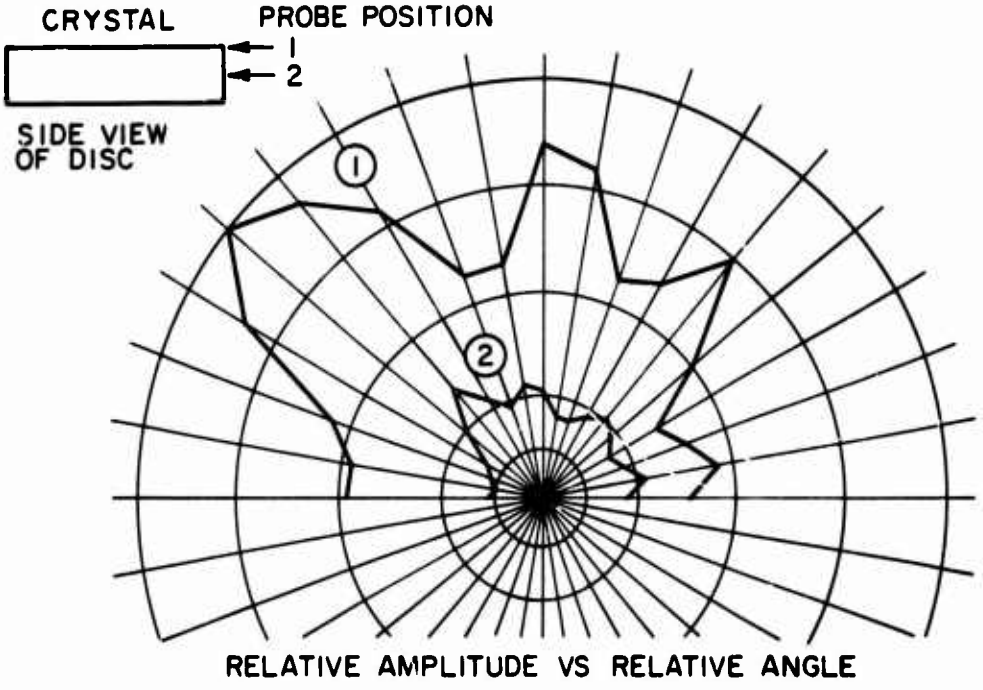

Figure 24. Response of the Edge Vibration of a Free Crystal in a Thickness Mode as Measured with a Small Crystal Probe

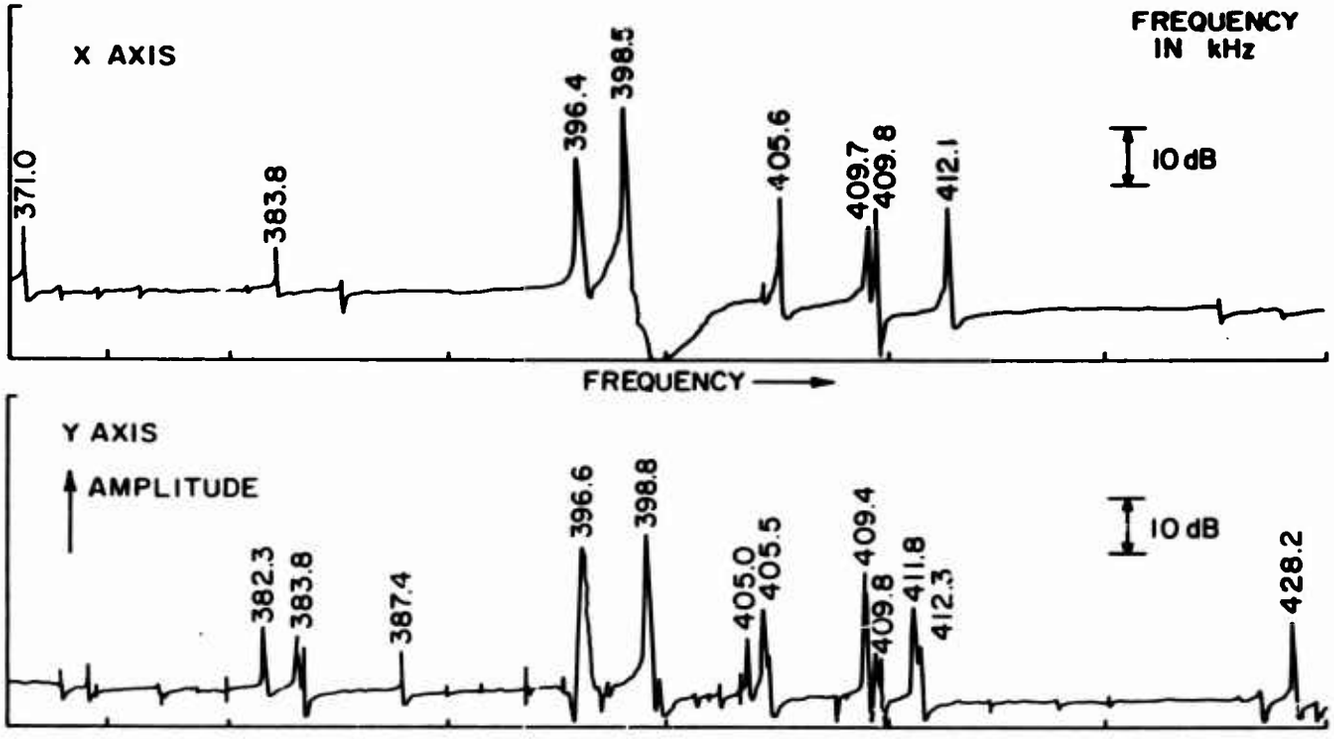

Figure 25. Frequency Response of the Electric Field Along the X and Y Axes When an X-cut Quartz Crystal is Excited Near its Fundamental Thickness Frequency

of resonances in a narrow frequency range near the frequency which the elementary theory would specify as the fundamental thickness resonance. It is not possible to decide which of the many neighbored peaks is the true thickness resonance, because at all of these resonances longitudinal and transverse displacement are of the same order of magnitude. The amplitude distribution differs considerably if the frequency is changed from that of one mode to that of the next one. The amplitude to which modes of similar frequency are excited by the electrostatic field is almost the same if the crystal is not loaded. The amplitudes of the field in the Y direction illustrates the intensities of the shear deformations that accompany each longitudinal mode.

Photographs of the decay of the electric field along the X and Y axes, Figure 26, show that the decaying vibration of a quartz crystal that was excited in thickness resonance was made up of several modes which appear as the peaks in the frequency response curves of Figure 25. The crystal has no memory built in, and at the instant of disconnecting the driving voltage only reacts to its instantaneous amplitude and velocity. Its decay is exclusively determined by these two quantities regardless of the frequency at which it was excited. Because the modes all have a strong longitudinal component they appear with about the same amplitude in decaying vibration. However, when the quartz crystal was loaded the elastically coupled shear modes seemed to be suppressed; this followed from comparison of the X and Y axis electric field response of a free and loaded crystal that is

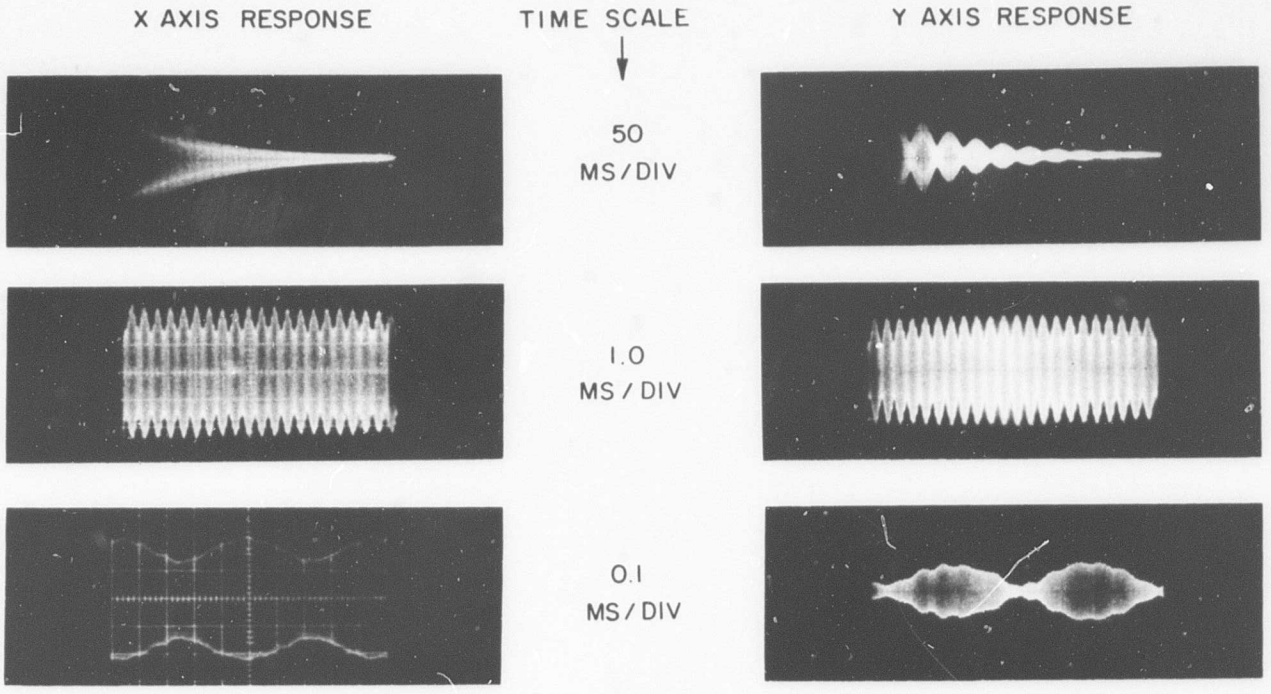

Figure 26. Photographs of the Electric Field Along the X and Y Axes for an X-cut Quartz Crystal Excited at its Fundamental Thickness Frequency

shown in Figure 27. At first sight, this would indicate a nonlinear mode structure, or a dependency of the relative shear and distortion on the boundary conditions. However, loading the crystal cannot have a great effect on the internal amplitude distribution. It will still take many hundred refelections of the various wave trains until their decay becomes noticeable. Because coupling between shear and dilatation is always strong in solids it is unlikely that the slight absorption at the boundary will change the equilibrium between shear and dilatation to any great extent. A second explanation seems to be more likely: If a crystal is excited in a mode for which the transverse displacements are significant, loading it with a film will reduce its amplitude considerably. The observer will believe that the mass load effects changed the resonant frequency, and will retune the crystal to the resonant frequency of an adjacent mode whose transverse component is smaller and the vibration amplitude will be great again. This did not correct for the load but tuned to a different mode of vibration. If, on the other hand, the initial mode was one of small transverse motion the film will have little effect on the vibration amplitude.

Liquid Drops

When a drop of fluid was placed on the flat surface of a disc shaped quartz crystal vibrating in a thickness mode, the decay time of the crystal decreased considerably. The attenuating effect of the drop was much larger than would be expected from the bulk loss factor of the liquid. The interaction of the liquid drop and the crystal

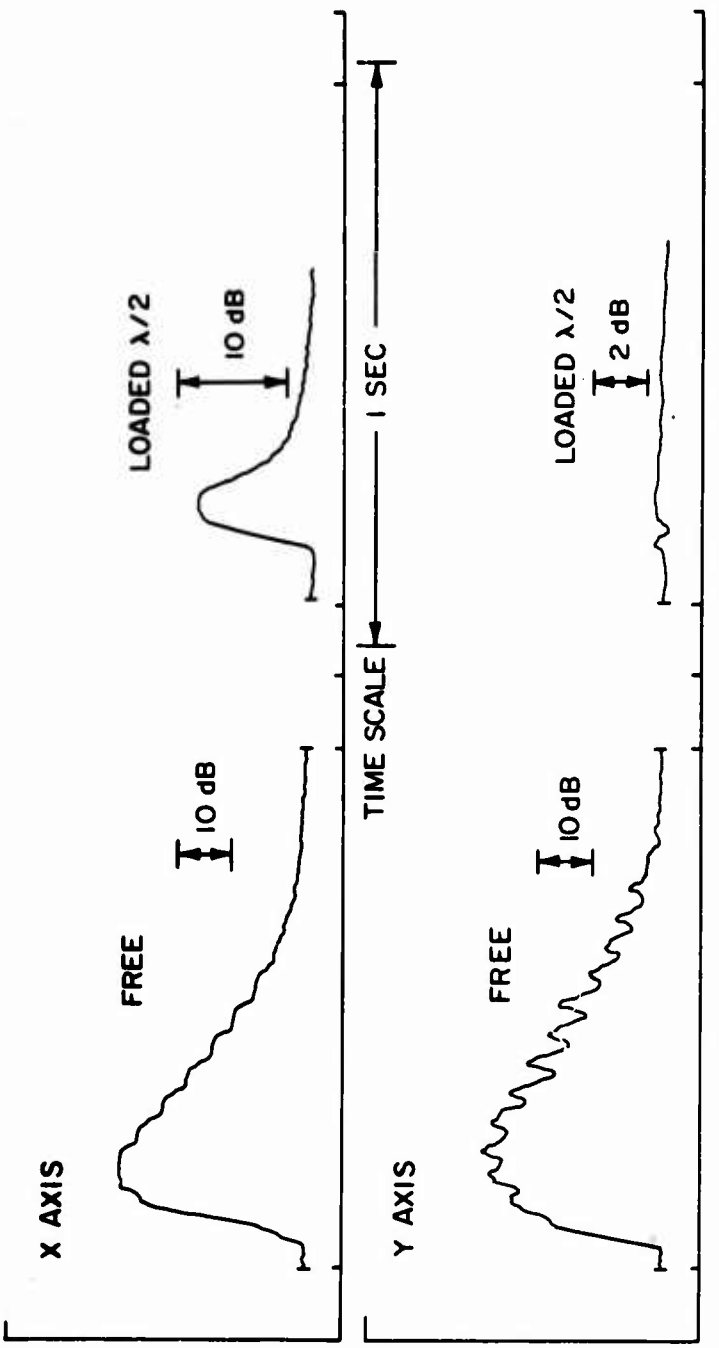

Figure 27. Envelope of the Electric Field Along the X and Y Axes for a Loaded and an Unloaded X-cut Quartz Crystal Excited at its Fundamental Thickness Frequency

produced a complicated response that depended on the drop volume, configuration, and surface contact area as well as the material in the drop. Surface tension phenomena and surface viscosity have been shown to exhibit a strong relaxation effect at higher frequencies which would increase attenuation. That the surface tension was not the cause of the increased damping in the fluids investigated during this study was shown by increasing the volume of a drop while keeping the contact area with the crystal the same. The decay time was found to be unaffected by this change. Figure 28a illustrates the variability of liquid drop measurements. The damping is seen to scatter by as much as a factor of 3 between different series of measurements. However, the results obtained for drops from various liquids differ by far more. Figure 28b illustrates results for different liquids. Detailed investigations showed that the area of contact between the liquid and crystal was the major variable associated with the added loss to the system.

The high absorption of water drops and its dependence on the contact area and not on the surface area of the drop was surprising. The results obtained during later tests showed that the vibrating quartz crystal excites shear waves at the contact surface. These waves decay over a distance that is an order of magnitude smaller than the thickness of the drop. Such shear waves cannot be excited at the free surface of the drop. This result seems to bear out Klemms prediction that the surface layer of free water would have a viscosity considerably greater (according to Klemm greater by a factor 10^4) than the regular viscosity of water.

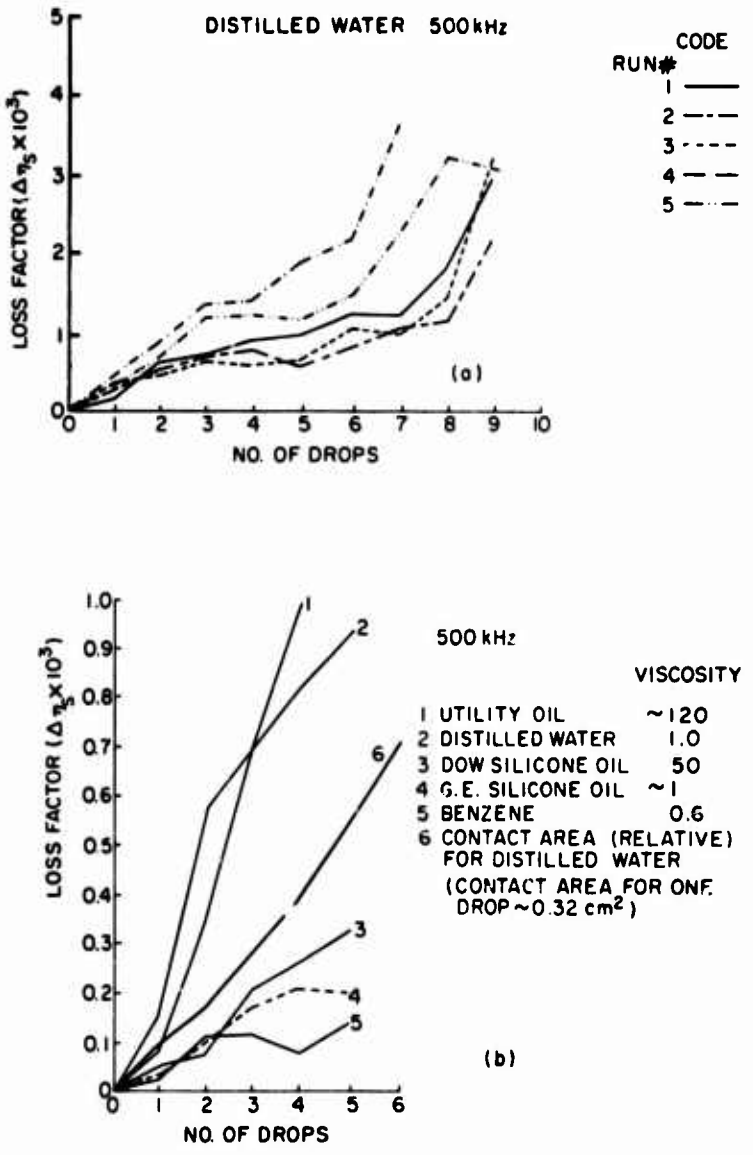

Figure 28. Attenuation Measurements of Small Volumes of Various Liquids Placed on the Surface of a Quartz Vibrator (a) Change in the System Loss Factor Plotted as a Function of the Number of Drops (b) Change in the System Loss Factor for Various Liquids Plotted as a Function of the Number of Drops

Free Films

Free films were generated by evaporating the film material onto a free surface of a single crystal. Figure 29 shows the film loss factor plotted vs film thickness of a free glycerin film and a free petroleum jelly film plotted as a function of film thickness. When these curves were measured the energy losses were assumed to be due to a relaxation phenomena. However, as the later results showed, the loss was due to shear waves set up between the two surfaces of the film. Energy losses due to the shear waves would be proportional to the surface area of the film. The bell shape of the curves is simply a consequence of the method of plotting the data and not of the physical background of the phenomenon. The ordinate represents the film loss factor (see Eq. 2.6) which refers to the energy loss of the volume of the film. Equation 2.7 shows that this volume loss factor is approximately equal to the increase of the loss factor of the system divided by the film thickness d.

The curves shown in Figure 30 are more proper. They represent the film losses per unit contact area. The losses caused by the film are negligible when the film is thin. They increase to a maximum when the film attains the thickness of a quarter of the shear wavelength, and then change little as the film thickness is increased further (see Theory Section). However, the plot of the data in Figure 29 is valuable from the point of experimental evaluation. The peak is sharp regardless of the viscosity; and the maximum which occurs at a wave number that is given by

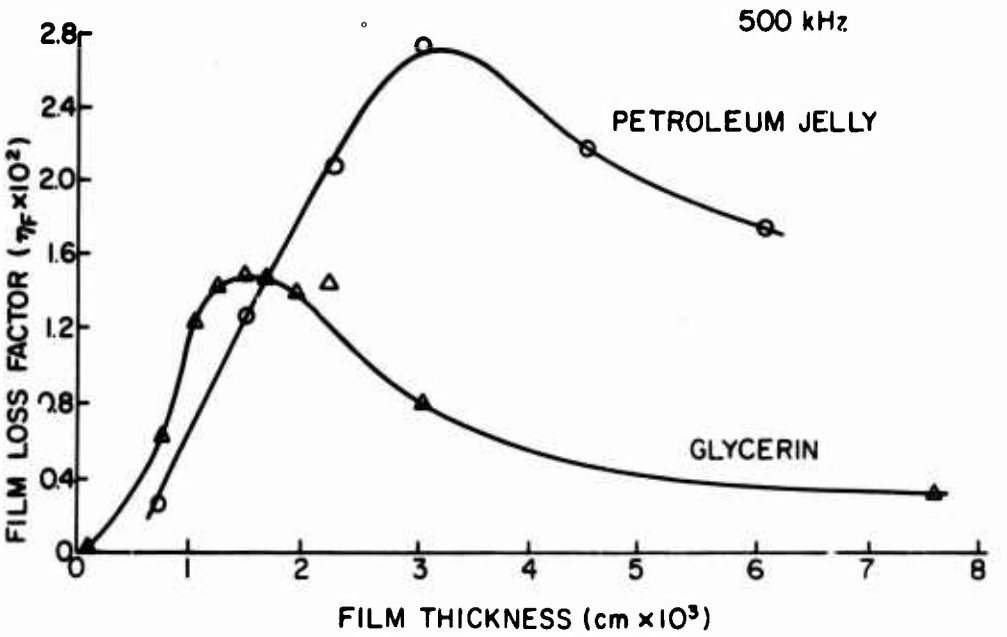

Figure 29. Film Loss Factor of a Free Glycerin Film and a Free Petroleum Jelly Film Plotted as a Function of the Film Thickness

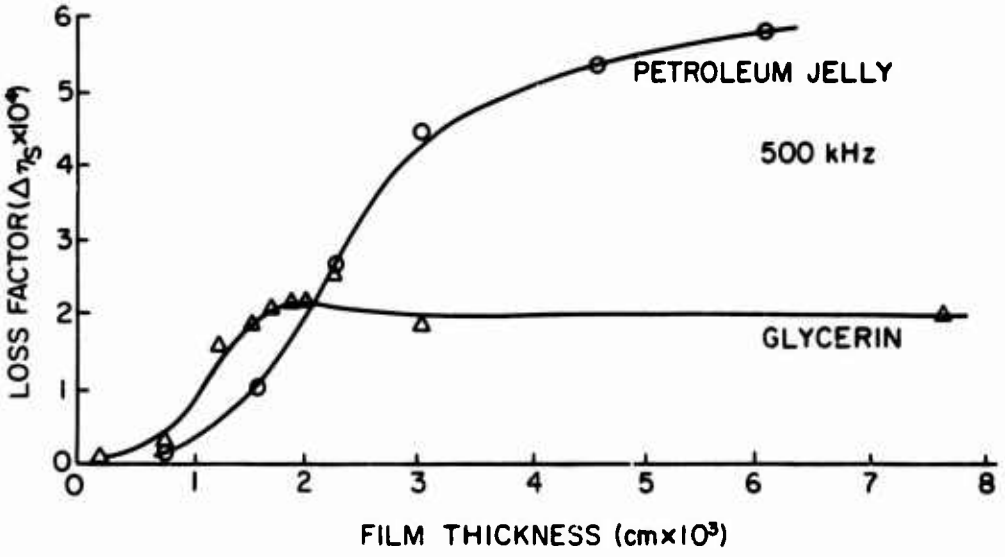

Figure 30. Change in the System Loss Factor for a Free Film of Glycerin and a Free Film of Petroleum Jelly Plotted as a Function of the Film Thickness

$$k_o d \approx \sqrt{\frac{\omega\rho}{2\mu}}\, d \approx 0.75$$

the thickness for which the peak occurs, measures the viscosity of the fluid. Thus, such measurements can be used to determine the viscosity of fluids in a wide frequency range. Data on the change of viscosity with frequency are not available. Viscosity measurements would best be performed with crystals vibrating in a shear mode. The height of the peak would determine the viscosity, so that a knowledge of the film thickness would be unnecessary.

The data for glycerin lead to a viscosity of 650 centistokes at 500 KHz. The value listed in the AIP Handbook is about 1200 centistokes for pure glycerin at room temperature. However, glycerin is hygroscopic and its viscosity is a function of the water content. The viscosity of the glycerin sample was measured with a Brookfield viscometer and found to be 550 centistokes at 20°C. This indicates about a 5% water content. The measurements on glycerin were taken in a vacuum so that the water content was probably less than 5%, and the measured value of viscosity should have been between 500 and 1200 centistokes. The measured value of 650 centistokes would indicate a water content of about 4%. The height of the peak indicates that about 8/10 of the vibrational energy of the longitudinally excited crystals was shear energy (see Theory Section). The solid vaseline has a shear rigidity and is viscous in addition. The measurements lead to a viscosity for vaseline at 70°F of about 3050 centistokes.

The free film measurements shown in Figure 31 for sugar solutions show an increase of the loss factor with viscosity that is somewhat less than the square root relationship predicted by Eq. 2.15. Such solutions are likely to exhibit non-Newtonian behavior at high frequencies, the (dynamic) viscosity being smaller than the (static) viscosity as the sugar concentration becomes high.

Loaded Films (between two surfaces)

The film was generated between the contact surfaces of two crystals or a crystal and a metal disc; the second crystal or metal disc having a thickness of either $\lambda/4$ or $\lambda/2$. Figure 32 shows the loss factor of various liquids as a function of the thickness of the liquid between two $\lambda/2$ crystals as the distance between the crystals was decreased. For these particular liquids the loss factor of the system decreased slightly as the sample thickness was increased.

A free film of water increased the loss factor of a single quartz crystal to 2×10^{-5} (see Figure 31). Loading the film even with such a light load as a $\lambda/2$ crystal increased the damping of a water film by a factor of about 50. For a frequency of 500 KHz, k_o is about 2×10^4 for water and for a film that is 2.5×10^{-4} cm thick, such a film already acts as if it were infinitely thick for shear waves. If viscous forces were the only forces present, a further increase in the film thickness should not affect the damping. But the curves show that for water, benzene, and various silicone oils losses decrease by a factor of two to four as the film thickness is increased from 2.5×10^{-3} to 2.5×10^{-2} cm.

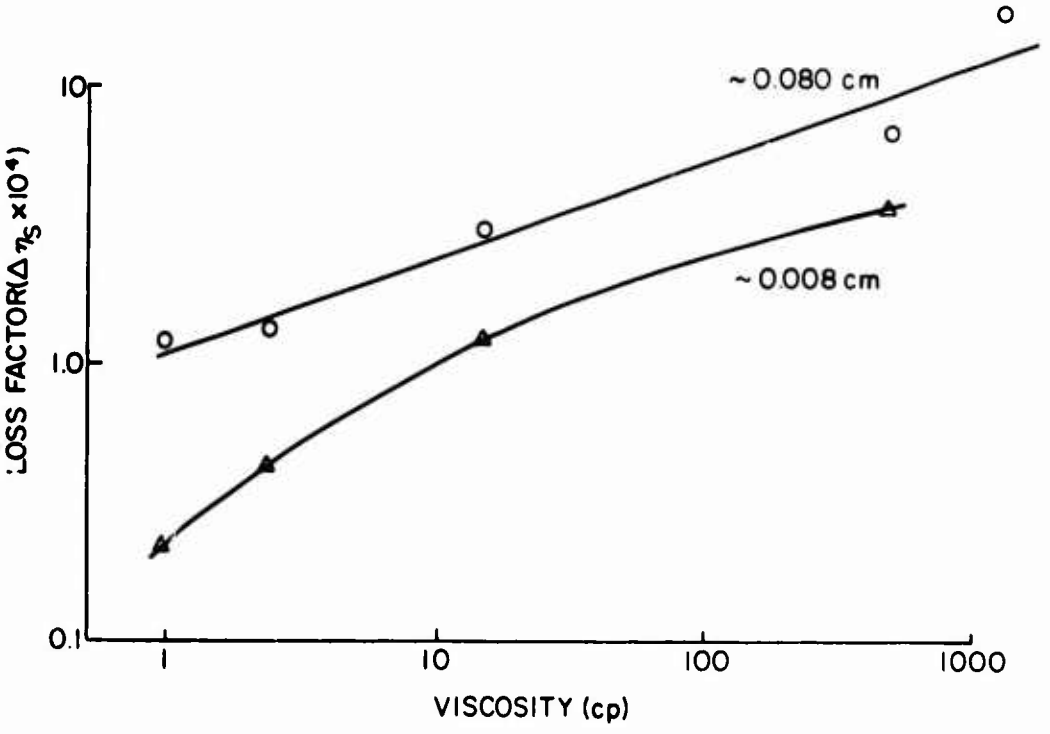

Figure 31. Change in the System Loss Factor for Free Films of a Sugar Solution Plotted as a Function of the Viscosity of the Solution

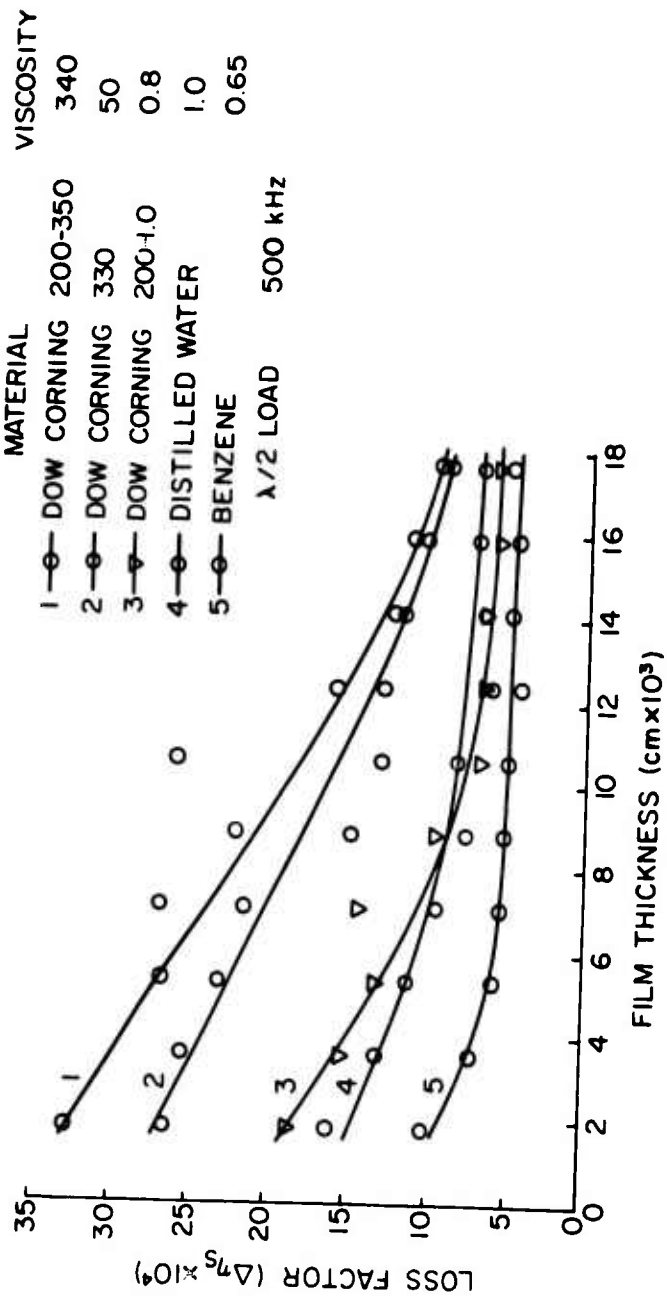

Figure 32. Change in the System Loss Factor for Various Liquids Between Two 500 KHz Crystals as the Distance Between the Crystals was Changed

Figure 33 shows the loss of a glycerin film under various loading conditions such as a free film, a film loaded with a half a wavelength thickness disc and a film loaded with a quarter wavelength thickness disc. The quarter wavelength loaded system resonated at 410 KHz. The surfaces in contact with each other were flat to the order of a few light fringes and when coupled to the crystal the loaded composite system behaved like a simple lumped system.

Glycerin is a highly viscous fluid. When a thin film is loaded with a $\lambda/2$ quartz, the difference of the transverse velocities of two contact surfaces is doubled. The system loss factor should therefore be increased by a factor of 2. The measurements indicate that the loss factor of glycerin is increased by this loading by a factor of about eight. When the film is loaded with a $\lambda/4$ disc, the losses would be expected to increase further. The measurements indicate an increase of about 40 compared to the unloaded films. For glycerin the loss factor for a $\lambda/2$ load increased with the film thickness, in contrast to the results obtained for other fluids as shown in Figure 32.

Glycerin has a high bulk viscosity that increases the damping by a factor of about two at 26°C over that expected for the shear viscosity.[24] Using Litovitz' value of $\alpha = 18.4\ (cm^{-1})$, $\alpha = \omega\eta_f/2C$, and $\Delta\eta_s = \eta_f\, M_f/M_t$ we get $\Delta\eta_s = 1.45\ 10^{-3}$ for a film thickness of 1.5×10^{-3} cm. The change in the system loss factor is proportional to the volume of the film for a volume type loss (see Eq. 2.7), thus the change in the system loss factor will increase as the film

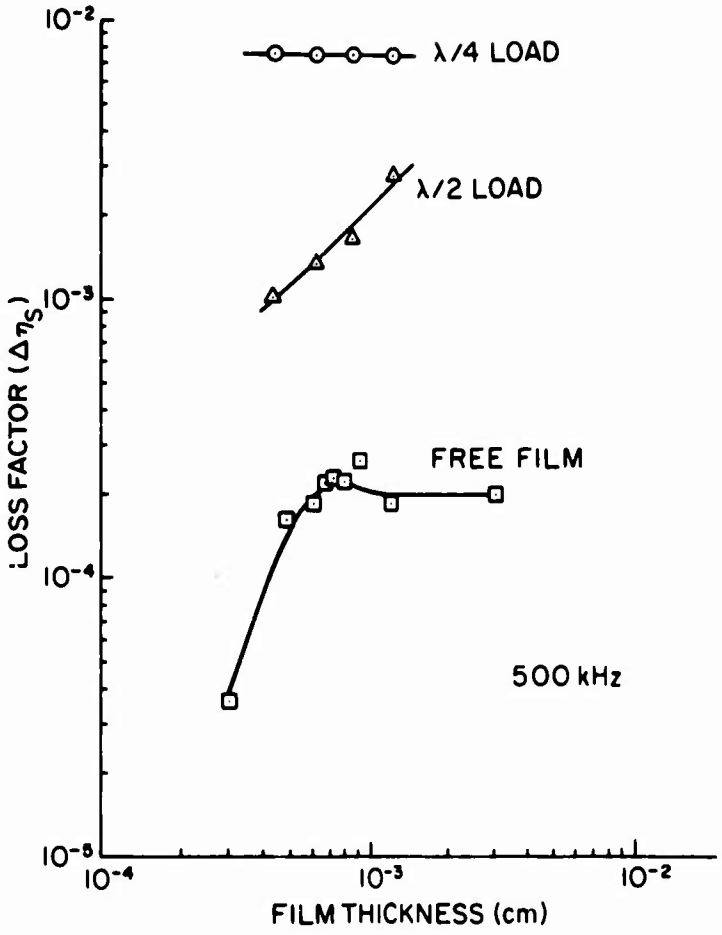

Figure 33. Change in the System Loss Factor for a Glycerin Film with Various Mechanical Loads Plotted as a Function of the Film Thickness

thickness increases. However, for most liquids the increase in loss because of sandwiching a film is even greater than would be expected on the basis of the bulk viscosity.

There seems to be a second possibility to generate losses. The normal components of the surface stress are coupled because of the dilatational pressure field in the film. Surface dislocations give rise to microscopic scattering centers that generate near fields. These near fields interact, the interaction increasing for decreasing film thickness.

Figure 34 shows the result of altering an aqueous solution of sugar (sucrose) to obtain a range of viscosities. The change in surface tension and density is also given. These readings were taken for a fixed film thickness of 1.5×10^{-3} cm with a $\lambda/2$ and $\lambda/4$ load as the percentage by weight of sugar was changed. The losses observed here were similar to those of a sandwiched glycerin film.

A $\lambda/2$ load is in resonance and represents a small normal loading (see Theory section). For a thickess of $\lambda/2$, the loading crystal is equivalent to a resistance of

$$\eta \omega M \approx \eta 2\pi \cdot \frac{3 \cdot 10^5}{d} \cdot d \rho \approx 2 \times 10^6 \eta \rho \approx 400 \rho \text{ grams/sec cm}^2 ,$$

where $\eta = 2 \times 10^{-4}$ has been assumed as the loss factor of a quartz crystal with a thick unloaded film; then, loading the film is equivalent to introducing a resistive load of about 15 times the wave impedance of air. Loading even by a $\lambda/2$ crystal will increase the film losses

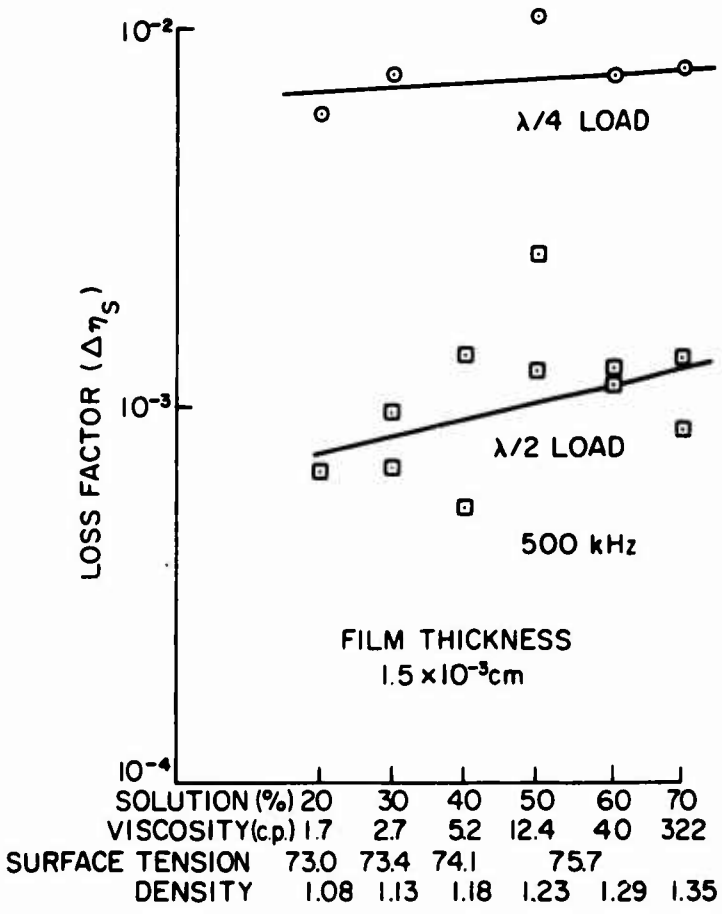

Figure 34. Change in the System Loss Factor for Sucrose Solutions with Various Mechanical Loads Plotted as a Function of the Solution Concentration

considerably because of the increase of the surface losses with loading as has already been pointed out in connection with Figure 32.

Furthermore, the loading crystal vibrates in antiphase to the excited crystal and increases the relative shear motion between the two surfaces of the film. If the crystals were isotropic, loading would increase the loss factor of the system by an additional factor of two; it would double the relative transverse velocity, thus increasing the energy loss by a factor of four, but would also increase the energy of the system by a factor of two. A $\lambda/4$ load acts like a rigid clamping (see Theory section). The quartz crystal then is heavily loaded, and the mass impedance of the film is negligible compared to that of the $\lambda/4$ load. The loss factor then does not depend on the film thickness.

Figure 35 shows the data for a methyl alcohol - H_2O solution which gave a surface tension range of 70 to 20 dynes/cm. The load was a disc and the film thickness was 1.5×10^{-3} cm. Two different crystals were used. The 400 KHz crystal was optically polished, the 500 KHz crystal was not polished. These measurements also indicate that a surface effect must be present. When the surface tension is high, both crystals lead to the same result. But if the surface tension is small, the rough surface crystal (not polished) has the smaller loss. The shear stress is responsible for much of the loss, and as the shear wavelength is short (~ 30 μ), coupling between film and surface will depend on the microscopic structure of the surface. For an optically flat surface, coupling seems to be good and the film losses go up. For a

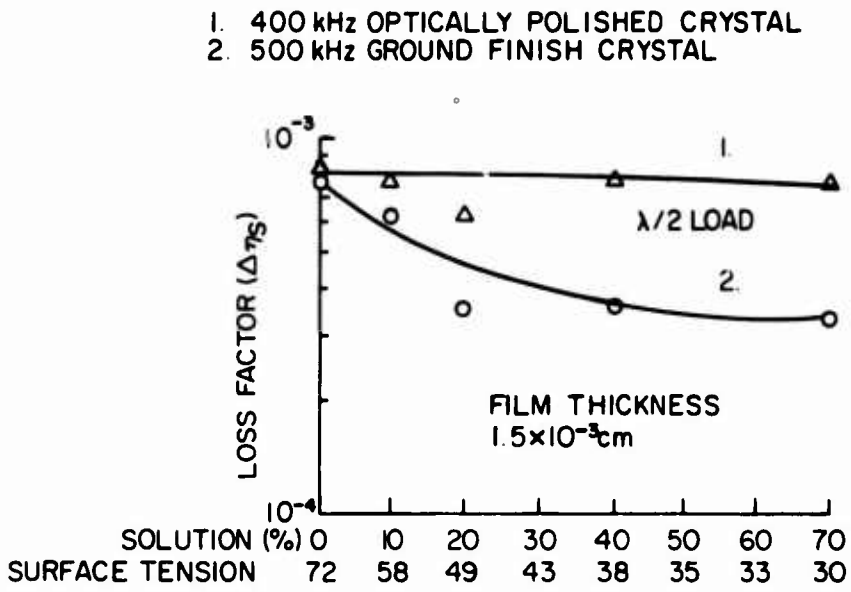

Figure 35. Change in the System Loss Factor for Methyl Alcohol-Water Solution for Two Different Crystals with a λ/2 Load Plotted as a Function of the Solution Concentration

ground surface, the surface tension is not enough to drag the water into the surface cracks and surface dislocations because of the trapped air pockets. Coupling between film and crystal surface may therefore be expected to be disturbed by microscopic and submicroscopic air spaces. As the surface tension is increased the air spaces are partially eliminated because of the better wetting and the losses go up. The above is offered as an explanation; other factors may be involved which would lead to a different explanation.

All the preceding measurements were taken with the relative positions of the driving crystal and the loading crystal or disc fixed. A series of measurements were taken for a given film thickness as the $\lambda/2$ loading crystal was rotated about its axis and the bottom $\lambda/2$ crystal was held stationary. Figure 36 represents the results of these measurements; they show that the coupling loss may be changed by a factor of ten for this series of arbitrary rotations of the top crystal. A detailed series of measurements with a precision arrangement to hold and also rotate the crystals would undoubtedly lead to a larger variation. For the measurements shown in Figure 36 $k_o d$ was about 30. The shear wave that is generated at the surface of the film is completely damped out before it reaches the other surface.

The coupling losses described here lead to energy losses large in comparison to the intrinsic losses of the quartz crystals or the losses of the materials used for the $\lambda/2$ or $\lambda/4$ loads. This was the situation that led to the investigation of coupling losses.

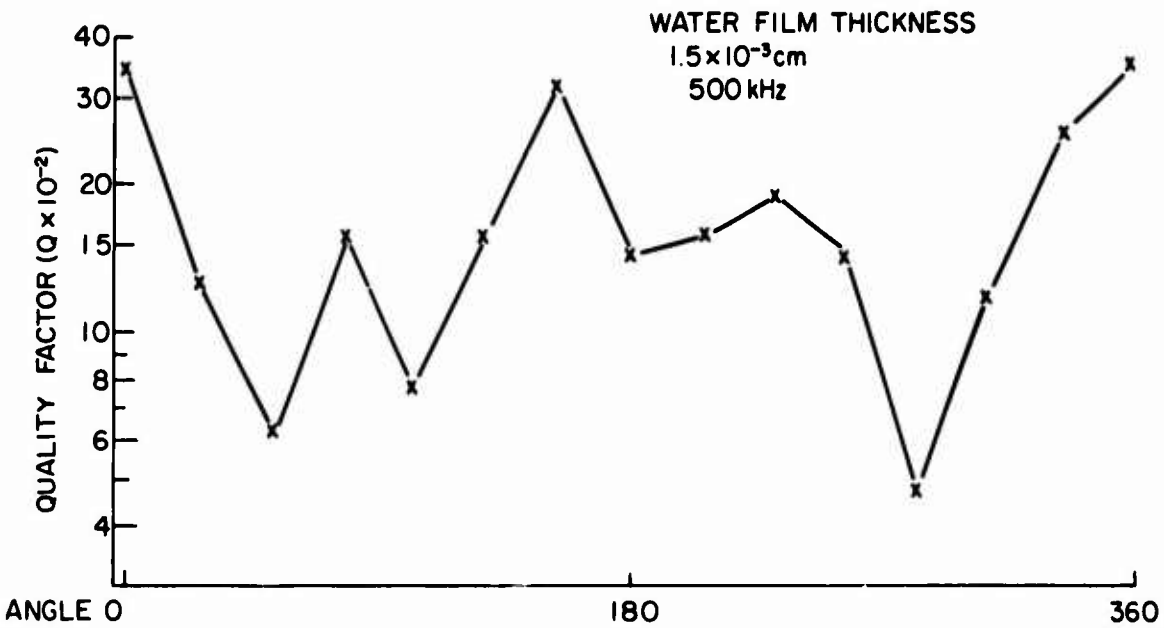

Figure 36. Quality Factor of a 500 KHz Quartz Crystal Loaded with a Similar Crystal Plotted as a Function of Arbitrary Relative Rotation

As far as the standard pulse echo technique is concerned, the situation is usually unencumbered by the previously described complications. The specimens are relatively long and the mass of the specimen large in comparison to that of the bond so that the attenuation in the specimen is large in comparison to the dissipation of energy by the bonding. If the increase in the loss factor by the bonding of two $\lambda/2$ quartz crystals is $\Delta\eta$; $2\pi\ \Delta\eta$ is the relative energy loss per cycle, i.e. per reflection. Such a bond would reduce the amplitude of a pulse by a factor $e^{-2\pi\Delta\eta} \sim (1 - 2\pi\ \Delta\eta)$ which for the usual case is small. It is only when the energy dissipation of the specimen is small and the energy of the specimen vibration also relatively small that bonding loss considerations become important.

Optical Contact

Figure 37 shows the variation of η_s of 10 MHz quartz crystals as the coupling film thickness is decreased. The right-hand curve is that of a single, optically polished, 0.95 cm diameter, X-cut quartz crystal. The left-hand curve is that of two 10 MHz crystals in optical contact. The set of curves between these two represent the measurements taken for two crystals coupled by a water film as the thickness of the film is varied from about 2.5×10^{-5} to 2.5×10^{-3} cm; the highest damping was noted for a film of about 2.5×10^{-5} cm. The transverse velocity gradient across the film increases and the losses increase correspondingly (see Figure 11). For very thin films the transverse motion of the film surfaces are tightly coupled and the behavior of the film approaches that of optical contact.

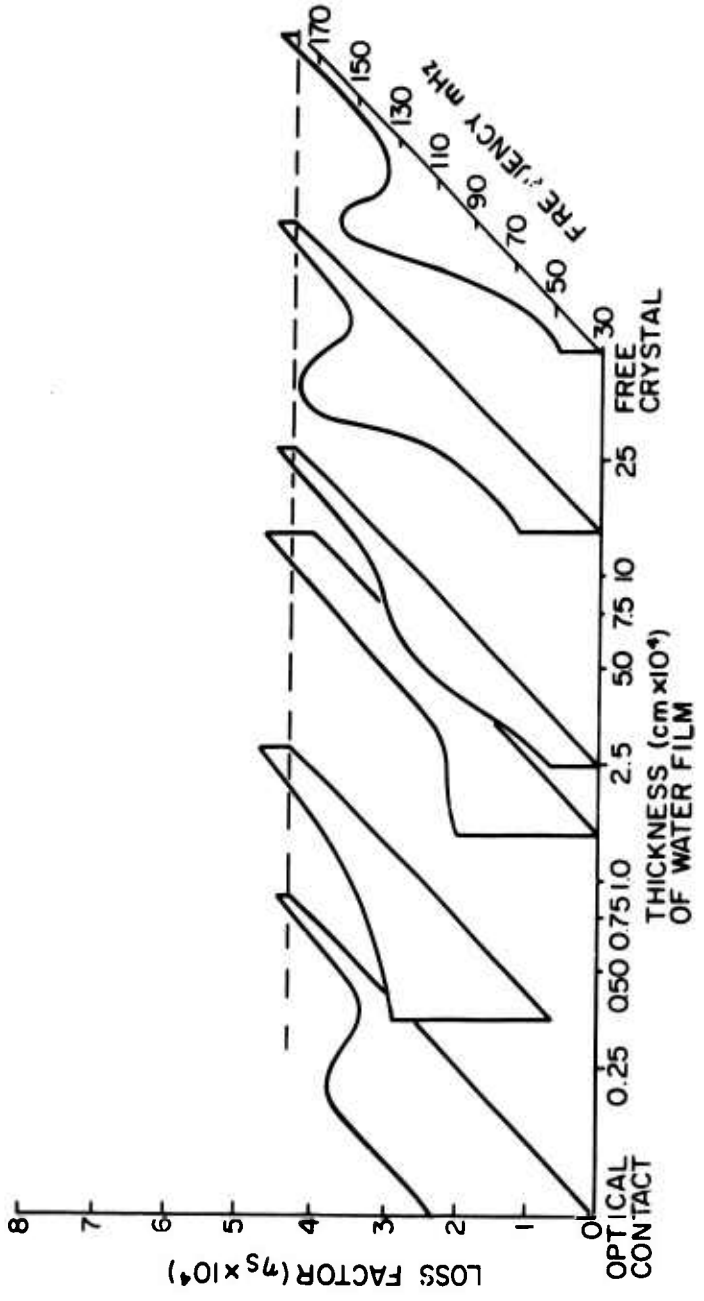

Figure 37. Variation of the Loss Factor of 10 MHz Crystals as the Thickness of the Coupling Film is Changed Plotted as a Function of Frequency

Quartz transducers can be placed in optical contact with polished crystalline surfaces. Figure 38 shows data obtained for commercial glass and also for fused quartz. The energy dissipation of glass is seen to be relatively independent of temperature and frequency. The fused quartz data show a low temperature relaxation. These two types of loss are characteristic of silica; a third type, temperature activated hysteresis, will be shown later.

To investigate optical contact losses measurements were taken using optically polished crystalline quartz transducers. Optically polished quartz crystals of frequency 10 MHz or greater could be easily placed in optical contact. The data represented in Figures 38 through 49 were taken as a function of frequency as the temperature was slowly varied. For instance, for a temperature of 90°K, the crystals were measured at 30 MHz, 60 MHz, 70 MHz, etc. Usually the temperature would vary several degrees during the measurements and an average value would be chosen to represent the series of measurements plotted in a curve.

Due to the large number of temperature points, the data were plotted initially as loss factor vs temperature for each resonant frequency; in the perspective format the same procedure was followed. In viewing the composite graphs it must be remembered that as far as a given set of data for a particular measurement is concerned, each curve would run from left to right angles to the given curves. Thus, the jumps between frequency curves cannot be attributed to changes in the system between different groups of measurements. The data for

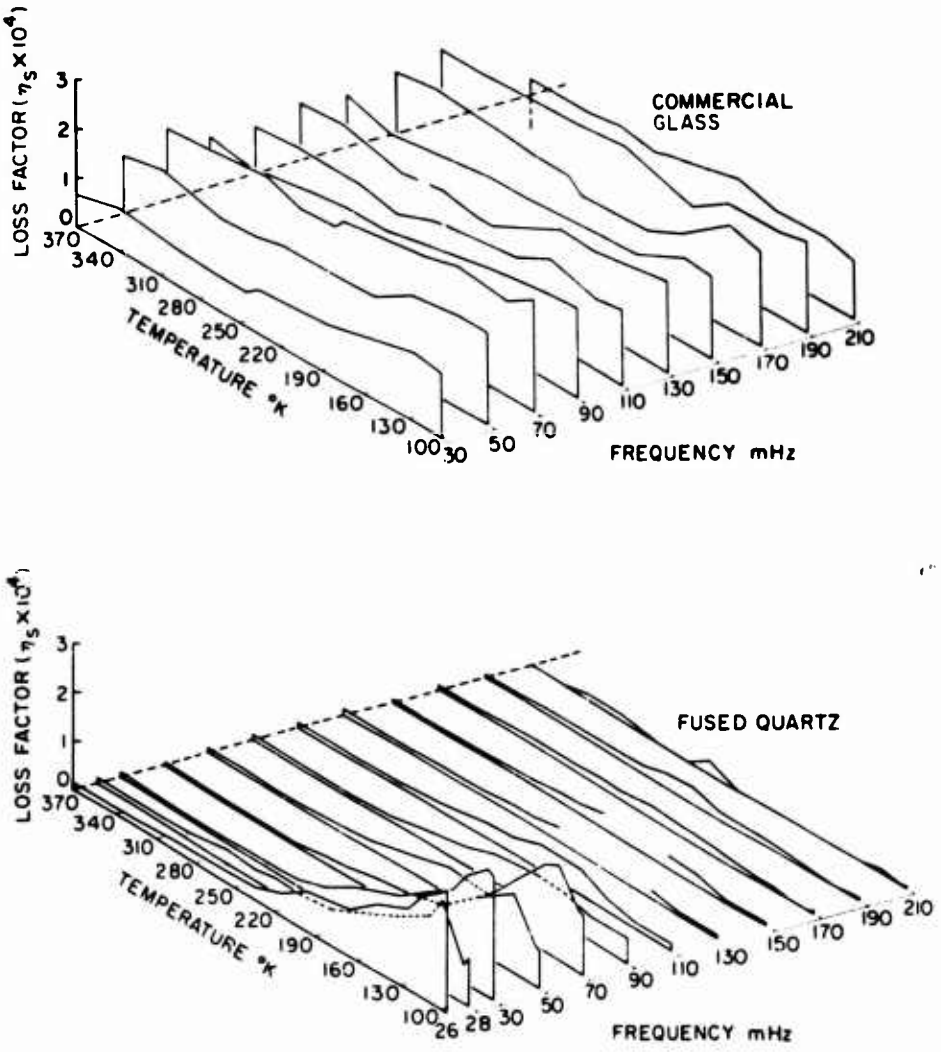

Figure 38. Loss Factor of Commercial Glass Specimen, and a Fused Quartz Specimen in Optical Contact with a 10 MHz Quartz Crystal Plotted as a Function of Temperature and Frequency

10 MHz have been left out of these graphs as it could not be measured with the same electronic components.

Figure 39 shows the loss factor of two single 10 MHz X-cut, quartz crystals plotted as a function of temperature and frequency. Both crystals show a small temperature activated hysteresis which follows the general form of $\eta_s = 1.0 \times 10^{-4} \exp(-1600/2T)$ for frequencies up to about 10 MHz.

Figure 40 shows the loss due to two 10 MHz crystals in optical contact (abbreviated as 10X-10X), compared to the preceding figures, a loss factor scale has been increased by a factor of 5. For frequencies less than 150 MHz the loss factor was approximately $\eta_s = 1.6 \times 10^{-3} \exp [-2000/2T]$. Bond breakage was effectively eliminated by exciting the system during heating and cooling cycles. A repetition of the measurements at the higher temperatures lead to a somewhat different result because of the variability of the crystal-crystal interaction. However, the fundamental shape of the curves was still the same.

Figure 41 shows a similar measurement when a 10 MHz X-cut crystal was placed in contact to a 20 MHz X-cut crystal (abbreviated as 10X-20X). The frequency curves are of interest as they exhibit coupled circuit behavior. The 10 MHz coupled crystal system resonated at multiples of the individual crystal frequency and also at the frequency corresponding to the total thickness.

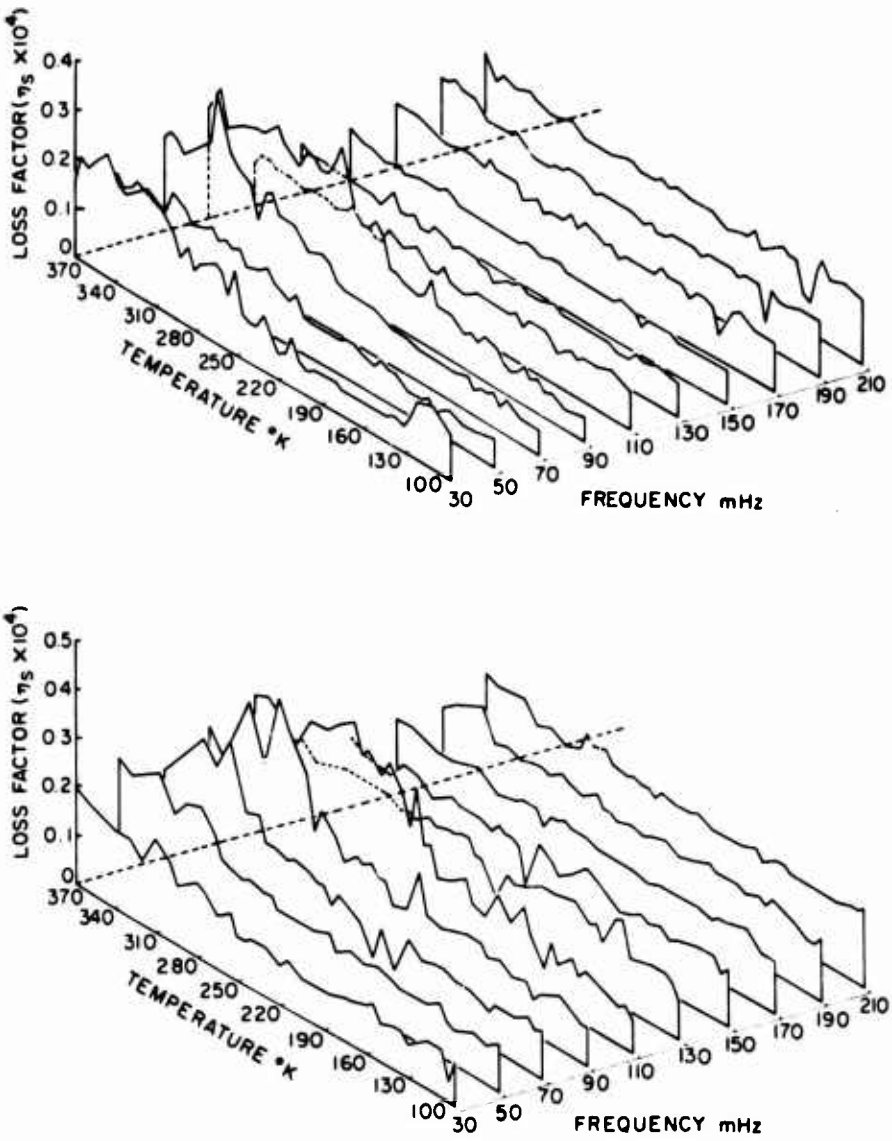

Figure 39. Loss Factor of Single 10 MHz X-cut Quartz Crystals Plotted as a Function of Temperature and Frequency

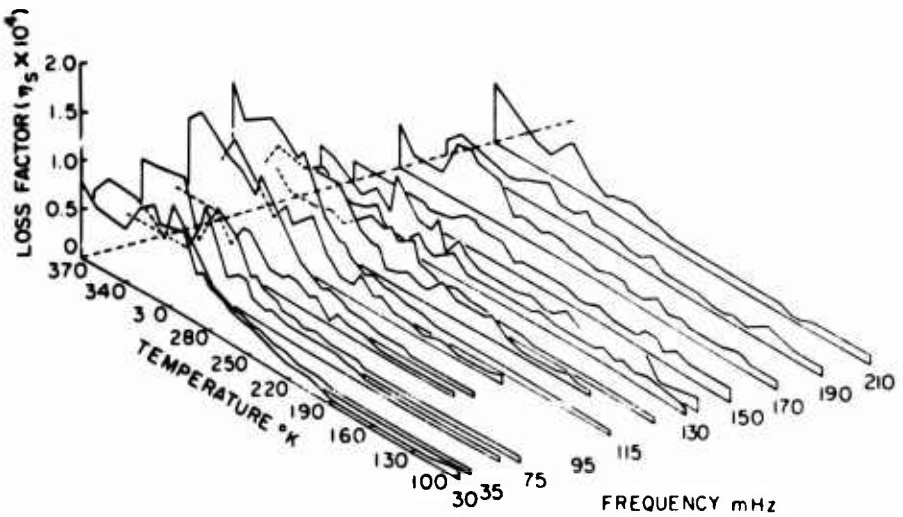

Figure 40. Loss Factor of Two 10 MHz X-cut Quartz Crystals in Optical Contact Plotted as a Function of Temperature and Frequency

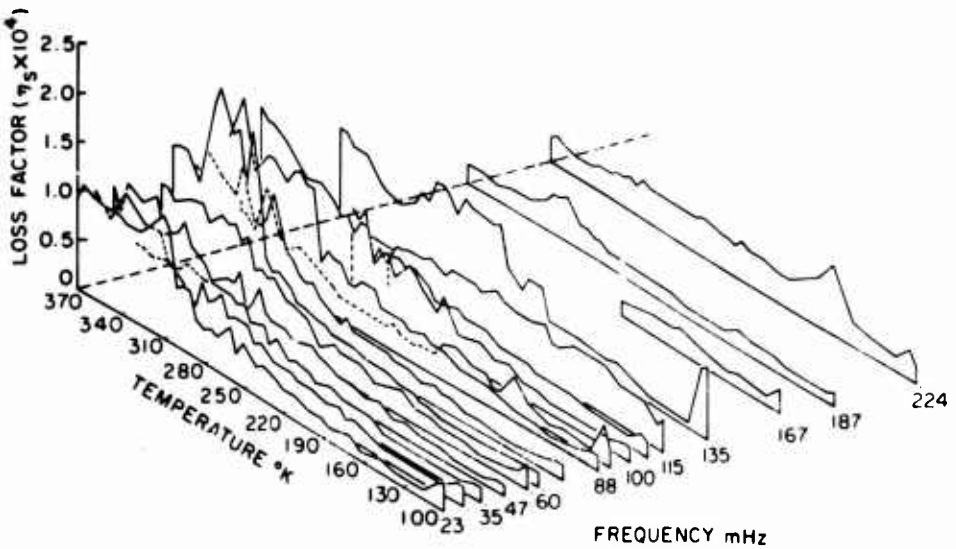

Figure 41. Loss Factor of 10 MHz X-cut Quartz Crystal in Optical Contact with a 20 MHz X-cut Quartz Crystal Plotted as a Function of Temperature and Frequency

For crystals of unequal fundamental frequency, the crystals interacted as a composite and as loaded individual crystals as follows from Figure 42. The behavior of the coupled system can be explained by the superposition of modes whose frequencies are that of the coupled composite, that of a frequency shifted 10 MHz crystal radiating into a quarter wavelength sample, and a 20 MHz crystal not frequency shifted and radiating into a multiple half wavelength sample. The results show that optical contact losses are small at high frequencies and low temperatures. Because of their high acoustic transmission the optically flat contact surfaces are particularly useful at the ultra high frequencies where bonding problems are critical.[4]

Figure 43 shows a contour representation of the data of Figures 43 and 44. The general characteristic of the 10X-10X and the 10X-20X crystals in optical contact is that of a hysteresis (independent of frequency) for the frequency range of 20 MHz to about 100 MHz.

The Effect of Crystal Alignment on Contact Losses

To determine the effect of crystal alignment on the contact losses, a series of relative measurements were made. The aligned coupled crystals had a broad response between 25 and 40 MHz; they did not vibrate at many of the higher frequencies where the nonaligned crystals previously resonated. The aligned crystals in optical contact were a completely new and different system with a different set of resonant modes. It was observed that a small frequency shift could induce a large change in the loss factor. As this coupled system exhibited a

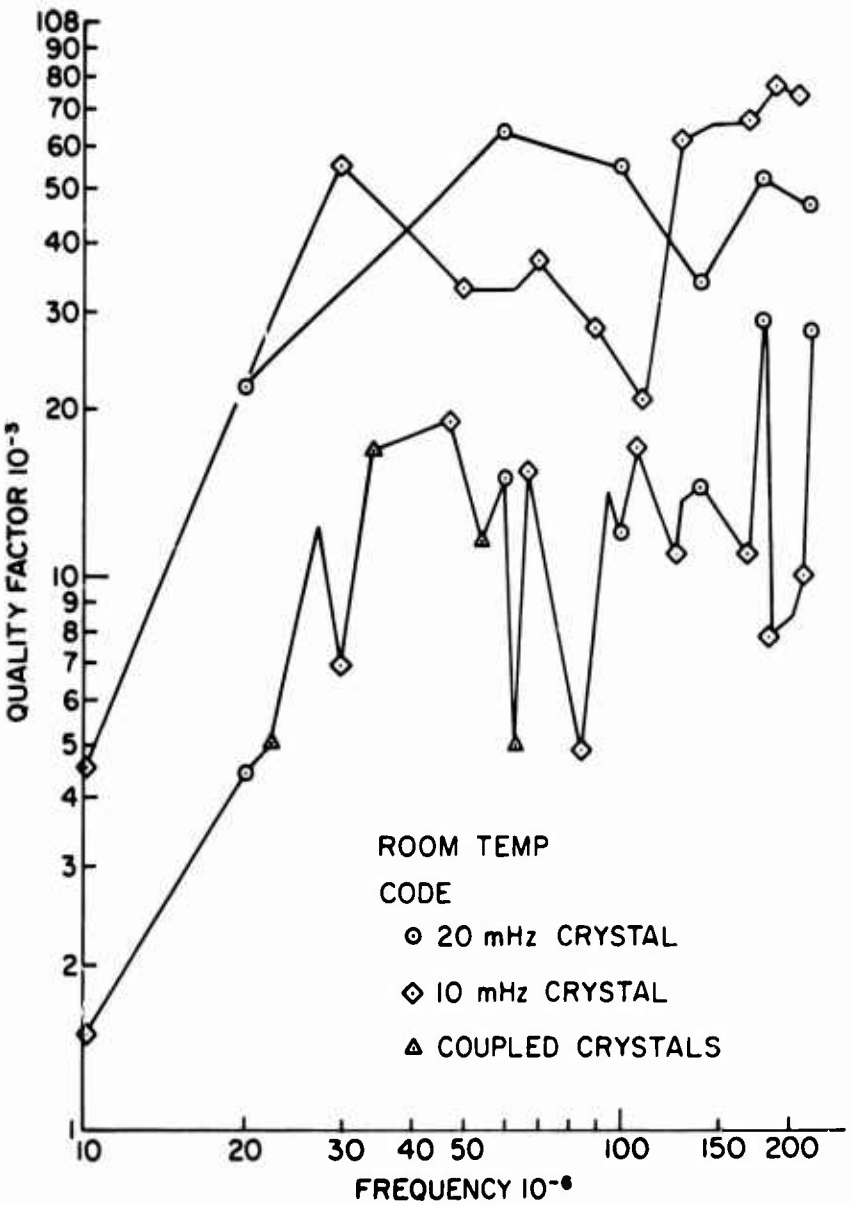

Figure 42. Frequency Behavior of a 10 MHz X-cut Quartz Crystal in Optical Contact with a 20 MHz X-cut Quartz Crystal

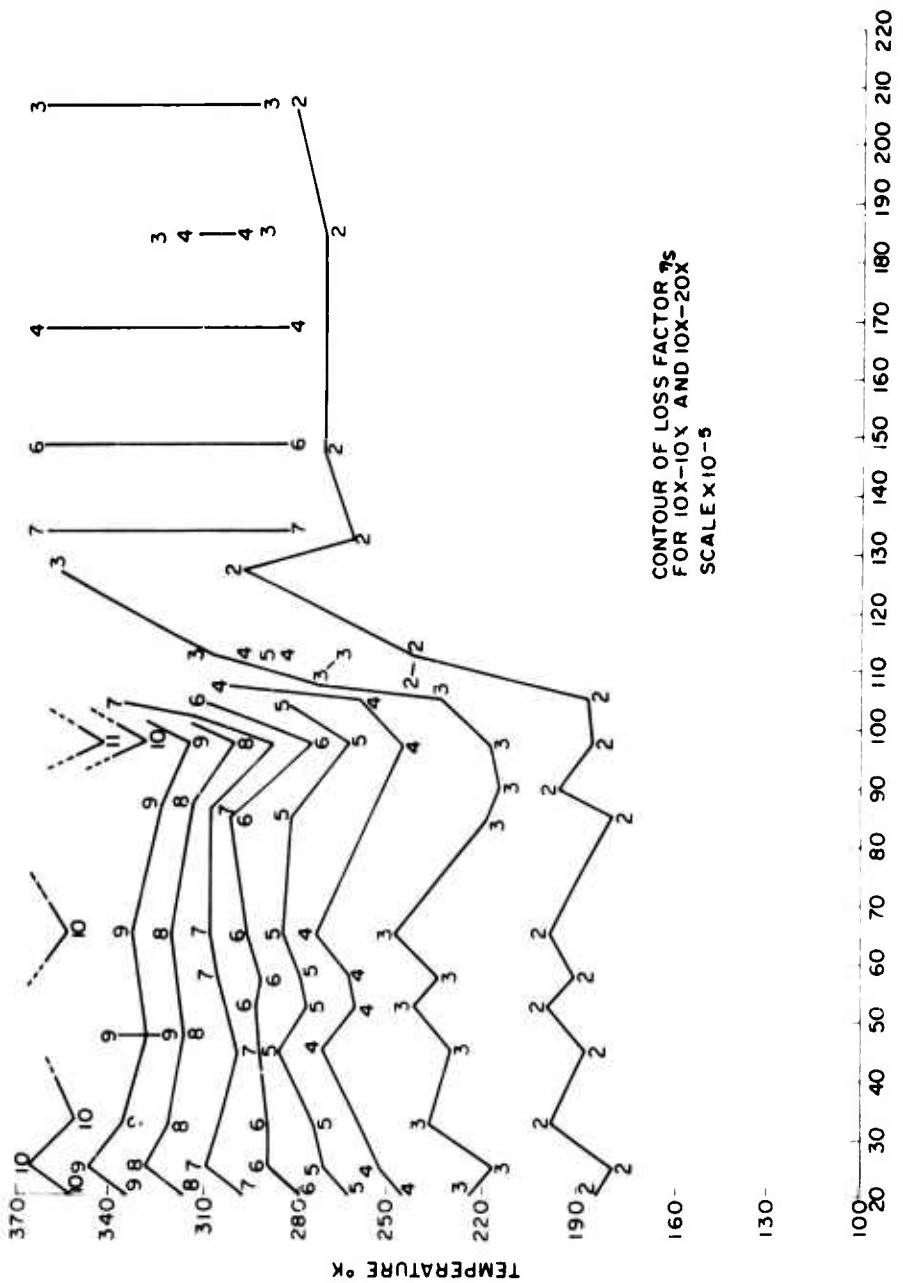

Figure 43. Contour Plot of Loss Factor for 10X-10X and 10X-20X Quartz Crystals in Optical Contact

new set of characteristics, the correlation between these measurements and those previously obtained was poor.

The measurements showed that testing the effect of the alignment or misalignment of the axes of two crystals in contact on the damping is difficult and would require special equipment such as very stable oscillators and means of measuring the vibration patterns of the quartz vibrators.

The Effect of Different Loading on Contact Losses

If an AC-cut 15 MHz quartz crystal and an X-cut 15 MHz quartz crystal were placed in optical contact with each other, the loss increased in some cases an order of magnitude. Figures 44 and 45 show experimental results. The 15 MHz AC-cut crystal showed temperature activated hysteresis in its fundamental mode of vibration, and the loss factor was given by $\eta_s = 1.2\ 10^{-2}\ \exp[-1700/2T]$. The 15 MHz X-cut crystal showed limited temperature activated hysteresis in its fundamental mode, but exhibited greater damping in the 100 MHz region; $\eta_s = 3.3\ 10^{-2}\ \exp\ [-2200/2T]$. The coupled (15 AC - 15X), Figure 45, system exhibited strong temperature activated for the lower frequency modes $\eta_s = 4.5\ 10^{-2}\ \exp[-2100/2T]$.

Carrying the mismatch one step further, an 15 MHz AC-cut crystal was placed in contact with a 30 MHz X-cut crystal. The results are represented in Figure 46. For the first three modes the loss factor was of the form $\eta_s = 3.1\ 10^{-3}\ \exp[-1300/2T]$ up to a temperature of about 230°K.

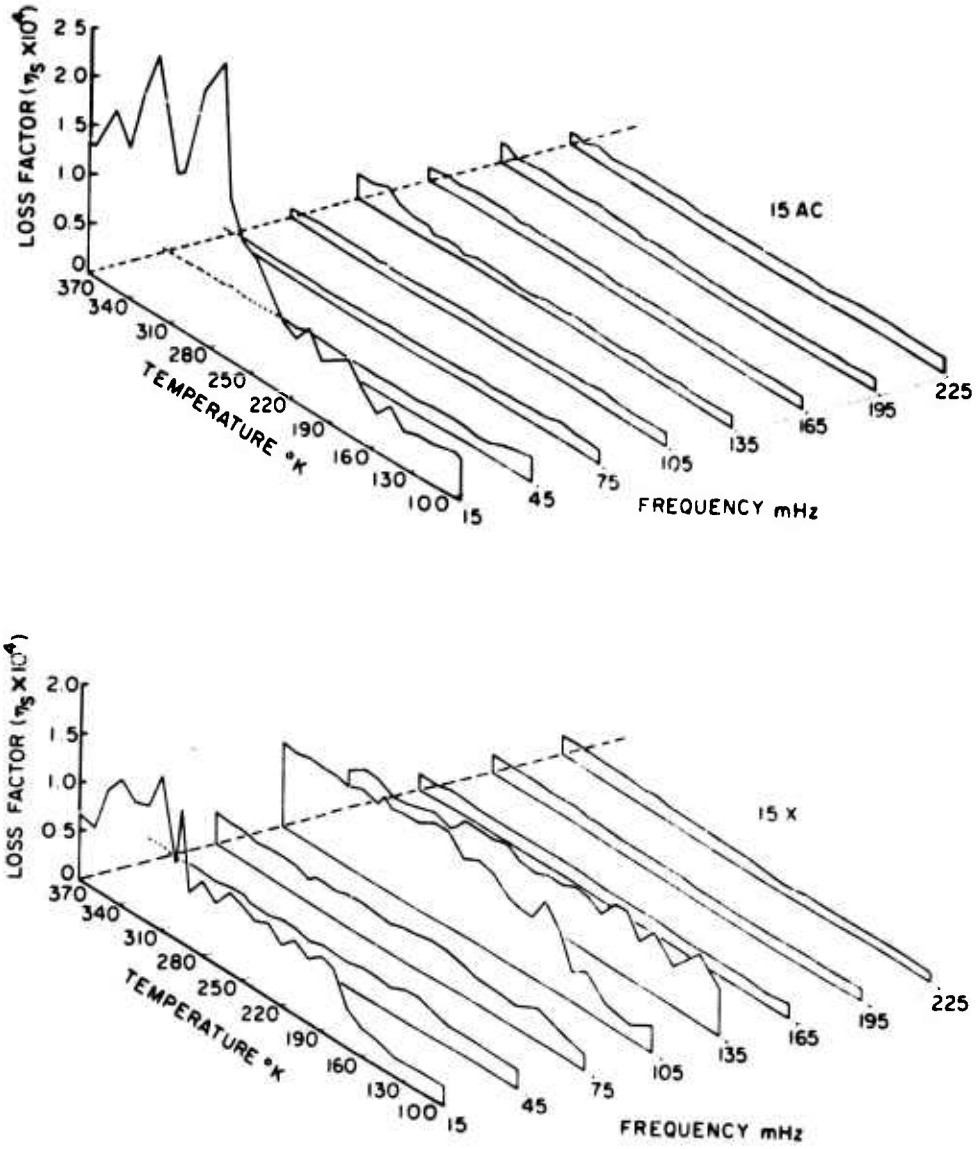

Figure 44. Loss Factor of a 15 MHz AC-cut Quartz Crystal and a 15 MHz X-cut Quartz Crystal Plotted as a Function of Temperature and Frequency

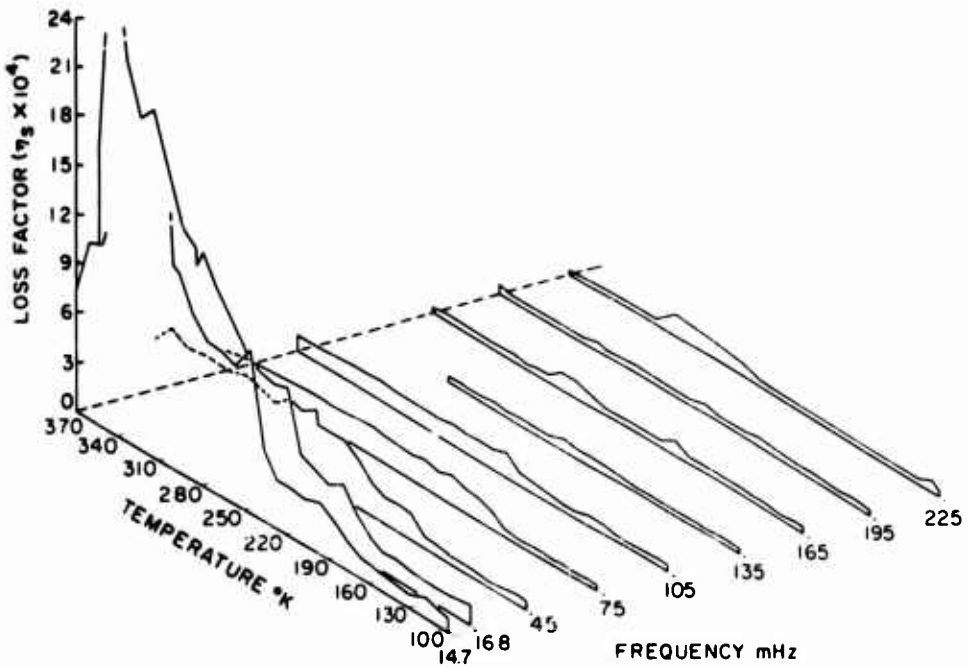

Figure 45. Loss Factor of a 15 MHz AC-cut Quartz Crystal in Optical Contact with a 15 MHz X-cut Quartz Crystal Plotted as a Function of Temperature and Frequency

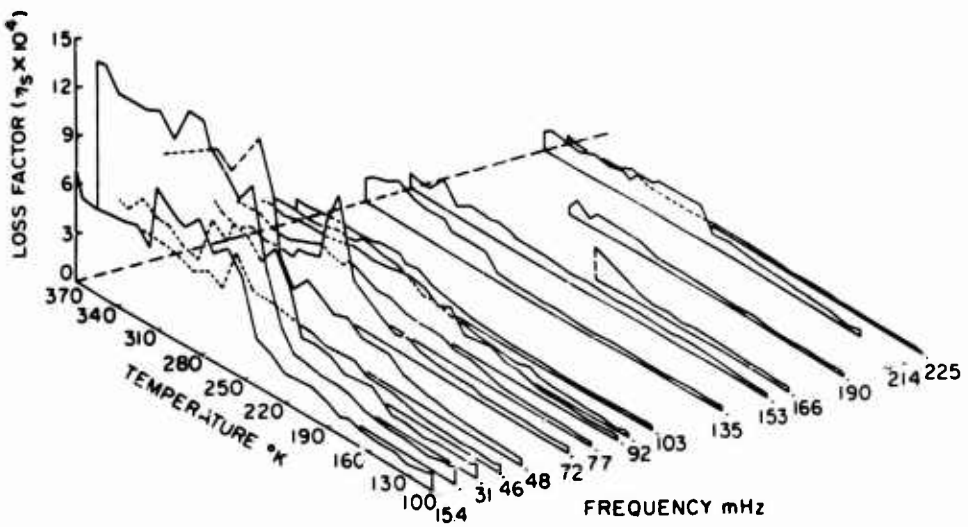

Figure 46. Loss Factor of a 15 MHz AC-cut Quartz Crystal in Optical Contact with a 30 MHz X-cut Quartz Crystal Plotted as a Function of Temperature and Frequency

The Effect of Etching on Optical Contact Losses

The surface of quartz can be altered by HF acid etching, Figure 47 shows that the temperature activated hysteresis of a single free crystal had been largely removed by having etched the crystal; as a consequence of the etching the losses increased considerably at the lower temperatures. To substantiate the above findings, two new 10 MHz X-cut quartz crystals were measured in the following three conditions: (1) the single crystals, (2) the single crystals after etching them, (3) the etched crystals placed in optical contact. Figures 48 and 49 show the results; the crystals in optical contact system are now tightly coupled since they do not resonate at multiples of the crystal frequency. Fewer temperature points were taken as only the general trends and characteristics were of interest now. The single crystals showed again a slight temperature activated hysteresis, etching eliminated much of the temperature activated hysteresis but increased the losses at low temperatures, this has been pointed out in findings connected with the preceding measurements. The coupled crystals showed temperature activated hysteresis for lower frequency modes of the form $\eta_s = 5.3\ 10^{-3} \exp[-2000/2T]$ up to about 240°K. For higher temperatures $\eta_s = 18 \exp[-6000/2T]$. For frequencies of 55 MHz and above the loss factor was greater at the lower temperatures than that for the two lower frequency modes.

It is convenient to divide optical contact losses into three types:

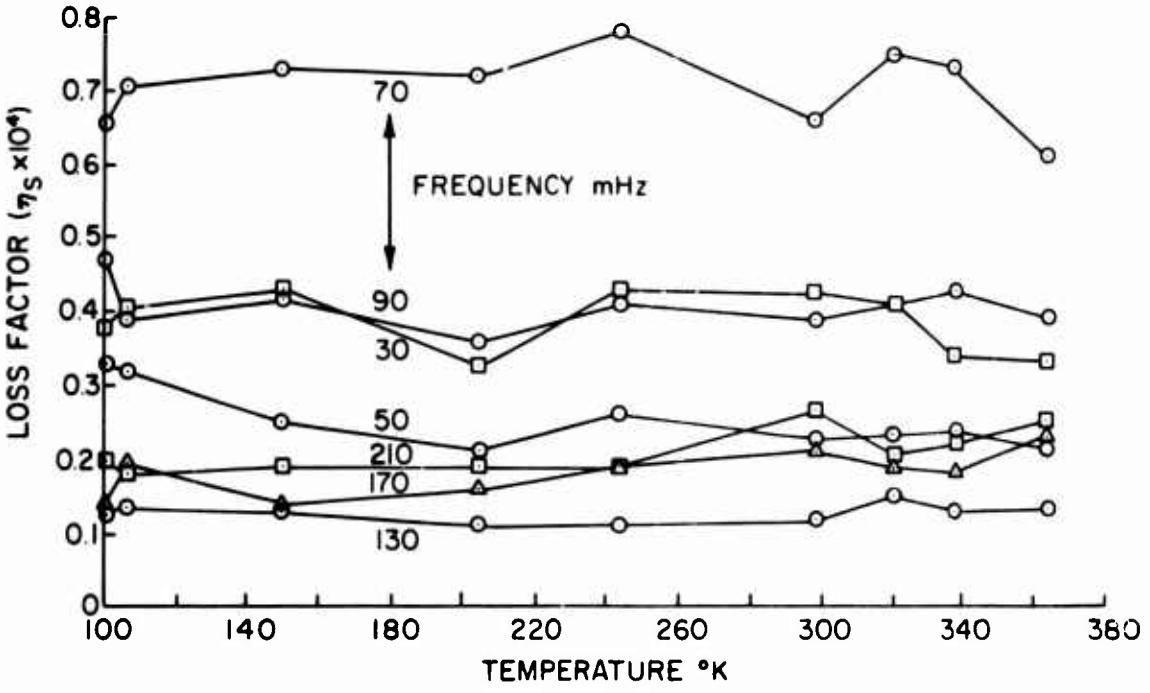

Figure 47. Loss Factor of 10 MHz X-cut Quartz Crystal After Etching in Hydrofluoric Acid.

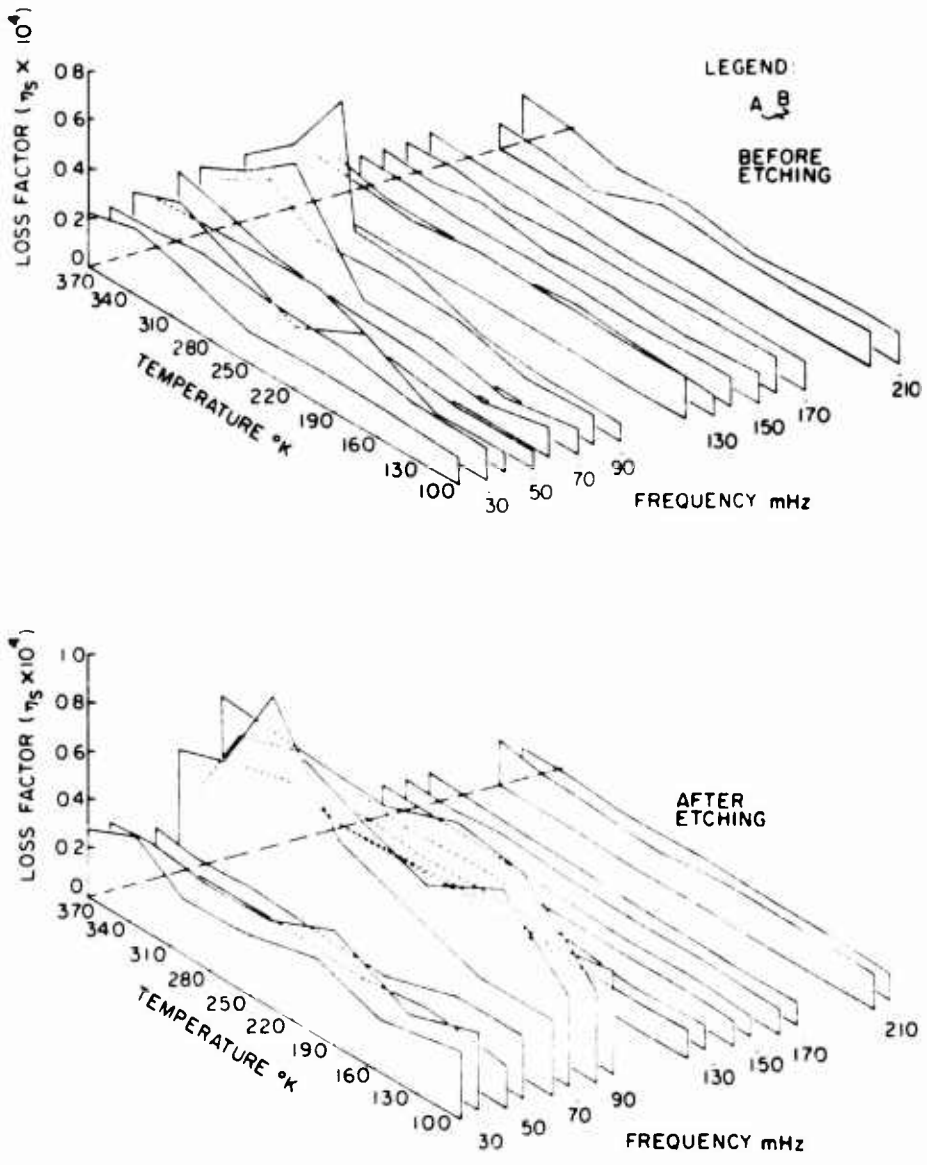

Figure 48. Loss Factor of Two Single 10 MHz X-cut Quartz Crystals Before and After Etching in Hydrofluoric Acid Plotted as a Function of Temperature and Frequency

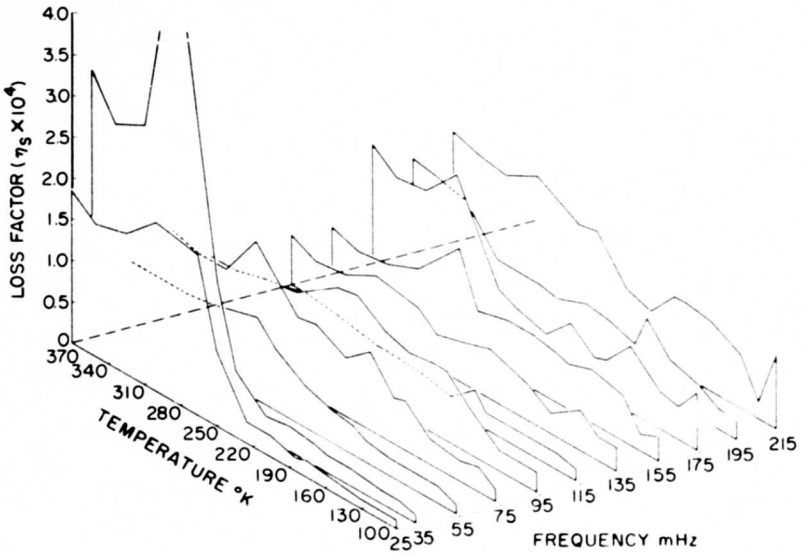

Figure 49. Loss Factor of Two 10 MHz X-cut Quartz Crystals in Optical Contact, after Etching, Plotted as a Function of Temperature and Frequency

1. Temperature activated hysteresis; the loss factor increases exponentially with the temperature. If the hysteresis is of the ideal type the loss factor will be frequency independent.

2. A loss similar to that of glass for which the loss factor is relatively high and independent of temperature (and of frequency).

3. A loss similar to that of fused quartz which exhibits a relaxation. Combinations of these types of loss were observed but the most significant loss was the temperature activated hysteresis type of loss which was usually restricted to the first few resonant modes.

The following is a summary of the loss for quartz and the measured losses observed for the different systems in optical contact with the abbreviations used above in this section.

crystal arrangement	η_s = const. exp[-ACT/RT]
single 10X	$\eta_s = 1.1\ 10^{-4}$ exp[-1600/RT]
coupled 10X-10X	$\eta_s = 1.6\ 10^{-3}$ exp[- 2100/RT]
single 15 AC	$\eta_s = 1.1\ 10^{-2}$ exp[-1800/RT]
single 15X	$\eta_s = 3.3\ 10^{-2}$ exp[-2200/RT]
coupled 15AC-15X	$\eta_s = 4.5\ 10^{-2}$ exp[-2100/RT]
coupled 15AC-30X	$\eta_s = 3.1\ 10^{-3}$ exp[-1400/RT]
coupled (etched) 10X-10X	$\eta_s = 5.3\ 10^{-3}$ exp[-2200/RT]

ACT = activation constant which according to Mason varies between 2 and 5 kilocalories per mole; this is the binding energy of impurity atoms. From the work of Cook and Breckenridge, Mason derives the equation

$$\eta = 7\ 10^{-4} \exp[-5000/RT] .$$

If we interpret these equations and their constants[19] (see Mason's theory of temperature activated hysteresis in Theory Section), we find that generally the activation constant is smaller and the leading coefficient is of comparable magnitude or larger than his constants for bulk quartz. This appears reasonable as it indicates that there are more defects in the surface of quartz than in the bulk and that the activation of surface defects takes less energy than for those in bulk. The surface energy of quartz, say X-face, should be in excess of 1000 ergs/cm^2 [25] and in light of the physical disruption of the crystal structure it appears reasonable that the binding energies of the surface dislocations and pinning points would be less than those in bulk.

In general the interpretation of the coupled crystals in optical contact would follow similar reasoning. The loss here is comparable or larger than that of the individual components, the contacted surfaces interacting similar to a surface of dislocations which are pinned by the peaks of the surface irregularities. To explain the experimental data the activation of the hysteresis loss must be possible by either temperature changes or by stress for certain specific modes, or a combination of the two working together. This is seen in the data where for low frequency and temperature there is small loss up to a certain frequency and then the loss factor changes to a value several times higher. Examples of this are the contacted 10X-20X, the aligned 10X-10X, the etched 10X-10X, the single 15X crystal, and the single etched 10X crystals.

The rapid increase of loss with temperature noted on the contacted, etched 10X-10X crystals and the contacted 15AC-30X crystals followed the form $\eta = 18 \exp[-6000/2T]$ and $\eta = 37 \exp[-5000/2T]$ respectively. This is similar to the form of the background loss observed in metals such as copper, aluminum, Mg, etc.[19] An explanation either for the metals or the contacted quartz crystals is not evident.

As hysteresis is a mechanical type loss a simple model can be used to compare crystal contacts to velocity independent friction. The optical contact surface would be in many respects like two pieces of fine sandpaper pressed together. The structure of the two sheets would fit together in an infinite number of stable configurations. Any relative motion between the two would produce a loss as work would be expended going through the vibration cycle. If the sheets were subjected to stress patterns similar to those experienced by the crystals there would be a tendency for relative motion which would increase as the pressure forcing the sheets together is reduced. Relatively high force would correspond to low temperature for the contacted crystals. Relative motion and thus loss would increase with the number of pinning points torn loose during the cycle. After a certain number of pinning points have been torn loose the surfaces could move relatively unrestricted, this would correspond to decreasing the pressure on the sandpaper sheets to the point that they could be slid over one another. This model would explain the tendency for the loss factor to increase to a certain value and then level off. Each mode of vibration with its stress distribution would work in conjunction with the temperature activation to produce the final resultant loss.

The model used here and the processes of the loss mechanism is largely speculation, but it appears that there is room for a reasonable explanation along these lines and there are enough variable parameters on hand to fit the data. Possibly it is just as important to simply note that these losses exist and in ultrasonic measurements they should be avoided or eliminated if possible or their value ascertained and taken into account.

IV. SUMMARY AND CONCLUSIONS

Procedure and Measurements

The original problem of this investigation was to measure the acoustic properties of small specimens. The measurements were to be taken by coupling the specimen to a high Q resonant vibrator, such as a quartz crystal, and then to observe the additional damping of the coupled system due to the specimen. However, it was found that energy losses due to the coupling were so large that measurements were not possible for small, high Q specimens. The main emphasis of the study was then shifted to the investigation of the characteristics of ultrasonic coupling losses.

The energy losses due to a coupling film or coupling by placing surfaces in optical contact were measured as a function of such varied parameters as frequency, bond thickness, bond composition, mechanical loading, surface conditions, relative alignment of transducer and specimen, and temperature. The equipment used in the measurements was designed so that the energy dissipation due to the mounting of the quartz crystal in order to measure its damping was negligible.

The experimental data obtained for small volumes of liquids, free films, and for loaded films was initially puzzling: the magnitude of the losses was much larger than would be expected on the basis of the theory of longitudinal vibrations. An investigation of the vibrational modes for a disc according to the Aggarwal solution indicated that the resonant modes near the fundamental thickness resonance exhibited shear

displacements at the surface of the disc which were comparable to the longitudinal displacement. Such radial or shear motion of the disc shaped vibrator leads to considerable losses when a liquid coupling film is used. A liquid does not support a shear wave and the transverse component of the vibration in the film is rapidly damped out.

The energy losses for a free film on the surface of a vibrator agree with the theory of shear losses. Still higher accuracy could be obtained if a shear transducer were used with a suitable support arrangement. The viscosity of films could then be determined accurately as a function of frequency.

When the film was loaded the energy dissipation increased much more than would be expected even when shear is taken into account. The vibrational modes of the system in a loaded condition are unknown, but even large shear motions would not account for the magnitude of the energy losses.

In order to account for the energy losses it must be assumed that a component of the losses is due to surface imperfections such as microscopic surface cracks and surface dislocations, and that loading the crystal increases these losses. The addition of a $\lambda/2$ load increased the losses for a glycerin film by approximately a factor of 10, while a $\lambda/4$ load increased the losses about a factor of 40 relative to that of a free glycerin film. Surface cracks and dislocations generate acoustic near fields and near field coupling may account for another part of the loss. Whereas for most of the investigated liquids

the loaded film measurements indicated that the energy losses were not directly proportional to the film thickness, some liquids like glycerin have a high bulk viscosity and the losses are then found to increase with the film thickness.

Further indication of surface effects were noted when the losses due to a coupling film on a commercially obtained "ground finish" transducer increased as a function of an increase in the surface tension of the liquid. In contrast to this, the damping of an optically polished crystal was not affected by the variation of the surface tension of the film.

A study of the energy dissipation due to surfaces in optical contact was made. Through variation of temperature and other relevant parameters a temperature activated hysteresis was observed for many of the measurements. According to the theory of temperature activated hysteresis the loss is proportional to the number of dislocations; the surfaces in optical contact seemed to act like a plane of dislocations. Energy losses due to optical contact also show dependency on the mode of vibration.

Suggestions for Future Research

In order to determine more accurately the physical causes of the losses, further studies would have to be made of the transverse and longitudinal velocity distribution of a vibrating quartz crystal. Surface treatment of the transducer and specimen would have to be rigidly controlled. The detailed effect of mechanically loading the

vibrator would have to be investigated in greater detail in order to determine the various interacting effects.

The transducer loss might be reduced with further preparation of the surface. The final polish of the crystals used in this investigation was with one micron grit. It may be necessary to use the process of Smagin[26] to reduce surface losses. In this lengthy process the final surface polishing is with 0.1 micron grit. Crystals polished in this manner are claimed to have surface damage of less than 100 Å and to have high Q, usually in excess of 10^6.

With the knowledge derived it ought now to be possible to proceed in a systematic manner and obtain detailed results. It was only through these studies, however, that the significant properties involved in the acoustical behavior of thin films, bonded surfaces, and surfaces in optical contact could be made apparent. Apart from deriving a method to measure viscosity in a wide frequency range the study showed that acoustic measurements can give a considerable amount of information about the mechanical behavior of surfaces of solids which cannot be obtained by other methods.

APPENDIX A

Quartz Crystallographic Axes[27]

A cartesian coordinate system is used to designate the crystallographic axes of quartz. Figure 50a shows a natural, right-hand, alpha-quartz crystal with its axes designated by X, Y, and Z. The X axis (electric axis) passes through a vertex of the hexagonal crystal, the Y axis (mechanical axis) is perpendicular to an edge of the crystal, and the Z axis (optic axis) is the principal axis of the crystal and completes the cartesian coordinate system determined by the X and Y axes. The Z axis is of the type called a "screw axis"; the SiO_2 groups occupy positions that wind themselves progressively about the axis. Figure 50b shows an X-cut crystal and its relation to the crystallographic axes. The X-cut crystal is perpendicular to the X axis and thus the plane of the crystal contains the Y and Z axes.

Quartz Structure[27]

Quartz is a natural piezoelectric material that is widely used for transducers. The structure of quartz, or more specifically α quartz, is class 18, trigonal holoxial. A simple explanation of this structure is that of Gibbs where he starts with the hexagonal symmetry of β quartz and rotates adjacent projections of the silicon atoms about 8 degrees, Figure 50. β quartz structure is shown because of its simplicity and ease of representation. The low symmetry of α quartz is typical of piezoelectric substances which must have a

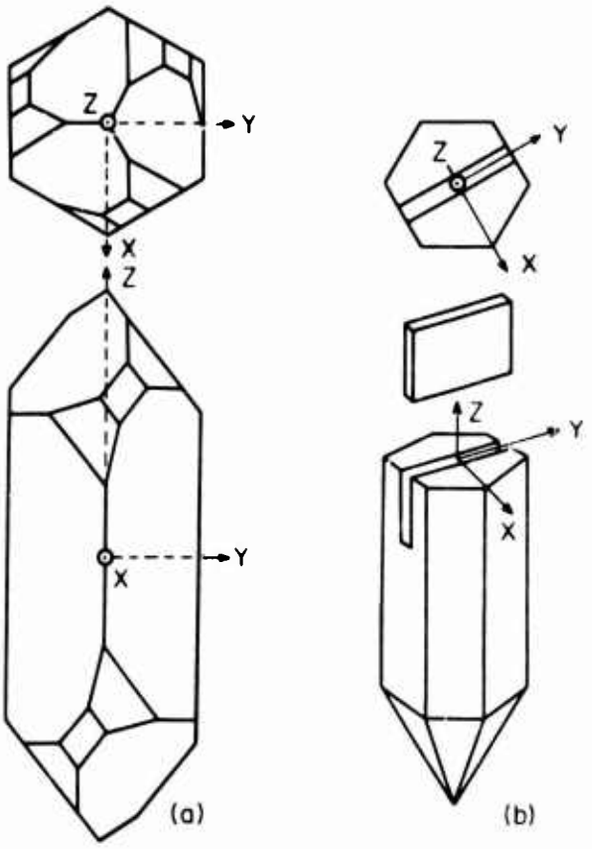

Figure 50. Quartz Crystallographic Axes (a) Natural, Right-Hand, Alpha-Quartz Crystal (b) X-cut Crystal

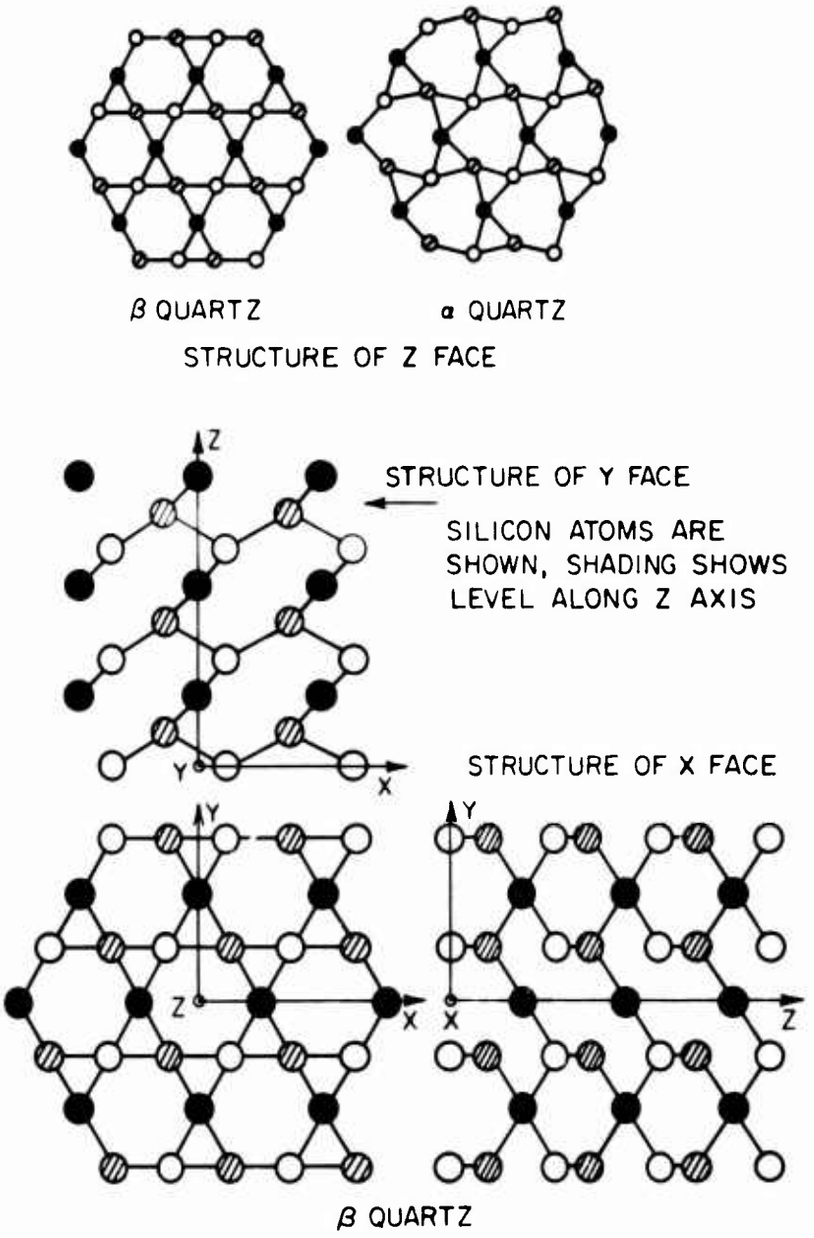

Figure 51. Crystal Lattice Structure for α and β Quartz

natural structural bias, or in other words, a non-centrosymmetric structure.

The low symmetry of a quartz necessitates the tensorial notation to express stress, strain, Poisson ratio, and piezoelectricity. Thus, a general solution of the vibration problem for a quartz crystal would be very involved and we must work either with partial solutions or devise a simple model. The stress-strain relations are expressed by the set of equations:

$$
\begin{aligned}
X_x &= c_{11}\, x_x + c_{12}\, y_y + c_{13}\, z_z + c_{14}\, y_z \\
Y_y &= c_{12}\, x_x + c_{11}\, y_y + c_{13}\, z_z - c_{14}\, y_z \\
Z_z &= c_{13}\, x_x + c_{13}\, y_y + c_{33}\, z_z \\
Y_z &= c_{14}\, x_x - c_{14}\, y_y + c_{44}\, y_z \\
Z_x &= + c_{44}\, z_x + c_{14}\, x_y \\
X_y &= + c_{14}\, z_x + \tfrac{1}{2}\,(c_{11}-c_{12})\, x_y
\end{aligned}
$$

and the piezoelectric relationships are given by the phenomenological equations:

$$
\begin{aligned}
X_x &= e_{11}\, E_x \\
Y_y &= -e_{11}\, E_x \\
Z_z &= 0 \\
Y_z &= e_{14}\, E_x \\
Z_x &= - e_{14}\, E_y \\
X_y &= - e_{11}\, E_y \,.
\end{aligned}
$$

These equations apply directly to the X-cut crystal as its axes coincide with the crystallographic axes. A crystal driven by an E_x

field does not only excite the thickness mode through the X_x stress but also excites the other modes through the Y_y and Y_z stresses which are coupled through both the elastic and the piezoelectric constants.

Quartz - Poisson's Ratio

Poisson's ratio for quartz is interesting as it gives some insight into the complexity of the vibration pattern. Cady[27] defines Poisson's ratio as $\sigma_{hk} \equiv s_{hk}/s_{kk}$. Figure 51 shows this ratio for X-cut quartz in the Y-Z plane.

Quartz - Surface Structure

X-ray studies of the surface structure of quartz have established additional characteristics. The surface structure of quartz is different than the bulk structure whether the surface is treated by either mechanical or chemical means.[28,29] Some investigators claim a surface poly-crystalline layer is formed by grinding and even by etching.[30] X-ray measurements[28] taken at the Bell Laboratories show that there is a relatively large amount of quartz misorientation by less than a minute and a smaller amount of misorientation by larger angles up to three or four degrees.

Quartz - Dislocations

Quartz in bulk has been shown to have a considerable number of imperfections and dislocations. Measurements of shear crystals by Bommel, et al[31] indicated that the limiting Q was due to dislocation relaxations. The following values were estimated:

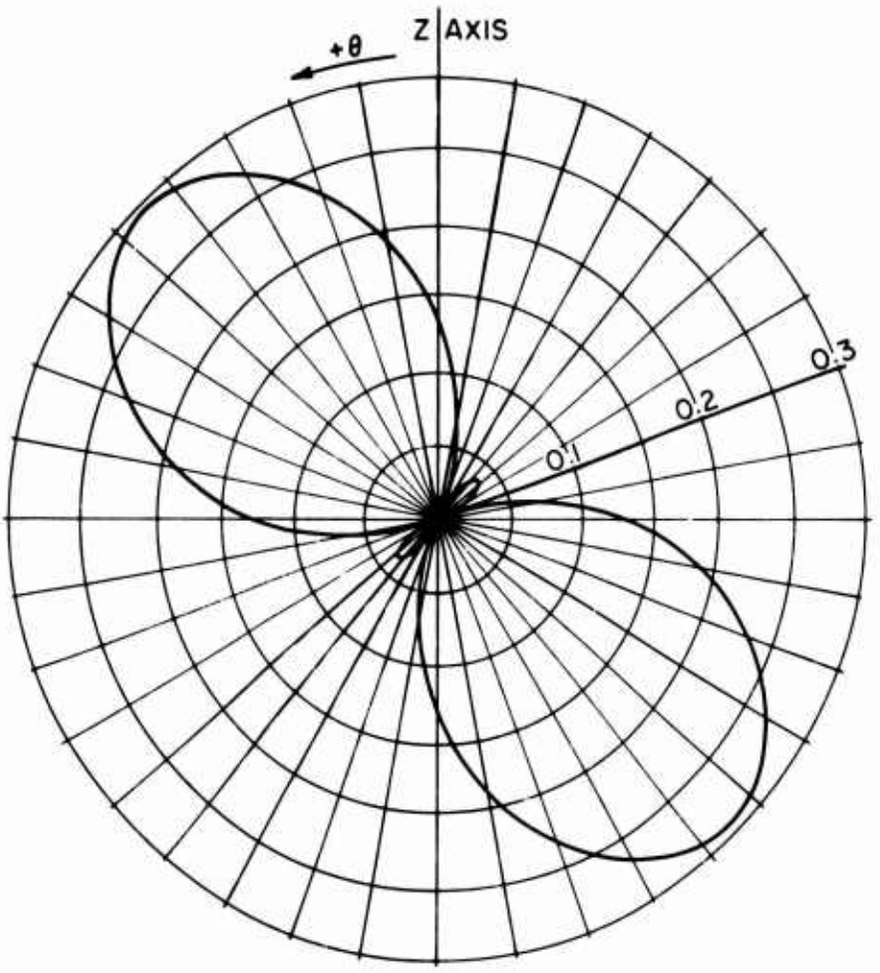

Figure 52. Poisson's Ratio for Quartz in the Y-Z Plane

	N dislocations/cm^2	loop length (cm)
Metal	10^5 to 10^6	$4\ 10^{-4}$
Quartz	10^3	$2\ 10^{-3}$.

Characteristic quartz losses are explained in terms of dislocations, imperfections, and impurities. At low temperatures a relaxation loss similar to that of fused silica is observed. This loss is attributed to the impurity distortion of the lattice and to a dislocation relaxation similar to that found in metals.[31] Another dislocation loss at higher temperature is attributed to the breakaway of dislocations from their impurity pinning points. The theory of this loss is discussed in the Theory Section.

BIBLIOGRAPHY

1. Alfred Klemm. Kataphorese von Gasblasen. Physikolische Zeitschrift 39, 783 (1938). Die Dämpfung von Kapillarwellen, Physikalische Zeitschrift 40, 483 (1939).

2. W. P. Mason. Acoustic Waves and Dislocation Motions. Lecture given at Penn State University March 16, 1967.

3. Valpey Corporation, private communication. August 1966.

4. H. Pfriem. Zur thermischen Dämpfung von Schallwellen in staub - und nebelhaltiger Atmosphare. Akust. Z 6, 109 (1941).

5. I. I. Abrikosova and B. V. Deriagin. Direct Measurements of Molecular Attraction of Solid Bodies, Soviet Physics JETP 4, 2 (1957).

6. H. I. Smith and M. S. Gussenhoven. Adhesion of Polished Quartz Crystals under Ultrahigh Vacuum. J. Appl. Phys. 36, 2326 (1965).

7. J. W. S. Rayleigh. The Theory of Sound, Vol. II, Dover Publications, Inc., New York (1945).

8. H. Osterberg. An Interferometric Method of Observing the Vibrations of an Oscillating Quartz Plate. Proc. N. A. S. 15, 982 (1929).

9. W. D. Dye. The Modes of Vibration of Quartz Piezo-Electric Plates as Revealed by an Interferometer. Proc. Roy. Soc. A. 1 (1932).

10. a. E. A. G. Shaw. On the Resonant Vibrations of Thick Barium Titanate Disks. J. Acoust. Soc. Am. 28, 38 (1956).

    b. E. A. G. Shaw and R. J. Sujir. Vibration Patterns of Loaded Barium Titanate and Quartz Disks. J. Acoust. Soc. Am. 32, 1463 (1960).

11. J. S. Arnold and J. G. Martner. Description of the Resonance of Short Solid Barium Titanate Cylinders. J. Acoust. Soc. Am. 31, 217 (1959).

12. T. R. Kane and R. D. Midlin. High Frequency Extensional Vibrations of Plates. J. of Appl. Mech. 78, 277 (1956).

13. D. C. Gazis and R. D. Midlin. Extensional Vibrations and Waves in a Circular Disk and a Semi-infinite Plate. J. of Appl. Mech. 82, 541 (1960).

14. a. L. Pochammer. Ueber die Fortpflanzungsgeschwindigkeiten kleiner Schwingungen in einem unbegrenzten isotropen Kreiscylinder. J. Rein. Angew. Math. 80, 324 (1876).

b. C. Chree. Longitudinal Vibrations of a Circular Bar. Trans. Camb. Phil. Soc. 14, 287 (1889).

15. H. D. McNiven. Extensional Waves in a Semi-Infinite Elastic Rod. J. Acoust. Soc. Am. 33, 23 (1961).

16. a. R. R. Aggarwal. Axially Symmetric Vibrations of a Finite Isotropic Disc, I. J. Acoust. Soc. Am. 24, 463 (1952).

b. R. R. Aggarwal. Axially Symmetric Vibrations of a Finite Isotropic Disc, II. J. Acoust. Soc. Am. 24, 663 (1952).

c. R. R. Aggarwal. Axially Symmetric Vibrations of a Finite Isotropic Disc, III. J. Acoust. Soc. Am. 25, 533 (1953).

d. R. R. Aggarwal and E. A. G. Shaw. Axially Symmetric Vibrations of a Finite Isotropic Disc, IV. J. Acoust. Soc. Am. 26, 341 (1954).

17. H. Kolsky. Stress Waves in Solids. Dover Publications, Inc., New York (1963).

18. R. K. Cook and R. G. Breckenridge. Anelasticity of Quartz. Phys. Rev. 92, 1419 (1953).

19. W. P. Mason. Physical Acoustics and the Properties of Solids. D. Van Nostrand Co., Inc., New York (1958).

20. W. P. Mason. Piezoelectric Crystals and their Application to Ultrasonics. D. Van Nostrand Co., Inc., New York (1950).

21. W. P. Mason. Relaxations in the Attenuation of Single Crystal Lead at Low Temperatures and their Relation to Dislocation Theory. J. Acoust. Soc. Am. 27, 643 (1955).

22. A. H. Cottrell. Dislocations and Plastic Flow in Crystals. Oxford University Press, London (1953).

23. B. E. Droney. Ultrasonic Reverberation in Solids for Loss Factors Exclusive of Scattering and Diffraction, a doctoral dissertation, The Pennsylvania State University, September, 1966.

24. T. A. Litovitz. Ultrasonic Absorption of Glycerin in the Liquid and Vitreous State. J. Acoust. Soc. Am. 23, 75 (1951).

25. W. F. Brace and J. B. Walsh. Some Direct Measurements of the Surface Energy of Quartz and Orthoclase, The American Mineralogist 47, 1111 (1962).

26. A. G. Smagin. Methods of Reducing the Energy Dissipated in the Surface Layers of Quartz. Soviet Physics, Crystall 4, 818 (1960).

27. W. G. Cady, Piezoelectricity, Vols. I and II, Dover Publications, Inc., New York (1964).

28. E. J. Armstrong. X-Ray Studies of the Surface Layers of Quartz, Bell Sys. Tech. J. 25, 136 (1946).

29. F. R. Hirsch, Jr. and J. M. W. DuMond. X-Ray Evidence on the Nature of the Surface Layers of Thin Ground Quartz Crystals Secured with the Cauchois Spectrometer. Phys. Rev. 54, 789 (1938).

30. D. D'Eustachio. Surface Layers on Quartz and Topaz. Phys. Rev. 70, 522 (1946).

31. H. E. Bommel, W. P. Mason, A. W. Warner, Jr. Experimental Evidence for Dislocations in Crystalline Quartz, Phys. Rev. 99, 1894 (1955).

32. H. I. Smith. Optical Contact Bonding. J. Acous. Soc. Am. 37, 928 (1965).

33. P. H. Carr. Reflection of Gigacycle-per-second Ultrasonic Waves from an Optical Contact Bond. J. Acoust. Soc. Am. 37, 927 (1965).

34. E. J. Skudrzyk. Vibrations of Complex and Radiating Vibratory Systems. The Penn State University Press (in publication).

35. R. A. Heising. Quartz Crystals for Electric Circuits. D. Van Nostrand Co., Inc., New York (1946).

VITA

The author [redacted].

After graduation from Edinboro High School, Edinboro, Pennsylvania in 1948 he was employed by General Electric Company as an apprentice machinist. He enlisted in the U. S. Navy in 1951 and qualified for a fleet appointment to the U. S. Naval Academy. After graduation from the Naval Academy at Annapolis, Maryland in 1956 he served with the Amphibious Forces of the Pacific Fleet. In 1960 he enrolled at The Pennsylvania State University, University Park, Pennsylvania and subsequently qualified for three degrees in physics: B.S., Physics, 1961; M.S., Physics, 1963; Ph.D., Physics, 1967. He is a member of Sigma Pi Sigma, Pi Mu Epsilon, and the Acoustical Society of America.